Service Altimetrie & Localisation Precise

CalVal Saral/ Altika

SARAL/Altika validation and cross calibration activities

Annual report 2021

Contract No 14026/00 – 160182 - lot 1.6.3

Reference : SALP-RP-MA-EA-23530-CLS

Nomenclature : SARAL Annual report 2021

Issue : 1rev 1

Date : March, 2022

CLS - 11 Rue hermès - Parc Technologique du Canal - 31520 Ramonville St-Agne - FRANCE
Telephone 33 5 61 39 47 00

Chronology Issues:		
Issue:	Date:	Reason for change:
1.0	Jan 22, 2021	Creation
1.1	Feb 16 , 2021	Update

People involved in this issue :				
	AUTHORS	**COMPANY**	**DATE**	**INITIALS**
Written by:	G. Jettou ; M.Rousseau	CLS		
Checked by:	G. Jettou	CLS		
Reviewed by:	F. Bignalet-Cazalet	CNES		
Approved by:	S. Labroue ; F. Bignalet-Cazalet	CLS ; CNES		
Application authorised by:	Y. Bernard; T. Guinle	CLS; CNES		

Index Sheet :	
Context:	
Keywords:	
Hyperlink:	

Distribution:		
Company	Means of distribution	Names
CLS/DOS	electronic copy	slabroue@cls.fr
CNES	electronic copy	thierry.guinle@cnes.fr
		nicolas.picot@cnes.fr
		Gerald.Dibarboure@cnes.fr
		Francois.Bignalet-Cazalet@cnes.fr
		Nadege.Queruel@cnes.fr
		dominique.chermain@cnes.fr
		aqgp_rs@cnes.fr

List of tables and figures

List of Tables

List of Figures

Contents

1. Introduction

1.1. SARAL/AltiKa Cal/Val activities

Since the beginning of the mission, SARAL/AltiKa data have been analyzed and monitored in order to assess the quality of SARAL/AltiKa products. Cycle per cycle reports summarizing mission performance are generated and made available through the AVISO web page (https://www.aviso.altimetry.fr/?id=1173&sat=4). Main performance metrics were also summarized in a paper published in the Marine Geodesy special issue on SARAL/AltiKa in 2015 [60]. Each year, the Cal/Val activity is described in a yearly report, which are also available through the AVISO website (https://www.aviso.altimetry.fr/en/data/calval/systematic-calval/annual-reports/saral.html).

The present report documents the activities undertaken in the framework of the SALP contract to assess and monitor Saral/AltiKa data quality. Depending on the sections the period considered may vary slightly. If not specified otherwize, all data from cycle 1 to 155 are considered (corresponding to March 2013 to November 2021). This period might be reduced for some plots if needed. We present a detailed description of the main performance metrics of the mission including:

- monitoring of missing and edited parameters,
- analysis of geophysical parameters and corrections,
- accuracy and stability of SLA measurements.

We also present the results of cross-calibration analysis performed between SARAL/AltiKa, Jason-2 and Jason-3. Even if the three satellites are on different ground tracks comparisons remain possible, and necessary, to ensure the continuity of ocean observations through high precision altimetry.

Routine validation of SARAL/AltiKa mission and cross-calibration with Jason-3 activities generate a large number of graphs, plots and figures. The purpose of the present report is to give the reader a useful and as much as possible reader-friendly summary of the most important results of the daily monitoring of the mission performed at CLS.

2. Processing status

2.1. Processing history

Four months after launch, SARAL/AltiKa OGDR and IGDR data were available to all users beginning of July 2013. They were first released under the version T label, with some flaws (unit problem for liquid cloud water,...), some corrections voluntarily disabled (atmospheric attenuation set at default value) or with disclaimers of product fields (ice_flag, altimeter wind not to use, ...).

Some of these issues were addressed by Patch 1, whose content is recalled in 11.1.. Beginning of September 2013 the GDR products were released with consistent Patch 1 standards since the beginning of the mission. A second processing upgrade, labeled Patch 2, containing several improvements for SARAL/AltiKa data, was applied on February 2014. The content of this Patch 2 is recalled in chapter 11.2. This included a full reprocessing of previous GDR cycles.

Further on, orbit standard changed from POE-D to POE-E from June 30th 2015 onwards on IGDR and from cycle 25 (July 3rd) on GDR, and from POE-D to POE-F from December 10th 2018 onward on IGDR and from cycle 125 on GDR. Also, the mean sea surface was updated from July 4th, 2016 onwards on IGDR data and from cycle 34 (May 12th) on GDR data.

Starting from cycle 135 for GDR and cycle 137 for IGDR, products are released with GDR-F standard including POE-F orbit and several improvements. The previous GDR cycles have been reprocessed. This is the reference dataset used for the report. Models and standards used in GDR-F are detailed in table 4 and in chapter 11.3..

Table 1 summarizes the processing history of SARAL/AltiKa products through the application dates of main product versions.

Data version	OGDR	IGDR	GDR
Version T	till cycle 4 segment 0609	till cycle 4 pass 394	-
Version T with Patch1 (chapter 11.1.)	from cycle 4 segment 0611 onwards (2013-07-18 13h44m04)	from cycle 4 pass 0395 onwards (2013-07-10 23h56m18)	from cycle 1 pass 0001 onwards
Version T with Patch2 (chapter 11.2.)	from cycle 10 segment 0407 onwards (2014-02-06 10h46m58)	from cycle 10 pass 0566 onwards (2014-02-11 23h17m37)	from cycle 8 to cycle 134 (cycles 1 to 7 have been reprocessed)
Version F (chapter 11.3.)	from cycle 138 onwards	from cycle 137 onwards	from cycle 135 onwards (cycles 1 to 134 have been reprocessed)

Table 1: *Product versions*

2.2. Payload history

2.2.1. Acquisition/tracking modes

Table 2 shows the acquisition/tracking modes used since the beginning of the SARAL/AltiKa mission.

cycle	pass	start time	stop time	altimeter mode
1	0001-0200	2013-03-14	2013-03-21	DIODE acquisition / median tracking
1	0201-0400	2013-03-21	2013-03-28	DIODE acquisition / EDP tracking
1	0401-0600	2013-03-28	2013-04-04	DIODE acquisition / median tracking
1	0601-0800	2013-04-04	2013-04-11	DIODE / DEM tracking
1	0801-1002	2013-04-11	2013-04-18	DIODE acquisition / EDP tracking
2	0001-1002	2013-04-18	2013-05-23	DIODE acquisition / median tracking
3	0001-0400	2013-05-23	2013-06-06	DIODE acquisition / median tracking
3	0401-0800	2013-06-06	2013-06-20	DIODE acquisition / EDP tracking
3	0801-1002	2013-06-20	2013-06-27	DIODE acquisition / median tracking
4 to 9	0001-1002	2013-06-27	2014-01-23	DIODE acquisition / median tracking
10	0001-0127	2014-01-23	2014-01-27	DIODE acquisition / median tracking
10	0128-0135	2014-01-27	2014-01-27	autonomous DIODE / median tracking
10	0136-1002	2014-01-27	2014-02-27	DIODE acquisition / median tracking
.../...				

cycle	pass	start time	stop time	altimeter mode
11 to 16	0001-1002	2014-02-27	2014-09-25	DIODE acquisition / median tracking
17	0001-0324	2014-09-25	2014-10-06	DIODE acquisition / median tracking
17	0414-0457	2014-10-09	2014-10-11	autonomous DIODE / median tracking
17	0457-1002	2014-10-11	2014-10-30	DIODE acquisition / median tracking
18 to 113	0001-1002	2014-10-30	2017-11-6	DIODE acquisition / median tracking
114	0001-0531	2017-11-06 15:58:04	2017-11-25 04:11:25	DIODE acquisition / median tracking
114	0532-0540	2017-11-25 04:13:19	2017-11-25 11:05:25	Autonomous acquisition / median tracking
114 to 155	0540-1002	2017-11-25 11:07:14	2021-11-15 20:23:35	DIODE acquisition / median tracking

Table 2: *Acquisition and tracking modes*

2.2.2. List of events

Table 3 summarizes the major events of the SARAL/AltiKa mission.

cycle	pass	start time	stop time	event
1		2013-03-14	2013-03-17	X-band stations acquisition problems (a few missing data)
1	0172-0175	2013-03-20 05:10:03	08:30	calibration I2+Q2 and I&Q for expertise
1	0266	2013-03-23 12:13:52	12:13:55	semi major axis maneuver
1	0372, 0374	2013-03-27		CAL2 long calibrations at 04:51 (28min missing data) and 06:40 (11min missing data)
1	0801	2013-04-11 04:42:00	04:59:45	altimeter gain calibration I2+Q2 (mostly over land)
.../...				

cycle	pass	start time	stop time	event
1	0868	2013-04-13 12:53:52	12:53:54	station keeping maneuver
1	0898	2013-04-14 13:42:00	13:59:45	altimeter gain calibration I&Q (mostly over land)
1	0984	2013-04-17 13:47:00	14:04:45	altimeter gain calibration I2+Q2 (mostly over land)
2	0034, 0035	2013-04-19 9:37	10:25	cross calibration test over S-band station Biak (Indonesia)
2	0057	2013-04-20 04:53	05:12	altimeter gain calibration I&Q (over land)
2	0127	2013-04-22 15:26	15:54	cross calibration maneuver
2	0206	2013-04-25 9:53		pitch maneuver (0.045°) to correct the PF/RF alignment (alignment between the platform and the radiofrequency axis)
2	0355	2013-04-30 14:35	15:03	cross calibration maneuver
2	0782	2013-05-15 12:48:23	12:48:26	station keeping maneuver
3	0438	2013-06-07 12:25:11	12:25:13	station keeping maneuver
3	0887-0890	2013-06-23 05:06:55	06:56:57	no O/I/GDR product due to PLTM lost
3	0926	2013-06-24 13:31:11	13:31:13	station keeping maneuver
4	0498	2013-07-14 14:42:44	14:42:47	station keeping maneuver
4	0556	2013-07-16 15:01:01	15:19:00	altimeter gain calibration I&Q (mostly over land)
4	0586	2013-07-17 16:13:01	16:30:45	altimeter gain calibration I2+Q2 (mostly over land)
4	0911	2013-07-29 00:54:25	00:58:26	inclination maneuver (1 burn on Y and Z axis)
4	0984	2013-07-31 14:08:03	14:08:11	station keeping maneuver

.../...

cycle	pass	start time	stop time	event
5	0182	2013-08-07 13:48:06	13:48:09	station keeping maneuver
5	0726	2013-08-26 13:51:02	13:51:05	station keeping maneuver
5	0958	2013-09-03 16:02:01	16:20:00	altimeter gain calibration I&Q (mostly over land)
6	0038	2013-09-06 12:44:01	13:01:45	altimeter gain calibration I2+Q2 (over land)
6	0812	2013-10-03 13:55:39	13:57:17	1st inclination maneuver to reach the Envisat ground track (1 burn on Z axis)
6	0926	2013-10-07 13:29:45	13:31:25	2nd inclination maneuver to reach the Envisat ground track
6	0984	2013-10-09 14:07:52	14:07:57	station keeping maneuver
7	0526	2013-10-28 14:11:24	14:11:26	station keeping maneuver
7	0586	2013-10-30 16:11	16:28:45	altimeter gain calibration I2+Q2
7	0812	2013-11-07 13:57:01	13:57:03	station keeping maneuver
8	0326	2013-11-25 14:31:29	14:31:32	station keeping maneuver
8	0812	2013-12-12 13:56:58	13:57:01	station keeping maneuver
9	0240	2013-12-27 14:25:41	14:25:44	station keeping maneuver
10	0128	2014-01-27 16:15	16:32:45	altimeter gain calibration I2+Q2 (mostly over land)
10	0152	2014-01-28 12:38:43	12:38:45	station keeping maneuver
11	0126	2014-03-03 14:50:53	14:50:56	station keeping maneuver
11	0782	2014-03-26 12:47:17	12:47:20	station keeping maneuver

.../...

cycle	pass	start time	stop time	event
12	0438	2014-04-18 12:24:16	12:24:19	station keeping maneuver
12	0728	2014-04-28 15:12:55	15:30:45	expertise calibration CAL1
13	0326-0327	2014-05-19 14:31:18	14:31:21	station keeping maneuver with two consecutive mispointing events between 14:38 and 14:43 and between 15:03 and 15:12
14	0782	2014-07-09 12:47:10	12:47:12	station keeping maneuver
15	0356	2014-07-29 15:22:00	15:39:45	altimeter gain calibration I2+Q2 (mostly over land)
15	0782	2014-08-13 12:47:06	12:47:08	station keeping maneuver
16	0539	2014-09-09		No TM from 01:02:30 to 01:06:16 and from 01:09:25 to 01:14:08 due to the update of MNT onboard parameters
16	0640	2014-09-12 13:44:34	13:44:36	station keeping maneuver
16	0406 0474 0690	2014-09-04 09:44:24 2014-09-06 18:38:32 2014-09-14 07:36:44	09:47:15 18:41:55 07:38:50	several platform mispointing events caused by a rise in reaction wheel friction due to movement of lubricant. Only the 3 largest events are shown.
17	0324	2014-10-06 12:40:00	12:40:02	station keeping maneuver
17	0324-0414	2014-10-06 13:03:22	2014-10-09 16:27:46	safe hold mode
17	0438	2014-10-10 12:14:14	12:14:34	station keeping maneuver
17	0610	2014-10-16 12:26:26	12:26:35	station keeping maneuver
17	0958	2014-10-28 16:02:00	16:19:45	altimeter gain calibration I2&Q2

.../...

cycle	pass	start time	stop time	event
18	0152	2014-11-04 12:26:39	12:26:41	station keeping maneuver
18	0640	2014-11-21 13:39:10	13:39:12	station keeping maneuver
19	0182	2014-12-10 13:47:02	13:47:04	station keeping maneuver
19	0640	2014-12-26 13:44:42	13:44:45	station keeping maneuver
20		2015-01-12 11:30		software patch applied by ISRO in order to avoid zero-crossings of RW speed
20		2015-01-17	2015-01-18	platform pointing disturbance (fluctuations in RW friction)
20	0412	2015-01-22 14:31:03	14:31:06	station keeping maneuver
20	0586	2015-01-28 16:11		CNG calibration
21	0268	2015-02-21 13:47:56	13:47:58	station keeping maneuver
22	0354	2015-03-31 13:50:16	13:50:18	station keeping maneuver. Delta_Vy twice more than expected.
22	0610	2015-04-09 12:28:10	12:28:14	station keeping maneuver to stop the westward drift.
22	0986	2015-04-22 15:30		CNG calibration
23	0954	2015-05-26 12:51:07	12:51:12	station keeping maneuver. Delta_V applied twice less than expected. thruster firing has taken place between 10:00 to 10:04 UT to control a reaction wheel error guidance has been performed with thrusters (instead of RW)
24	0554	2015-06-16 13:23	13:39	station keeping maneuver (to calibrate satellite rotation with thrusters). The main objective is not to recover the nominal ground track but to calibrate this new way of performing satellite rotation

.../...

cycle	pass	start time	stop time	event
24		2015-06-30		introduction of a leap second =¿ UTC = TAI-36s The sequence of dates of the UTC second markers is: 2015 June 30, 23h 59m 59s 2015 June 30, 23h 59m 60s 2015 July 1, 0h 0m 0s
24		2015-06-30		First MOE with GDR-F orbit standard
25				Orbit standard = GDR-F
25	0182	2015-07-08 13:40:55	13:40:58	station keeping maneuver (only with thrusters). Thruster activity is expected from 13:31:50 UT to 13:50 UT
25	0758	2015-07-28 16:22		Altika quarterly expertise CNG calibration
26	0152	2015-08-11 12:32:56	12:32:59	station keeping maneuver (to stop western drift and stay in the +/-1km ground track window) only with thrusters
26	0524	2015-08-24 12:24:12	12:24:14	station keeping maneuver, performed only with thrusters.
26		2015-09-05	2015-09-06	mispointing events attributed to sudden changes in friction torque of reaction wheel (RW-4).
27		2015-09-15		Update of CoG historic file: the initial value of Zcog value has been updated by POD team and propagated to IDS teams through CoG historic file ; new value -0.6105 (instead of -0.6583)
28	0182	2015-10-21 13:41:40	13:41:43	station keeping maneuver
28	0195	2015-10-22		mising data due to issues on X-band stations network and the amount of TM_gaps
28	0614	2015-11-05 15:39		CNG Calibration
28	0812	2015-11-12 13:40:32	13:59:33	station keeping maneuver (3 bursts)
29	0210	2015-11-26 13:08:18	13:24:57	station keeping maneuver
30	0412	2016-01-07 14:28:48	14:44:39	station keeping maneuver
30	0986	2016-01-27 15:30:00	15:47:45	CNG calibration

.../...

cycle	pass	start time	stop time	event
31	0441-0442	2016-03-18 15:08:55	15:25:40	collision avoidance maneuver
33	0010	2016-04-07 13:18:44	13:34:31	station keeping maneuver
33	0528	2016-04-25 15:33:00	15:50:45	CNG Calibration
35	0522	2016-07-04 12:13:35	12:31:15	orbit change maneuver, cycle 35 ends at pass 522
101	0090	2016-08-11 15:54:00	16:11:45	CNG Calibration
103	0290	2016-10-27 15:47:00	16:04:45	CNG Calibration
105	0862	2017-01-25 15:43:00	16:00:45	CNG Calibration
108	0432	2017-04-25 15:38:00	15:55:45	CNG Calibration
111	0202	2017-07-31 15:11:00	15:28:45	CNG Calibration
113	0660	2017-10-25 15:30:00	15:47:45	CNG Calibration
114	0742	2017-12-02 12:32:08	12:48:47	collision avoidance maneuver
116	0316	2018-01-26 15:30:00	15:47:45	CNG Calibration
119	0058	2018-05-02 15:37:00	15:54:45	CNG Calibration
121	0544	2018-07-28 15:23:00	15:40:45	CNG Calibration
124	0458	2018-11-07 15:40:00	15:57:45	CNG Calibration
125	0923	2018-12-28 22:14:55	22:14:55	HD mode sequence
126	0944	2019-02-02 15:23:00	15:40:45	CNG Calibration

.../...

cycle	pass	start time	stop time	event
126	0322-0337	2019-01-11 22:15:34	2019-12-01 10:38:54	HD mode sequence
126	0780-0795	2019-01-27 22:16:10	2019-28-01 10:39:32	HD mode sequence
126	964	2019-02-03 08:01:55	onwards	Star Sensor Anomaly (SSA) *
127	0236	2019-02-12 22:16:47	22:16:47	HD mode sequence
127	0251	2019-02-13 10:40:08	10:40:08	HD mode sequence
127	0694	2019-02-28 22:17:26	22:17:26	HD mode sequence
127	0709	2019-03-01 10:40:46	10:40:46	HD mode sequence
128 to 147	0982 - 0579	2019-04-15 00:00:00	2021-01-25 00:00:00	HD mode sequence
132	0170	2019-08-04 15:12:00	15:29:45	CNG Calibration
134	0628	2019-10-29 15:31:00	15:58:45	CNG Calibration
137	0284	2020-01-30 15:30:00	15:47:45	CNG Calibration
142	0112	2020-07-17 16:04:00	16:21:45	CNG Calibration
145	0798	2020-11-23 15:28:00	15:45:45	CNG Calibration
147	0654	2021-01-27 14:58:00	15:15:45	CNG Calibration
152	0377 - 0979	2021-07-12 00:00:00	2021-08-02 00:00:00	HD mode sequence
153	0024	2021-09-03 15:27:00	15:44:45	CNG Calibration
154	0034 - 0978	2021-09-08 00:00:00	2021-11-01 00:00:00	HD mode sequence

.../...

cycle	pass	start time	stop time	event
155	0778 - 1002	2021-11-08 00:00:00	2021-11-15 20:23:35	HD mode sequence
155	0682	2021-11-04 15:29:00	15:46:45	CNG Calibration

Table 3: *Main SARAL/AltiKa mission events (red rows indicates safe hold mode event)*

* In February 2019, SARAL/AltiKa satellite encountered a Star Sensor Anomaly (SSA), affecting the nadir pointing accuracy. Since that day, the spacecraft regularly goes through mispointing issues, most of which remain within the altimeter pointing specifications.

2.3. Models and Standards

Table 4 summarizes the contents regarding altimeter standards and geophysical correction models of the current version (F) of SARAL/AltiKa products.

Model	Product version "F"
Orbit	Based on Doris onboard navigator solution for OGDR. DORIS tracking data for IGDR. DORIS+SLR tracking data using POE-F for GDR.
Altimeter Retracking	"Ocean MLE4" retracking: MLE4 fit from 2nd order Brown analytical model. The retracker MQE format changed into "integer" in GDR-F in order to allow a better precision. MLE4 simultaneously retrieves 4 parameters from the altimeter waveforms: • Epoch (tracker range offset) → altimeter range, • Composite Sigma → SWH, • Amplitude → Sigma0, • Square of mispointing angle.
Altimeter Retracking	"Ice 1" retracking: Geometrical analysis of the altimeter waveforms, which retrieves the following parameters: • Epoch (tracker range offset) → altimeter range, • Amplitude → Sigma0.
Altimeter Retracking	"Ice 2" retracking: The aim of the ice2 retracking algorithm is to make the measured waveform coincide with a return power model, according to Least Square estimators. The ice-2 retracking account for the antenna gain effect. Retrieval of the following parameters: • Epoch → altimeter range, • Width of the leading edge → SWH, • Amplitude → Sigma0, • Slope of the logarithm of the waveform at the trailing edge → Mispointing angle/surface slope, • The thermal noise level (to be removed from the waveform samples).
Altimeter Retracking	"Ice 3" retracking: Ice 3 retracking is a TFMRA retracking based on [2] and [3].
	.../...

Model	Product version "F"
Altimeter Retracking	"Sea Ice" retracking: In this algorithm, waveform parameterization based on peak threshold retracking is applied to the Ka-band waveform. From this parameterization, a tracking offset and backscatter estimate are determined. Tests are made on the extent of the tracking offset, and extreme values are flagged as retracking failures. The sea-ice waveform amplitude is determined by finding the maximum value of the waveform samples and the tracking offset is determined by finding the point on the waveform (by interpolation) where the waveform amplitude exceeds a threshold determined from the above sea-ice amplitude. A tracking offset is determined. The Centre Of Gravity offset correction must be included in the range measurement as the correction is not available separately in the L2 product. • Amplitude → Sigma0, • Tracking offset → altimeter range, • Centre Of Gravity offset correction → correction to altimeter range measurement. N.B.: the Ice2 retracking algorithm has been tuned to Ka-band since Patch2, but not the Ice1 nor the Sea Ice algorithms.
Altimeter Instrument Corrections	consistent with MLE4 retracking with instrumental Look Up Tables taking into account the actual antenna pattern. Theses LUT are used, including new LUT for waveform off nadir angle.
Saral/AltiKa Radiometer Parameters	Using on-board calibration.
Dry Troposphere Range Correction	From ECMWF atmospheric pressures and model for S1 and S2 atmospheric tides.
Wet Troposphere Range Correction from Model	From ECMWF model.
Ionosphere correction	Based on Global Ionosphere TEC Maps from JPL.
Sea State Bias Model	SSB tables based on SWH&wind, computed using 2015 GDR-F dataset based on the method proposed by [33] and [34].
Mean Sea Surface	MSS_CNES_CLS15 [42]
Mean Dynamic Topography	MDT_CNES-CLS18
Geoid	EGM2008
Bathymetry Model	ACE-2
Inverse Barometer Correction	Computed from ECMWF atmospheric pressures after removing S1 and S2.
	.../...

Model	Product version "F"
Atmospheric tides	Non-tidal High-frequency De-aliasing Correction & Mog2D high resolution ocean model on (I)GDRs. None for OGDRs. Ocean model forced by ECMWF atmospheric pressures after removing S1 and S2 atmospheric tides.
Tide Solution 1	GOT4.10
Tide Solution 2	FES2014B [37] and [38]
Equilibrium long-period ocean tide model	From Cartwright and Taylor tidal potential.
Non-equilibrium long-period ocean tide model	Mm, Mf, Mtm, and Msqm from FES2014B.
Solid Earth Tide Model	From Cartwright and Taylor tidal potential.
Pole Tide Model	Shailen Desai 2015 with 2017 coefficients [36].
Wind Speed from Model	ECMWF model
Altimeter Wind Speed	Wind table N.Tran [33].
Trailing edge variation Flag	Derived from Matching Pursuit algorithm (from J. Tournadre, IFREMER).
Ice flag	Initialized in climatological areas based on wind speed values and updated by comparing the model wet tropospheric correction and the dual-frequency wet tropospheric correction retrieved from radiometer brightness temperatures.

Table 4: *Models and standards adopted for the SARAL/AltiKa version F products. Adapted from [52].*

3. Data coverage and edited measurements

This section details the SARAL/AltiKa mission performance regarding data availablity. The ratio of missing and edited measurements is carefully monitored through routine Cal/Val analysis to detect any anomalies, either on the instrument itself or on ground processing.

3.1. Missing measurements

Determination of missing measurements relative to the theoretically expected orbit ground pattern is an essential tool to detect missing telemetry or satellite events for instance. It also permits to measure the tracking performances of the altimeter, especially over non ocean surfaces that remain more challenging for the radar altimeter signal acquisition. The number of missing measurements is routinely monitored by Cal/Val tools. SARAL/AltiKa's performance regarding the number of missing measurements was so far compared to Jason-2.

Note that the interleaved phase that started in October 2016 along with several SHM periods experienced in 2017 (15-30 Mars , 17 May-12 July , 14 Sept-13 Oct) have severely impacted the number of available measurements for Jason-2 (see [65] for more details). To have suitable comparisons over SARAL/AltiKa's lifetime and to cover up the gaps of Jason-2's datased, all the monitoring will from now on include Jason-3's data over its whole available period.

Note that several SHM periods in 2019-2020 (24 Feb 2019 - 06 March 2019, 06 Apr 2019 - 12 Apr 2019, 31 Jan 2020 - 05 Feb 2020, 05 Feb 2020 - 13 Feb 2020, 15 Jun 2020 - 19 Jun 2020) have impacted the number of available measurement for Jason-3. Doris anomaly caused a gap in Jason-3's data between 27 Oct 2020 and 19 Nov 2020. Over-ocean calibration resulted in a slightly higher percentage of missing data over ocean in Aug/Sep 2021.

SARAL/AltiKa's performance regarding the number of missing measurements through the comparison of the percentage of missing measurements is estimated in a consistent manner for all the missions.

3.1.1. Over land and ocean

Missing 1 Hz measurements are estimated by comparing actual measurements to the theoretical ground track, resampled from the ENVISAT one. From cycle 100 onward, the actual ground track is drifting and the theoretical track from the repetitive phase can't be used any more. Missing measurements are then estimated using a theoretical ground track generated from predicted orbit files. As long as a record exists for a given date, the measurement is accounted as present, even if there is no useful science data (default values).

SARAL/AltiKa can use several on board tracking modes: median, Earliest Detectable Part (EDP) and Diode/DEM (see chapter 2.2.1.). The median mode is similar to the one used by Envisat and for most cycles of Jason-2. EDP tracker should improve the tracker behavior above continental ice surfaces and hydrological zones. Finally, Diode/DEM mode is a technique using information coming from Diode and a digital elevation model available on board. It was already tested on Jason-2. For

more information about the different on board tracker algorithms see [8]. The information about the acquisition / tracking mode used is available in the GDR (fields alt_state_flag_acq_mode_40hz and alt_state_flag_tracking_mode_40hz).

From cycle 4 onwards, SARAL/AltiKa used the **DIODE acquisition / median tracking mode**, except for two short periods of autonomous DIODE acquisition at cycles 10 and 17:

- at cycle 10, the altimeter switched to autonomous DIODE acquisition mode after a CNG I2+Q2 calibration, this mode was used for about 6 hours before switching back to the nominal DIODE acquisition mode,
- at cycle 17, the altimeter switched to the autonomous DIODE acquisition mode after it was turned on again after the SHM, this acquisition mode was used for a day and a half before switching back to the nominal DIODE acquisition mode.

Considering all surface types, SARAL/AltiKa has more data available than Jason-2 (which also uses most of the time the median tracker), independently from the tracker mode used for Saral. Figure 1 shows the percentage of available measurements for SARAL/AltiKa, Jason-2 and Jason-3 over all surfaces. The interleaved phase and the many SHM periods experienced in 2017 have clearly dropped the mean number of available measurements for Jason-2 (see [65] for more details) which ultimately lowers the performances of the mission. On the other hand, SARAL/AltiKa has only **1.1%** less available data than Jason-3, even if it experienced one SHM period in October 2014, and a severe attitude deviation in February 2019.

Except these punctual events, the main differences between the three missions appear over land surfaces as shown in figure 2. The missing data are highly correlated with the mountains location. Note that the routine calibrations for SARAL/AltiKa are mainly done over desert regions (Sahara, Australia, south of Africa and Mongolia), the percentage of available data is therefore low in these regions. When excluding these calibration areas and the highest mountains, SARAL exhibits an improved coverage compared to Jason-2. This can be noted over the Amazonian region (see figure 2) for instance where the percentage of available observations is **10%** higher than Jason-2's. In periods when the ground track was loosely maintained, and at the beginning of the drifting phase, routine calibrations also drifted and some of them were performed over ocean, resulting in short track sections missing.

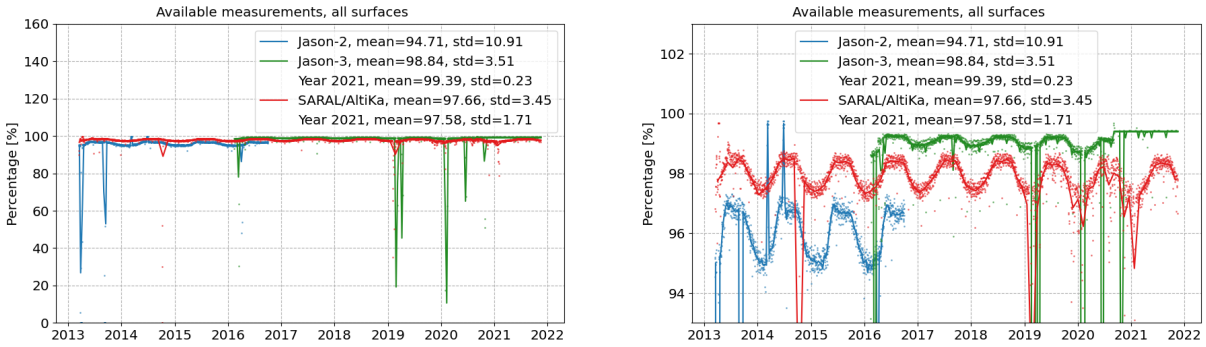

Figure 1: *Percentage of available measurements over all surfaces for SARAL/AltiKa, Jason-2 and Jason-3. Dots are daily averages while solid lines correspond to cycle averages.*

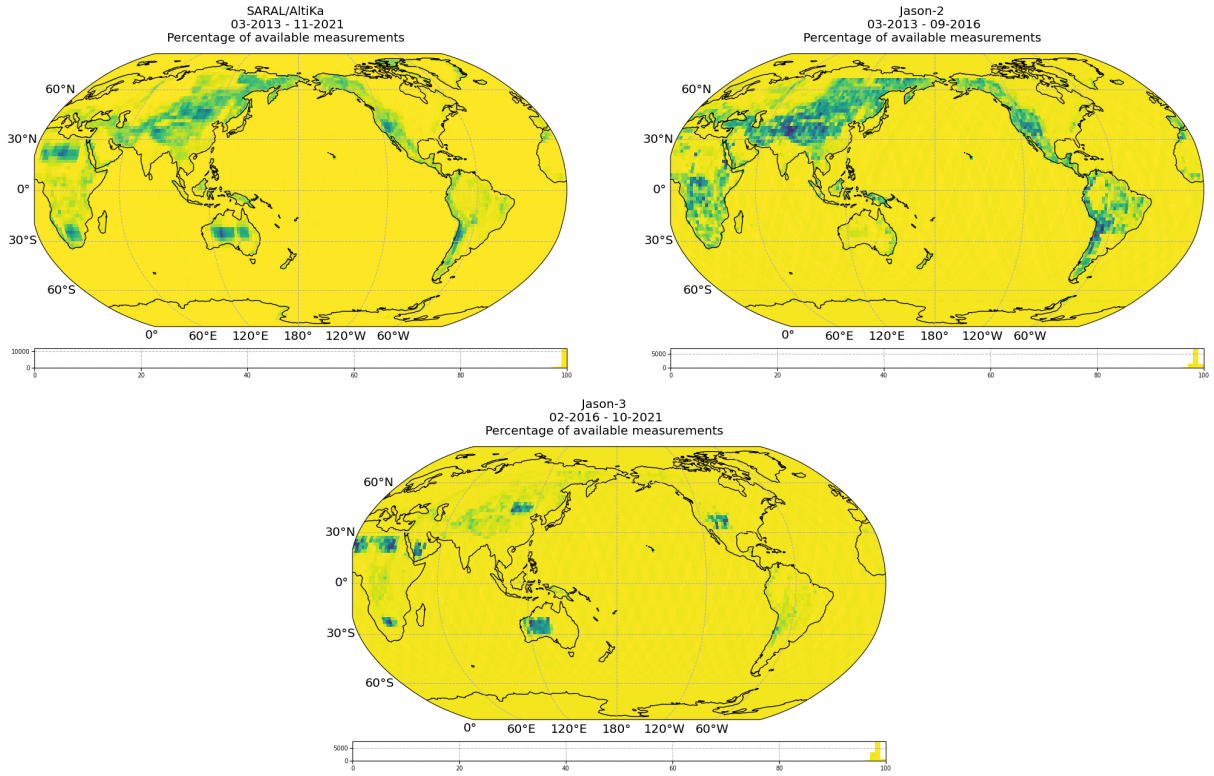

Figure 2: *Map of the percentage of available measurements over land for SARAL/AltiKa (left) Jason-2 (right) and Jason-3 (bottom).*

3.1.2. Over ocean

When considering only the ocean surface, the same analysis method leads generally to slightly less available data for SARAL/AltiKa compared to Jason-3 data coverage, as shown on figure 3, which represents the percentage of available measurements limited to ocean surfaces. Over the shown periods, the mean value is about **98.54%** for Jason-2, **99.74%** for Jason-3, and **99.71%** for SARAL/AltiKa, and we can still see the impact of SHM periods over Jason-2's globally lower value. SHM periods also impact Jason-3's. SARAL/AltiKa had other periods with reduced data availability. All these events are described in table 3.

In any case, these figures largely exceeds the specifications for SARAL/AltiKa, which were (see [51]) **95%** of all possible over-ocean data during a 3-year period with no systematic gaps plus the specific Ka-band limitation (**5%** of measurements may be not achieved due to rain rates $>$ **1.5 mm/h** according to geographic areas).

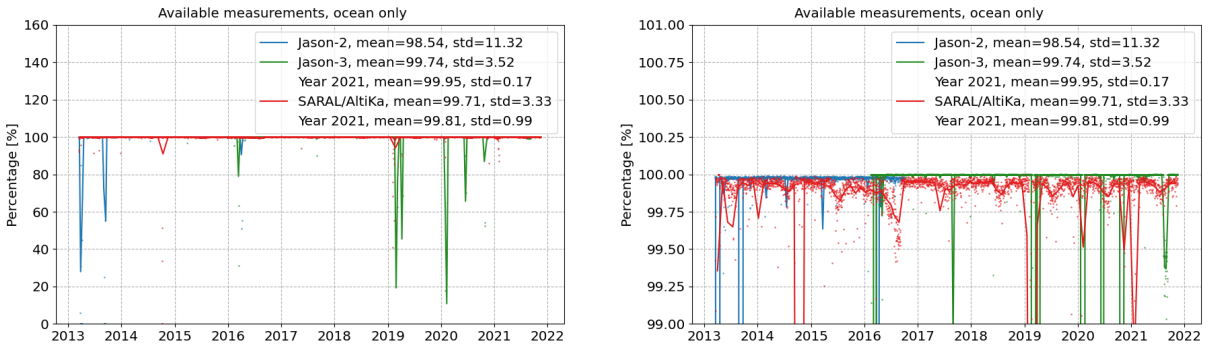

Figure 3: *Percentage of available measurements over ocean for SARAL/AltiKa Jason-2 and Jason-3. Dots are daily averages while solid lines correspond to cycle averages.*

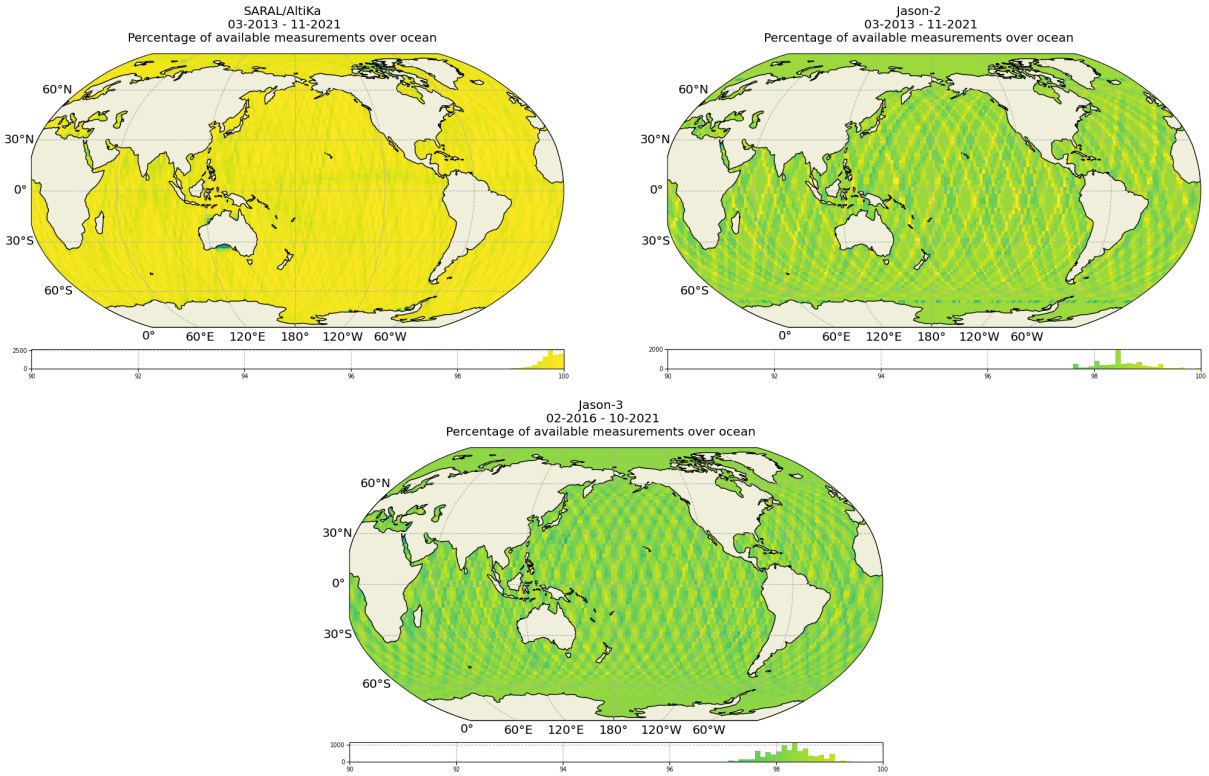

Figure 4: *Map of the percentage of available measurements over ocean for SARAL/AltiKa (left) Jason-2 (right) and Jason-3 (bottom).*

3.2. Edited measurements

The editing step of the Cal/Val process intends to remove for further analysis any measurement that is considered as erroneous. The definition of an erroneous measurement, and of the accepted error level on the final sea level anomaly is of course a trade off between accuracy and data coverage.

3.2.1. Editing criteria definition

Editing criteria are used to select valid measurements over ocean. The editing process is divided into 3 main parts:

- removal of all measurements affected by sea-ice (see section 3.2.2.),
- removal of all measurements which exceed given thresholds on different parameters (see section 3.2.3.),
- further checks on along-track sla consistency (see section 3.2.17.).

For each step of the editing process, the number of edited measurements, per track, per day and per cycle are routinely monitored at Cal/Val level. This allows the detection of anomalies through the number of removed data, which could come from instrumental, geophysical or algorithmic changes.

The editing performed here (and more generally SARAL/AltiKa Cal/Val activities) are dedicated to ocean applications. All data over land are removed using a land/water mask prior to the analysis described in this section. There are some variations over time (mainly at the beginning of the mission's life) of the number of measurements over land. These variations are directly related to the tracking mode used: when the DEM mode is used, more measurements are acquired over land compared to the median tracking periods.

Furthermore, as a very first step of the editing process, all passes are checked for latitude monotony (either increasing or decreasing). On SARAL/AltiKa this has not led to the removal of a single measurement yet.

Figure 5 gives an overview of the behavior of the edited measurements (all criteria combined) over the mission's lifetime. On average **22.38%** of ocean measurements are edited, the majority of which are removed due to the sea ice flag. As for the higher values observed since February 2019, they are mainly due to out of threshold square off nadir values (see dedicated section 3.2.11.). These values are the result of attitude deviations due to the star sensor anomaly (see 2.2.2.).
The results of each editing step are presented in the subsections hereafter.

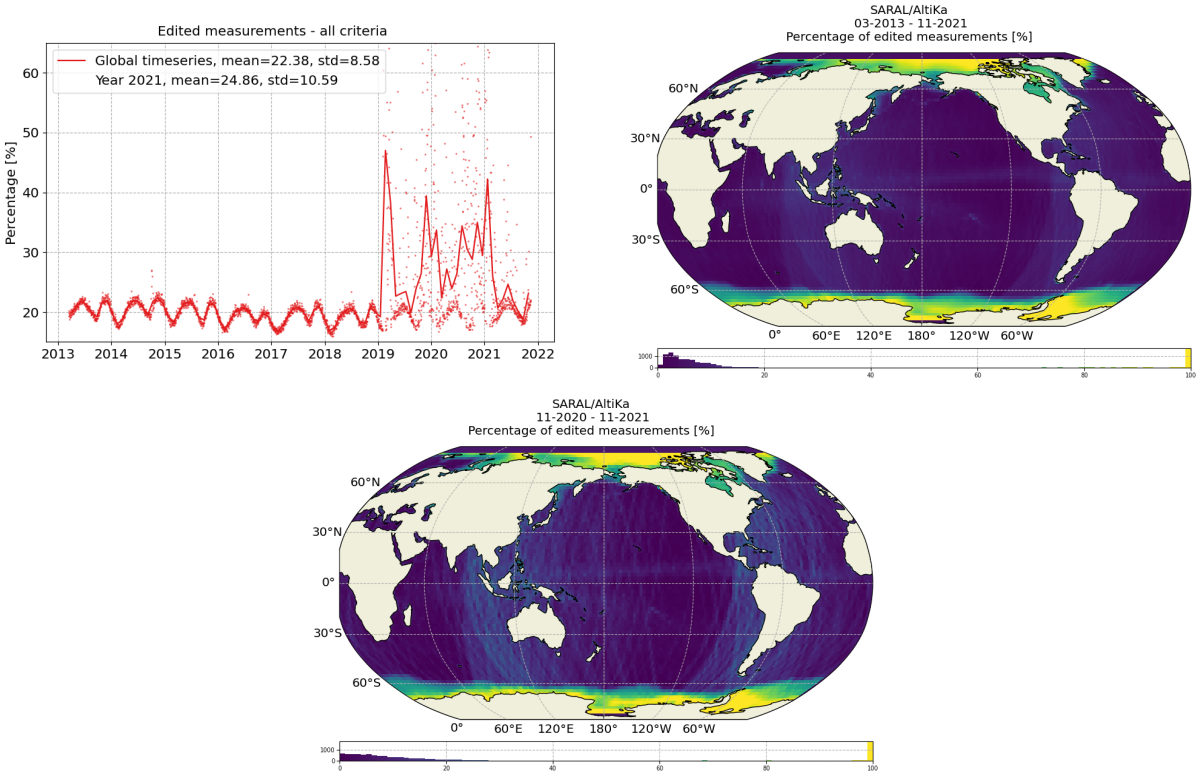

Figure 5: *Total percentage of SARAL/AltiKa edited measurements. [left] monitoring for GDR data, [right] map since the beginning of mission (cycles 1 to 155) and [bottom] map over the past year (2021). Dots are daily averages while solid lines correspond to cycle averages.*

3.2.2. Flagging quality criteria: Ice flag

The ice flag (ice_flag in the GDR products) is used to remove measurements affected by sea ice in the altimeter footprint. Left panel of figure 6 shows the evolution of the percentage of measurements edited by this criterion. Over the shown period, several characteristics are visible:

- a large seasonal cycle, due to annual growth and retreat of sea ice extent,
- two yearly minimums of the percentage of edited SARAL/AltiKa data (∼**16%** of edited data) are observed in February and September, corresponding respectively to periods where the Antarctic and Arctic sea ice extension are minimum,
- maximums of edited data are reached around June/July and November/December,
- a decreasing trend starting around march 2016.

The ice flag is set if the absolute value of the difference between the model wet tropospheric correction and the dual frequency wet tropospheric correction retrieved from 23.8 GHz and 37.0 GHz brightness temperatures exceeds **0.1 m**, OR if the number of valid 40-Hz altimeter range of the processed measurement is smaller than a specified threshold (see [52] for further details). The percentage of points for which the difference between the two wet tropospheric correction is greater than the threshold is clearly decreasing since march 2016 hence the lower percentage of edited measurement by the ice flag (∼**18%** before March 2016 and ∼**16.5%** after). As for the unusual peak observed in February 2019 (cycle 127), it is mainly due to the impact of the attitude deviation on the number of valid 40-Hz altimeter range (see figure 11).

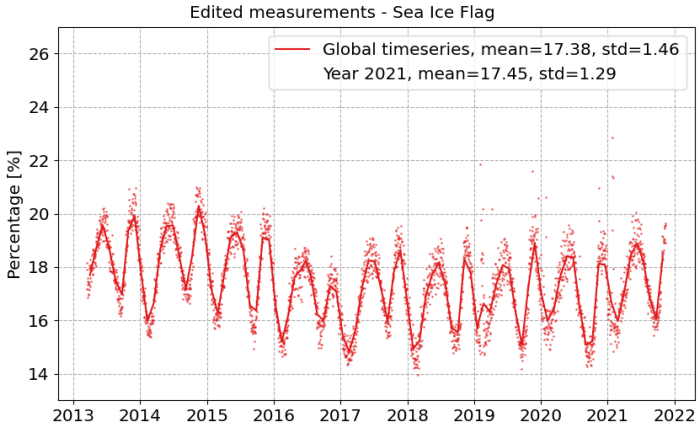

Figure 6: *Percentage of edited measurements by ice flag criterion. Monitoring for GDR data (all latitude). Dots are daily averages while solid lines correspond to cycle averages.*

The spatial distribution of the percentage of measurements edited by ice flag is plotted in the right panel of figure 6, over the whole mission lifetime.
Please note that an improved ice flag algorithm will be implemented in the L2E products (Level 2 Expertise) that can be made available on request [22]. As it is not yet in the GDR products, we do not consider this flag here.

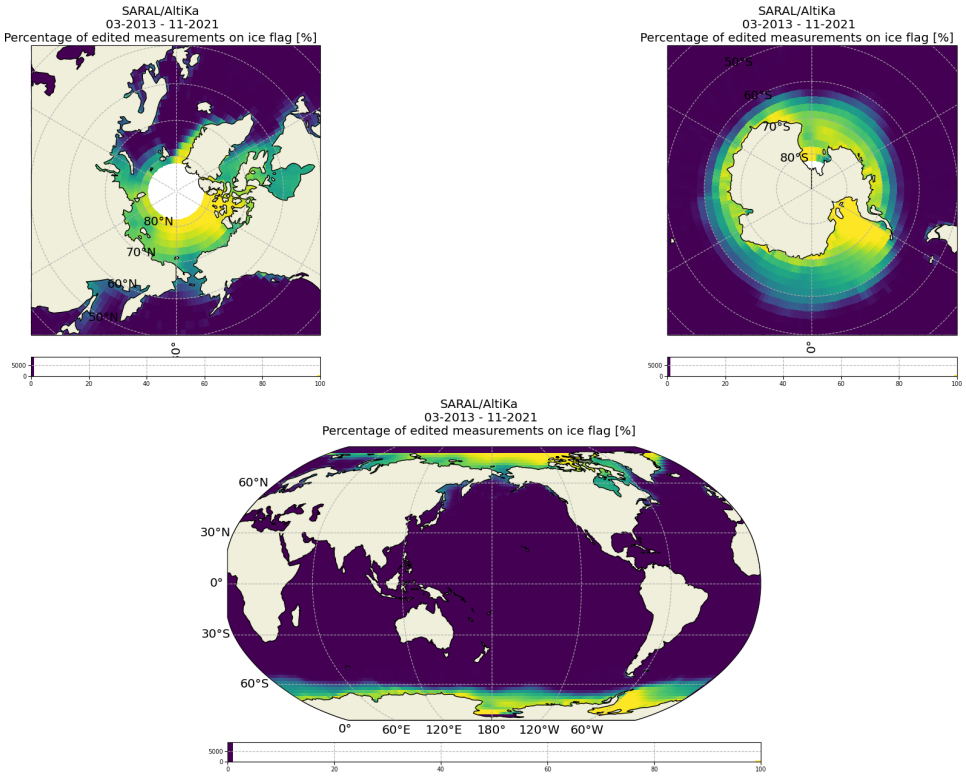

Figure 7: *Percentage of edited measurements by ice flag criterion. Maps since the beginning of the mission (cycles 1 to 155).*

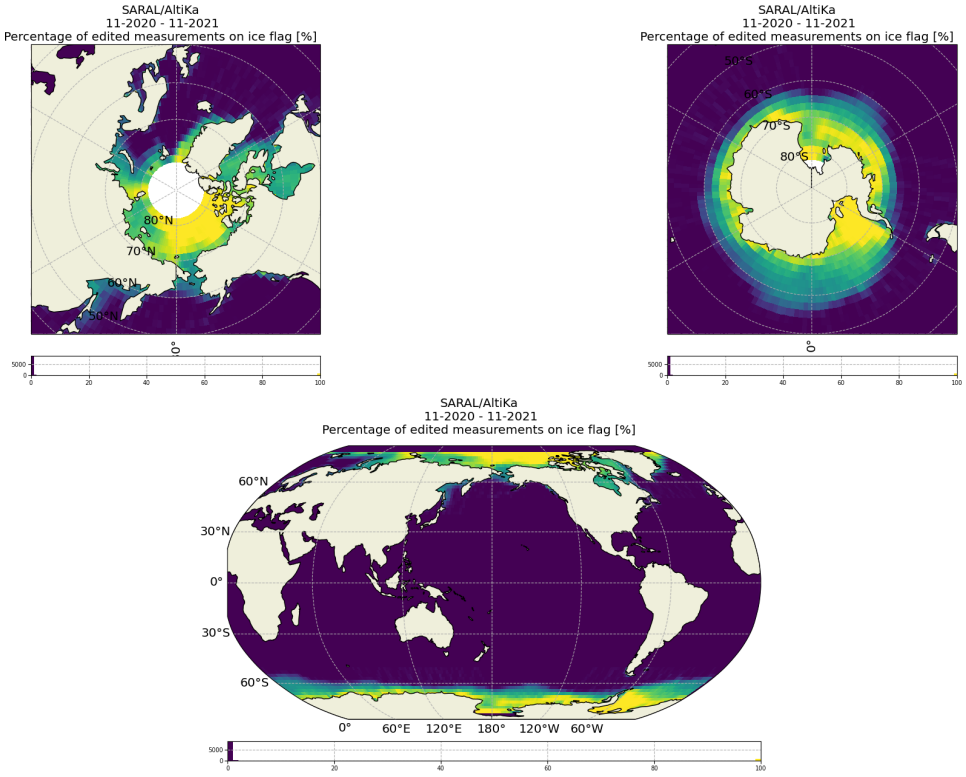

Figure 8: *Percentage of edited measurements by ice flag criterion. Maps on 2021.*

3.2.3. Threshold criteria: Global

Parameter	Min thresholds	Max thresholds	mean rejected	mean rejected over the past year (2021)
Sea surface height	$-130\,m$	$100\,m$	0.64%	0.86%
Sea level anomaly	$-2\,m$	$2\,m$	1.30%	3.86%
Number of range measurements	20	*Not applicable*	1.38%	1.67%
Standard deviation of range	0	$0.2\,m$	3.87%	5.86%
Squared off-nadir angle	$-0.2\,deg^2$	$0.09\,deg^2$	3.60%	6.51%
Dry troposphere correction	$-2.5\,m$	$-1.9\,m$	0.00%	0.00%
Dynamical atmopsheric correction	$-2\,m$	$2\,m$	0.00%	0.00%
Radiometer wet troposphere correction	$-0.5m$	$0\,m$	0.98%	1.45%
Significant wave height	$0\,m$	$11\,m$	2.23%	3.71%
Sea State Bias	$-0.5\,m$	$0.0025\,m$	0.39%	0.53%
Number measurements of Ka-band Sigma0	20	*Not applicable*	1.29%	1.58%
Standard deviation of Ka-band Sigma0	0	$1\,dB$	1.07%	1.26%
Ka-band Sigma0	$3\,dB$	$30\,dB$	0.40%	0.55%
Ocean tide	$-5\,m$	$5\,m$	0.00%	0.00%
Equilibrium tide	$-0.5\,m$	$0.5\,m$	0.00%	0.00%
Earth tide	$-1\,m$	$1\,m$	0.00%	0.00%
Pole tide	$-0.15\,m$	$0.15\,m$	0.00%	0.00%
Altimeter wind speed	$0\,m.s^{-1}$	$30\,m.s^{-1}$	0.39%	0.53%
All together	-	-	5.72%	8.67%

Table 5: *Editing thresholds, statistics obtained for cycles 1 to 155*

The quality of instrumental and geophysical parameters is checked with respect to thresholds, after selecting only ocean measurements and removing sea ice data. Thresholds used are summarized in table 5, along with the average percentage of edited data for each parameter/threshold pair over SARAL/AltiKa's lifetime and over the past year. Please note the evolution of the threshold used to stake out unvalid data with respect to square off-nadir angle parameter. The value of $\mathbf{0.09}\,deg^2$ represents indeed the square of half the altimeter antenna aperture ($Antenna aperture/2 = 0.6/2 = 0.3\ deg$). It corresponds to the upper limit of validity of the Brown analytical model used to estimate the altimeter waveform derived parameters. The value of $0.0625\ deg^2 = (0.25deg)^2$ was too conservative given the attitude deviations experienced since 2019. To have an homogeneous follow up, the editing process was run over the whole time serie using the new threshold.

On the other hand, no measurements are edited by the following corrections:

- dry troposphere correction,
- dynamical atmospheric correction,
- equilibrium tide,
- earth tide,
- and pole tide.

Indeed these parameters are all derived from models, and are only checked in order to detect default values, which would point to a processing anomaly.

For each parameter and threshold, the percentage of edited data are monitored on a cycle per cycle, day per day and pass per pass basis by Cal/Val routines. Figure 9 presents the monitoring of the percentage of data points rejected by all thresholds combined. Considering all parameters and thresholds, the mean percentage of edited measurements is **5.72%**. The editing rate is steady over time (up to February 2019) but shows a large seasonal signal due to annual growth and retreat of sea ice extent. This annual signal highlights the ice flag's limitations and shows that it is no fully accurate especially in the Southern Ocean (map of figure 9). As demonstrated in figure 10, there is no more annual variations when selecting only low latitudes data. The rise of this parameter around October 2014, and since February 2019 is a result of several mispointing events that occured respectively before the SHM and after the SSA (as shown on figure 9 with track like patterns). Note that one measurement can be edited by several different thresholds, so the sum of individual criterion percentages does not equal the all thresholds combined percentage.

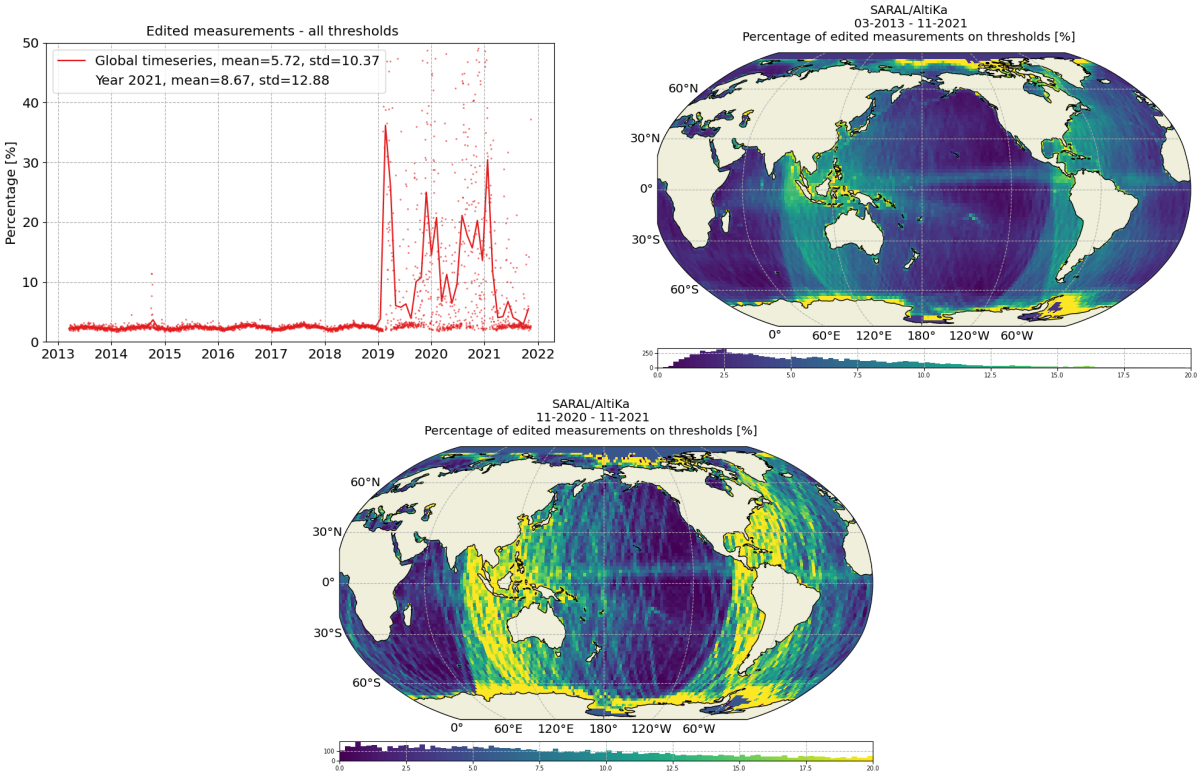

Figure 9: *Percentage of edited measurements on all thresholds combined. [left] monitoring for GDR data, [right] map since the beginning of mission (cycles 1 to 155) and [bottom] map over the past year (2021). Dots are daily averages while solid lines correspond to cycle averages.*

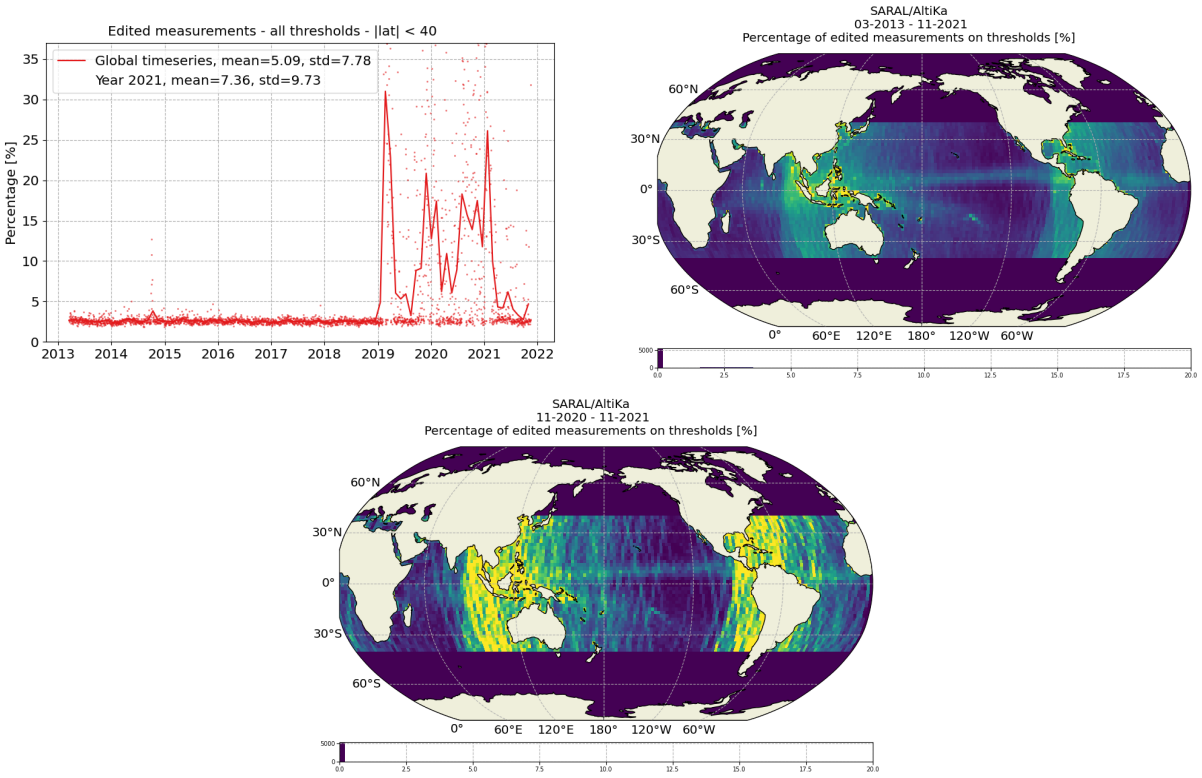

Figure 10: *Percentage of edited measurements on all thresholds combined, for |latitudes| < 40°. [left] monitoring for GDR data, [right] map since the beginning of mission (cycles 1 to 155) and [bottom] map over the past year (2021). Dots are daily averages while solid lines correspond to cycle averages.*

3.2.4. Number of 40-Hz measurements

The percentage of edited measurements because of a too low number of 40-Hz measurements is represented on the left side of figure 11. On SARAL/AltiKa all the 1 Hz measurements resulting from the compression of less than 20 high rate waveforms are discarded from further analysis. The map of measurements edited by 40-Hz measurements number criterion is plotted on the right panel of figure 11 and shows a correlation with wet and heavy rain areas (in general regions with disturbed sea state), as well as regions close to sea ice (actual limitation of the ice flag accuracy). Indeed waveforms are distorted by rain cells or sigma bloom events, which makes them often meaningless for SSH calculation. As a consequence, edited measurements due to several altimetric criteria are often correlated with wet areas (rain cells/sigma bloom events). Coastal regions are also impacted due to land contamination within the altimeter footprint. Also note the peaks observed since February 2019 that are linked to the attitude deviation impact on the tracking performances.

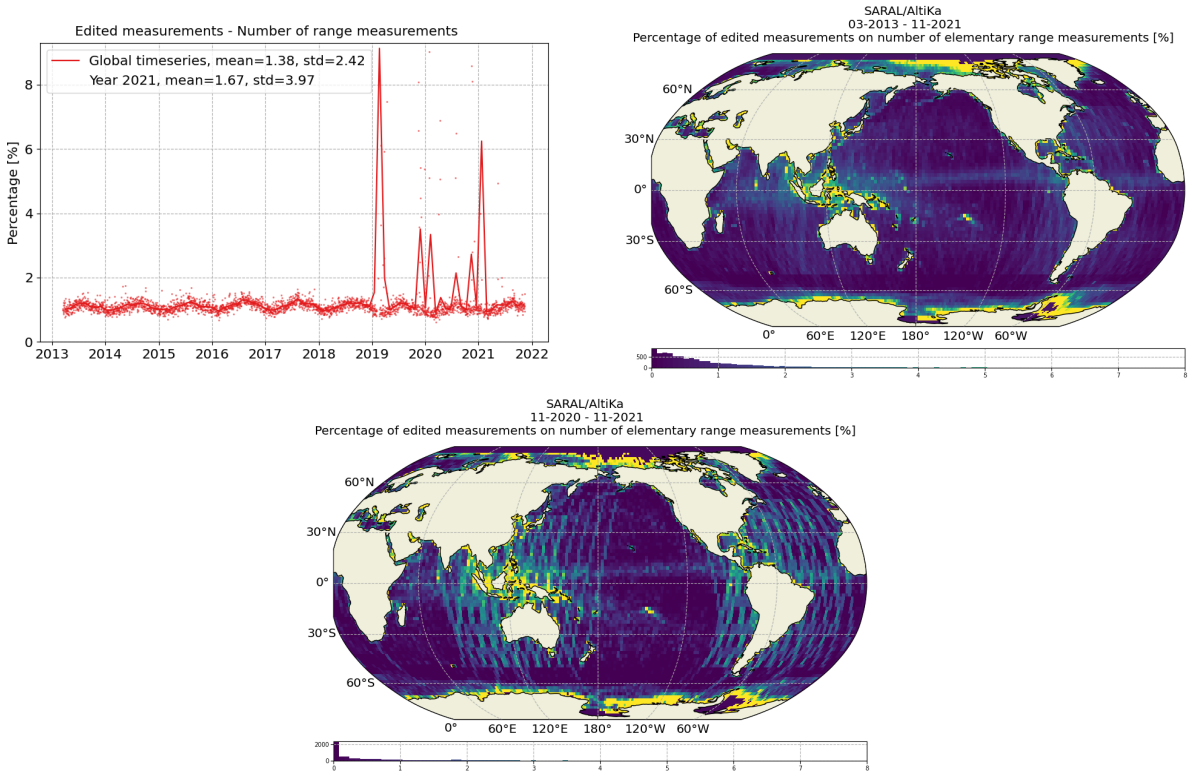

Figure 11: *Percentage of edited measurements on the number of 40-Hz measurements criterion. [left] monitoring for GDR data, [right] map since the beginning of mission (cycles 1 to 155) and [bottom] map over the past year (2021). Dots are daily averages while solid lines correspond to cycle averages.*

3.2.5. Standard deviation of 40-Hz range measurements

The percentage of edited measurements due to a high standard deviation (of the 40-Hz measurements) of the range is shown in figure 12. On average, **3.87 %** of the measurements are edited on this criterion.

Several days show a slight increase in the percentage of data edited by this criterion. These are mostly related to mispointing episodes before the SHM (October 2014),around maneuver burns, and after SSA (February 2019). In both cases, the data is edited (in general several parameters are out of thresholds) as a consequence of the lower platform pointing accuracy. Since cycle 24, platform pointing during maneuvers is achieved by the thrusters instead of the reaction wheels. The impact of this change on the number of edited GDR data is small.

The right panel of figure 12 shows a map of the percentage of measurements edited by the 40-Hz measurements standard deviation criterion. As in section 3.2.4., edited measurements are correlated with wet and costal areas, but also to mispointing episodes since SSA (track-like patterns).

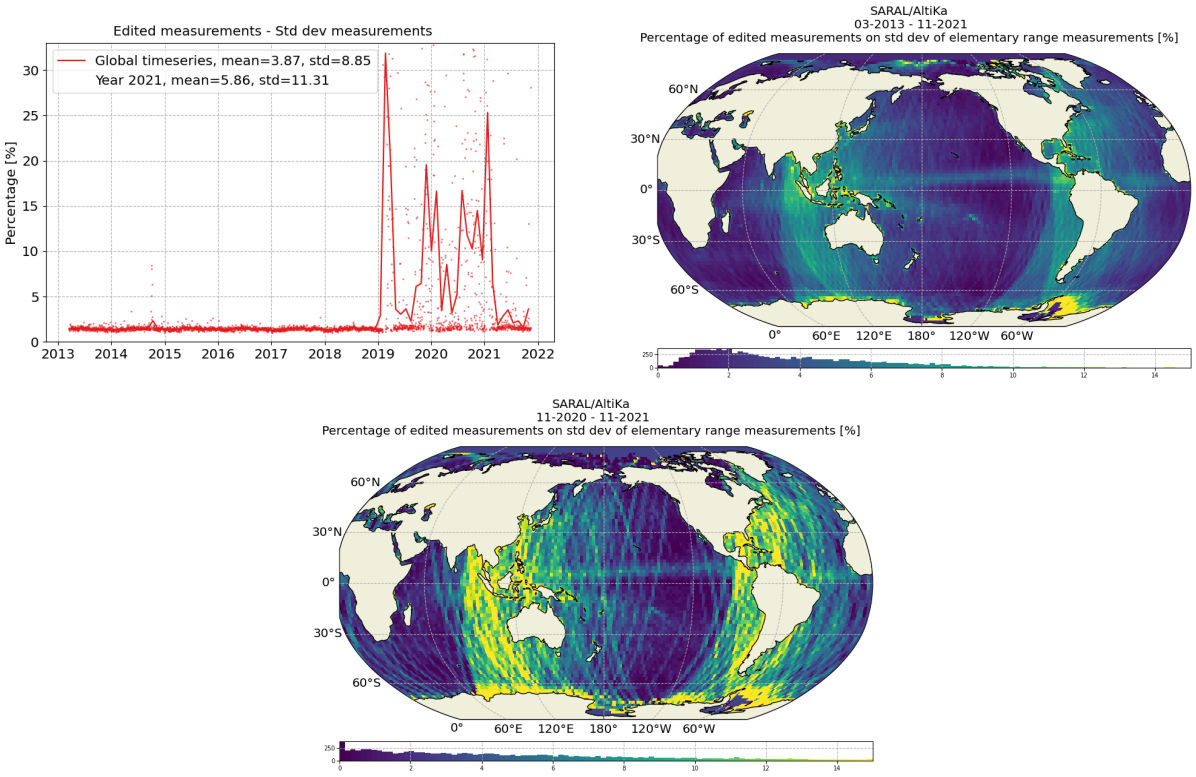

Figure 12: *Percentage of measurements edited due to high standard deviation of 40-Hz range measurements . [left] monitoring for GDR data, [right] map since beginning of mission (cycles 1 to 155) and [bottom] map over the past year (2021). Dots are daily averages while solid lines correspond to cycle averages.*

3.2.6. Significant wave height

The percentage of edited measurements due to significant wave height out of thresholds is represented on figure 13. On average, **2.23%** of the measurements are edited on this criterion.

As for the 40 Hz range standard deviation, several days show an increased number of edited data mostly due to mispointing events and maneuver burns, leading to a lower tracking performance and an out of threshold SWH estimate. Except from along track bands related to the late mispoiting events, figure 13 (right panel) shows that measurements edited by the SWH criterion are especially found in wet regions where heavy rains and sigma bloom events can occur, as well as in high sea state regions and costal areas.

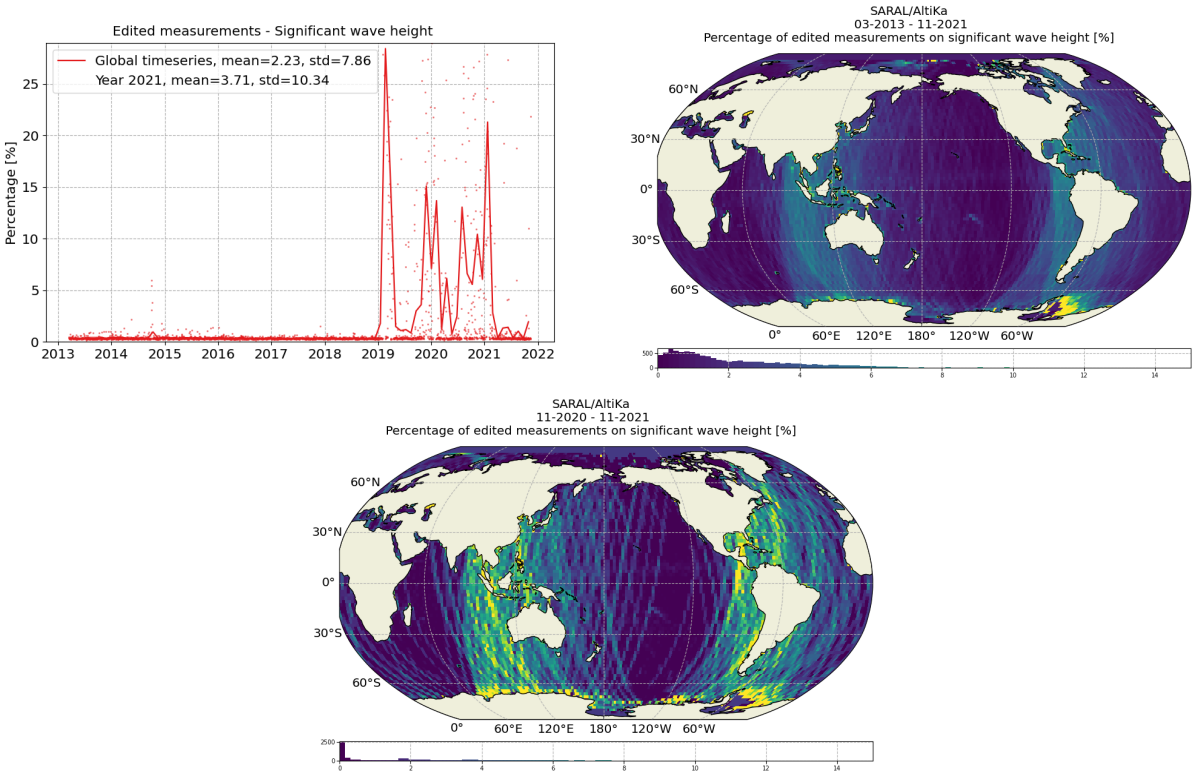

Figure 13: *Percentage of edited measurements by SWH criterion. [left] monitoring for GDR data, [right] map since the beginning of mission (cycles 1 to 155) and [bottom] map over the past year (2021). Dots are daily averages while solid lines correspond to cycle averages.*

3.2.7. Backscatter coefficient

The percentage of edited measurements due to backscatter coefficient out of thresholds is represented on figure 14. On average, **0.40%** of the measurements are edited on this criterion.

High editing rates (see right panel of figure 14) are generally found at the coast, and in rain areas. Nevertheless this quantity is affected by mispointing events to a lesser extent compared to the other waveform related parameters. This weaker sensitivity to platform pointing can be explained by the fact that the backscatter coefficient is more related to the power of the received signal than to its geometry.

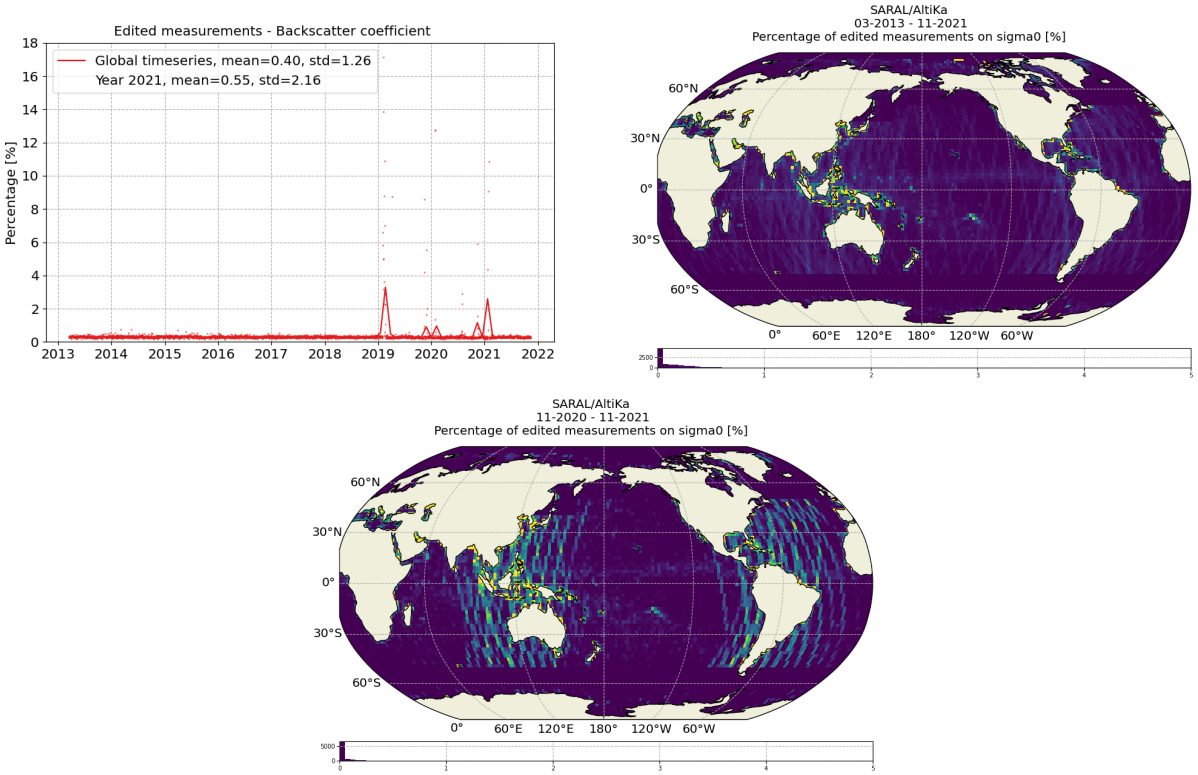

Figure 14: *Percentage of edited measurements by Sigma0 criterion. [left] monitoring for GDR data, [right] map since the beginning of mission (cycles 1 to 155) and [bottom] map over the past year (2021). Dots are daily averages while solid lines correspond to cycle averages.*

3.2.8. Number of backscatter coefficient measurements

The percentage of edited measurements due to too few 40 Hz measurements for each 1 Hz measuremet is represented on figure 15. On average, **1.29%** of the measurements are edited on this criterion. High editing rates (see right panel of figure 15) are generally found at the coast, and in rain areas. This quantity is also affected by mispointing events which lead to higher editing rates. The number of elementary measurements of backscatter is occasionally related to the number of elementary range measurements, and metrics are very similar.

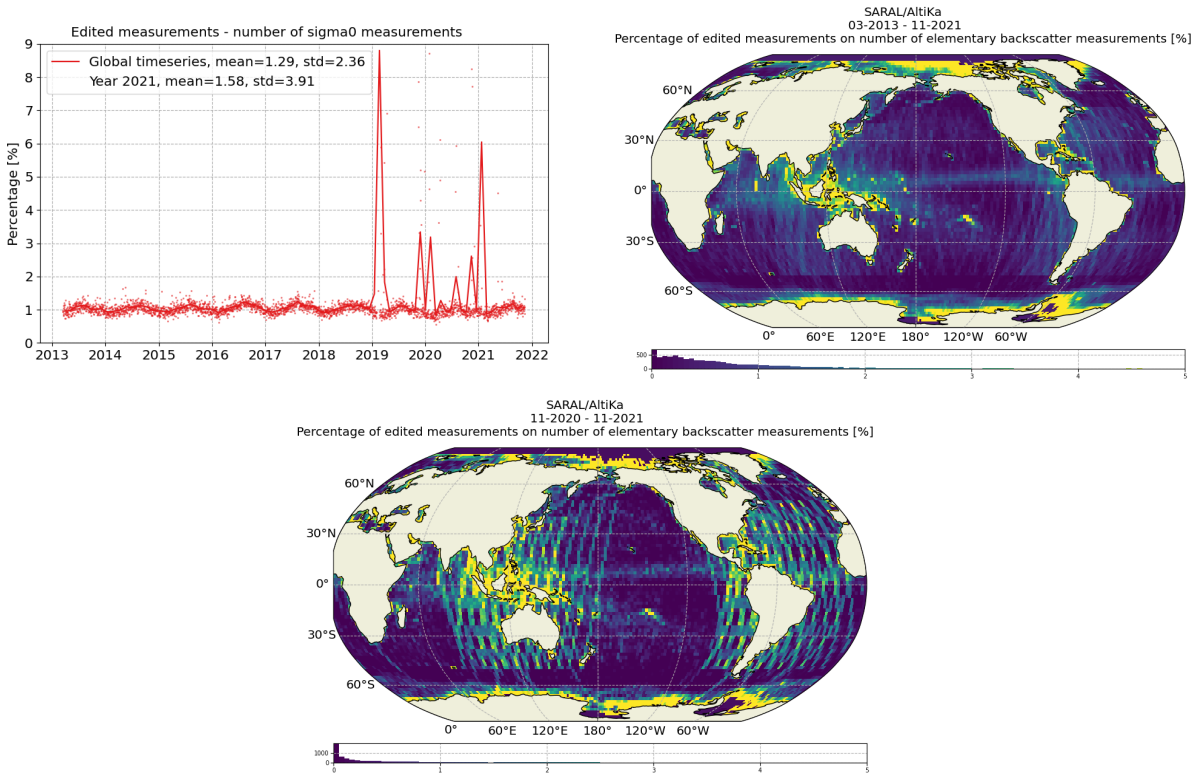

Figure 15: *Percentage of edited measurements by number of high rate backscatter coefficient measurements. [left] monitoring for GDR data, [right] map since the beginning of mission (cycles 1 to 155) and [bottom] map over the past year (2021). Dots are daily averages while solid lines correspond to cycle averages.*

3.2.9. Standard deviation of backscatter coefficient

The percentage of edited measurements on the 40 Hz backscatter coefficient standard deviation criterion is represented on figure 16. On average, **1.07%** of the measurements are edited on this criterion.

The right panel of figure 16 shows that measurements edited on 40 Hz backscatter coefficient standard deviation criterion are found in coastal areas, and in regions affected by rain events, which can be either related to the contribution of the Ka backscatter attenuation that depends on atmospheric water content, or related to the high variability of the backscatter coefficient in theses regions. The spatial distributions of edited measurements due to high standard deviation of backscatter and of range measurements are quite similar, except the impact of mispointing events that is smaller in this case (see 3.2.7.).

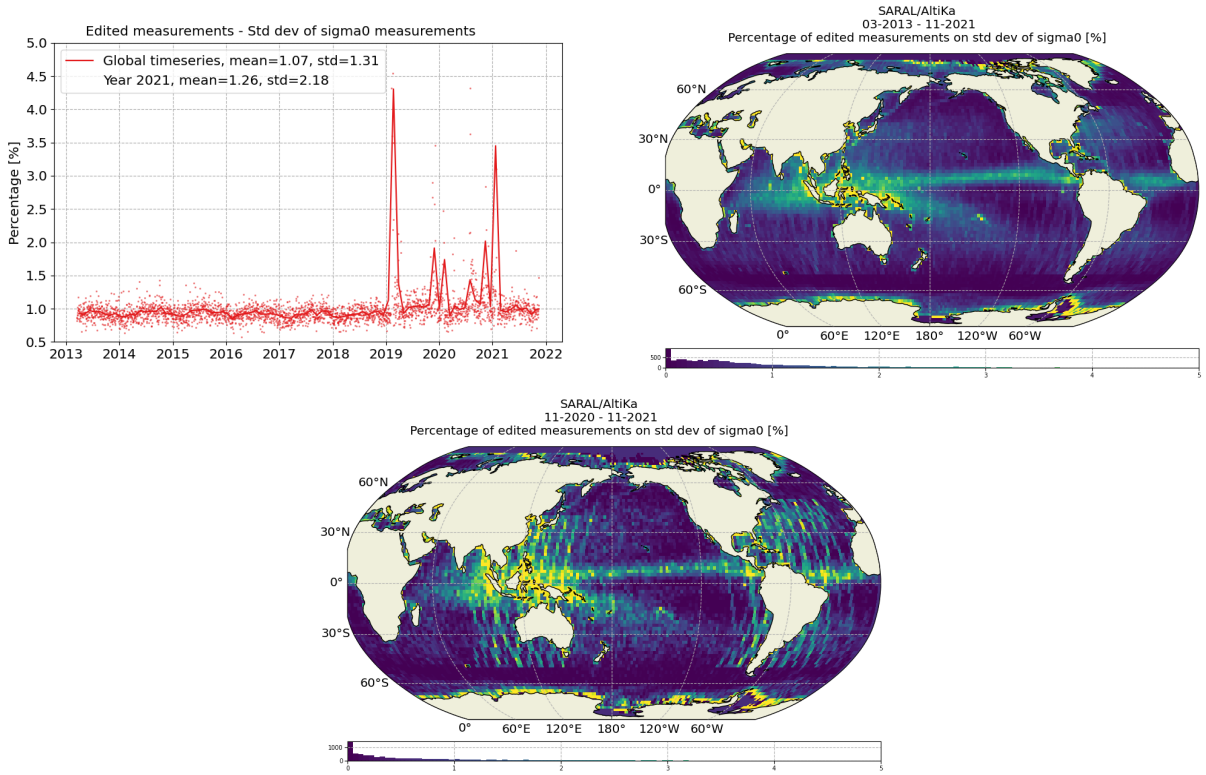

Figure 16: *Percentage of edited measurements by 40 Hz Sigma0 standard deviation criterion. [left] monitoring for GDR data, [right] map since the beginning of mission (cycles 1 to 155) and [bottom] map over the past year (2021). Dots are daily averages while solid lines correspond to cycle averages.*

3.2.10. Radiometer wet troposphere correction

The percentage of edited measurements due to radiometer wet troposphere correction criterion is represented in figure 17. On average, **0.98%** of the measurements are edited on this criterion. The edited data for Saral/AltiKa are generally due to wet troposphere path delay values that are larger than the tolerated **-0.5 m** threshold. The GDR-F (Patch 4) retrieval algorithm is sensitive to low sigma 0 / high mispointing values. Wet troposphere is not defined when sigma 0 is at default value (in costal areas). Large editing percentages are mainly observed in coastal regions suggesting that land effects on radiometer measurements and impacts the quality of the wet troposphere path delay retrievals. Other editing events happen in known wet areas in the inter tropical band where the retrieval algorithm may be less efficient in some cases of high rain rates or unusal sea states (sigma blooms).

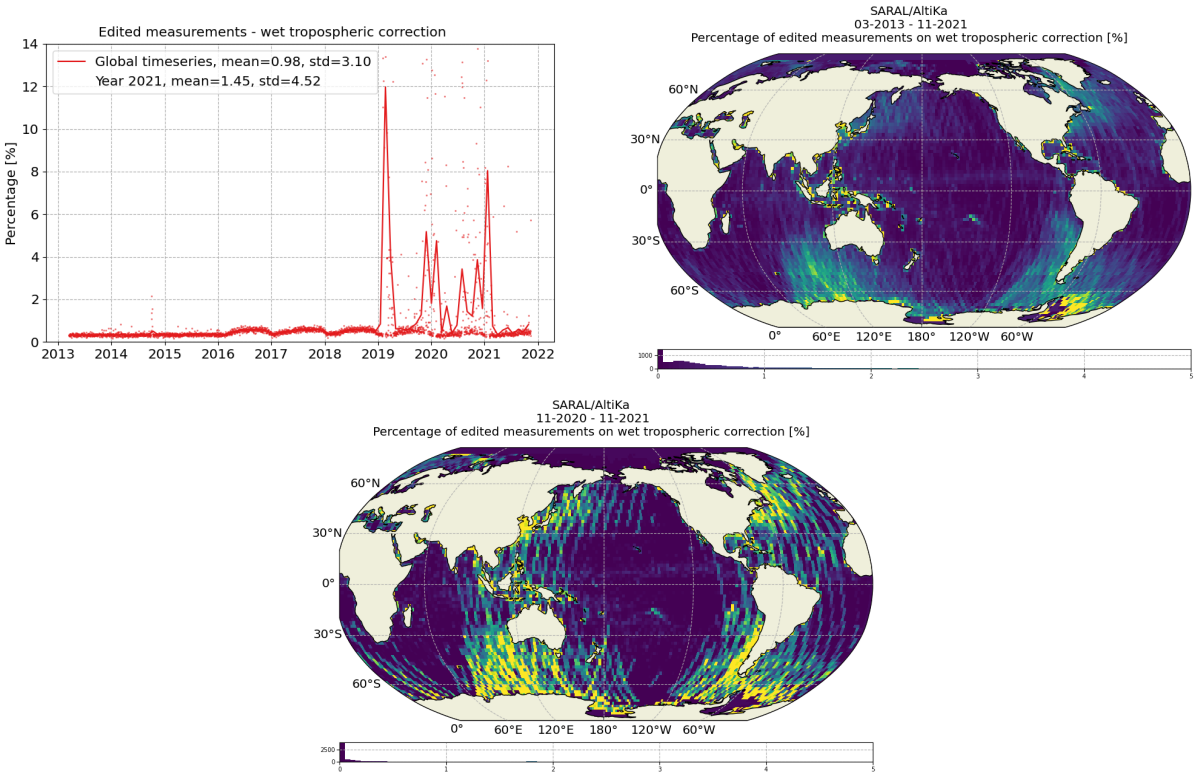

Figure 17: *Percentage of edited measurements due to radiometer wet tropospheric correction out of thresholds. [left] monitoring for GDR data, [right] map since the beginning of mission (cycles 1 to 155) and [bottom] map over the past year (2021). Dots are daily averages while solid lines correspond to cycle averages.*

3.2.11. Square off-nadir angle

The percentage of edited measurements due to square off-nadir angle criterion is represented in figure 18. On average, **3.60%** of all measurements are edited due to high mispointing values.

Maneuvers have a strong impact on mispointing values because the platform has to rotate from nadir to geodetic pointing before thrusters activity. As a result, nearly all maneuvers are edited due to high mispointing values. After the SHM, systematic mispointing was observed at zero-crossings of reaction wheel (RW) speed, resulting in a slightly higher percentage of edited points. This was corrected and the percentage of measurements edited due to high mispointing values came back to normal values. As for the peaks observed since February 2019, they are mainly related to attitude deviations experienced by the spacecraft since the SSA (see section 2.2.2.).

The spatial distribution of the percentage of edited values (right panel of figure 18) shows different patterns. There are several features visible in this map, such as:

- editing due to maneuvers in the Indian Ocean,
- a patch in the North Atlantic Ocean, resulting from zero crossings of RW speed over the regions between Greenland and Svalbard,
- several track-like patterns due to attitude deviations resulting from the SSA.
- a pattern similar to the one observed for several other parameters: coastal areas and wet areas, as off-nadir angle estimation is based on the waveform trailing edge slope which is highly impacted by rain cells and surface roughness.

Since the SHM, mispointing is a carefully monitored parameter. More information on mispointing events can be found in section 4.3. of this report .

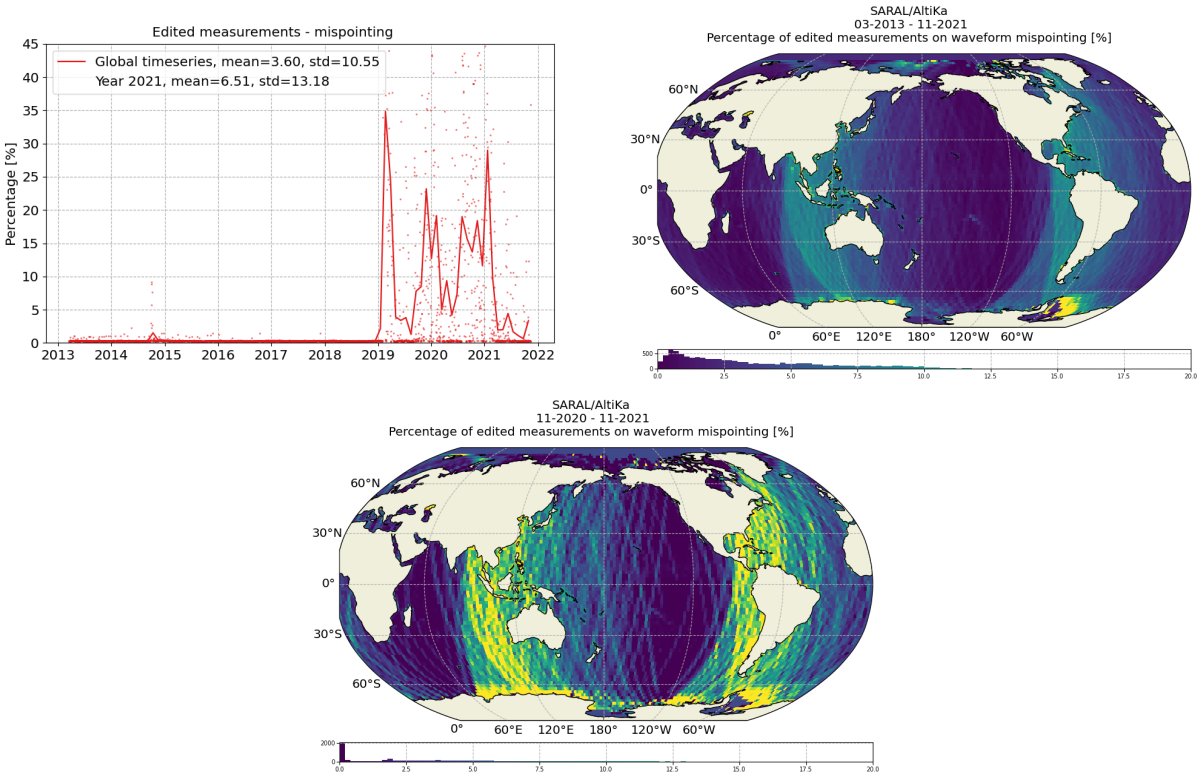

Figure 18: *Percentage of edited measurements by square off-nadir angle criterion. [left] monitoring for GDR data, [right] map since the beginning of the mission (cycles 1 to 155) and [bottom] map over the past year (2021). Dots are daily averages while solid lines correspond to cycle averages.*

3.2.12. Sea state bias correction

The percentage of edited measurements due to sea state bias correction criterion is represented in figure 19. On average, **0.39%** of measurements are edited due to sea state bias values out of thresholds. The percentage of edited measurements is stable over time, although some days have higher values. It is mainly due to mispointing events or platform manoeuvres. The spatial distribution is consistent with what is observed regarding editing on SWH / Wind values, and areas with low sea states may be edited due to erroneous sea state bias estimation (default values). This does not happen for high sea states (high northern and southern latitudes) where no measurements are edited on the sea state bias threshold criterion.

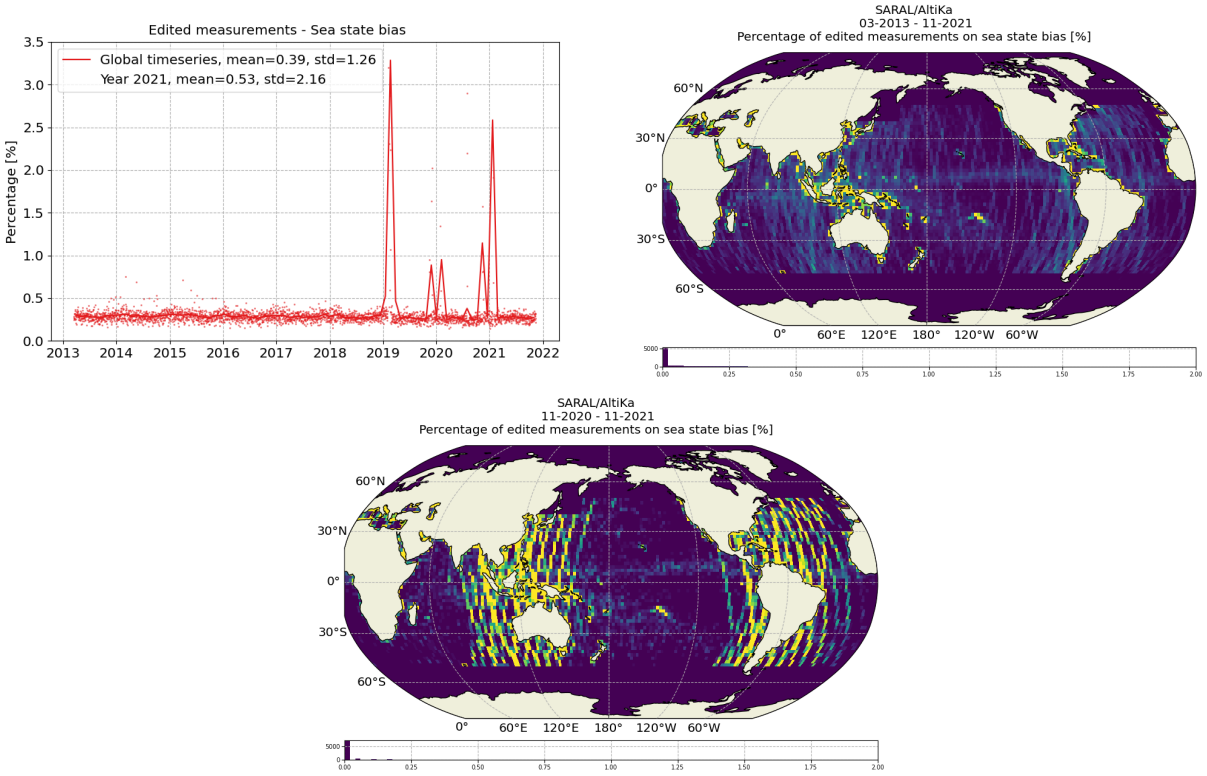

Figure 19: *Percentage of edited measurements by sea state bias criterion. [left] monitoring for GDR data, [right] map since the beginning of the mission (cycles 1 to 155) and [bottom] map over the past year (2021). Dots are daily averages while solid lines correspond to cycle averages.*

3.2.13. Altimeter wind speed

The percentage of edited measurements due to altimeter wind speed criterion is represented in figure 20. On average **0.39%** of measurements are edited. This map exhibits the same patterns as the one related to the backscatter coefficient (which is used to derive the wind speed).

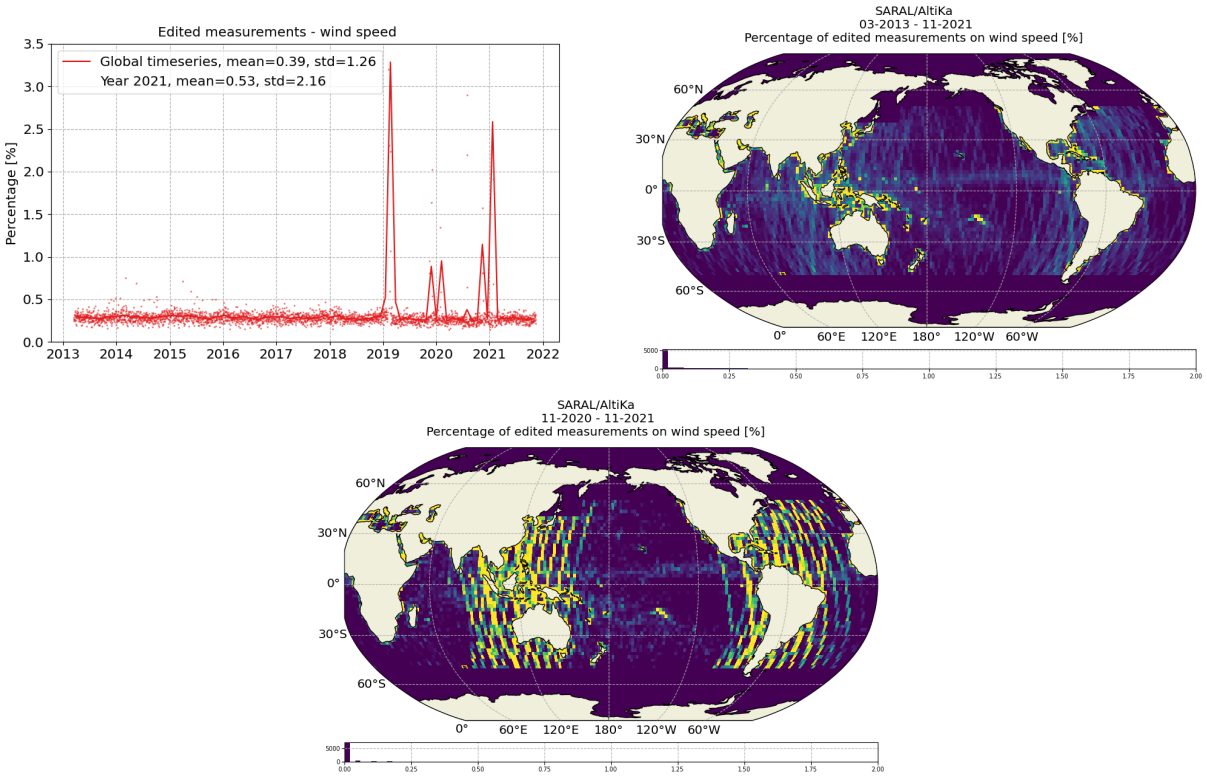

Figure 20: *Percentage of edited measurements by wind speed criterion. [left] monitoring for GDR data, [right] map since the beginning of the mission (cycles 1 to 155) and [bottom] map over the past year (2021). Dots are daily averages while solid lines correspond to cycle averages.*

3.2.14. Ocean, pole and earth tide corrections

No measurements are edited due to the pole tide or the solid earth tide components whereas very few measurements with no (default values) ocean tide values (FES14B) are edited. The percentage of edited measurements due to the threshold on the latter is represented in figure 21. Less than **0.01%** of the measurements are edited due to the ocean tide correction. FES14 tide atlas includes closed seas so the ocean tide is now (GDR-F) defined over the Caspian Sea.

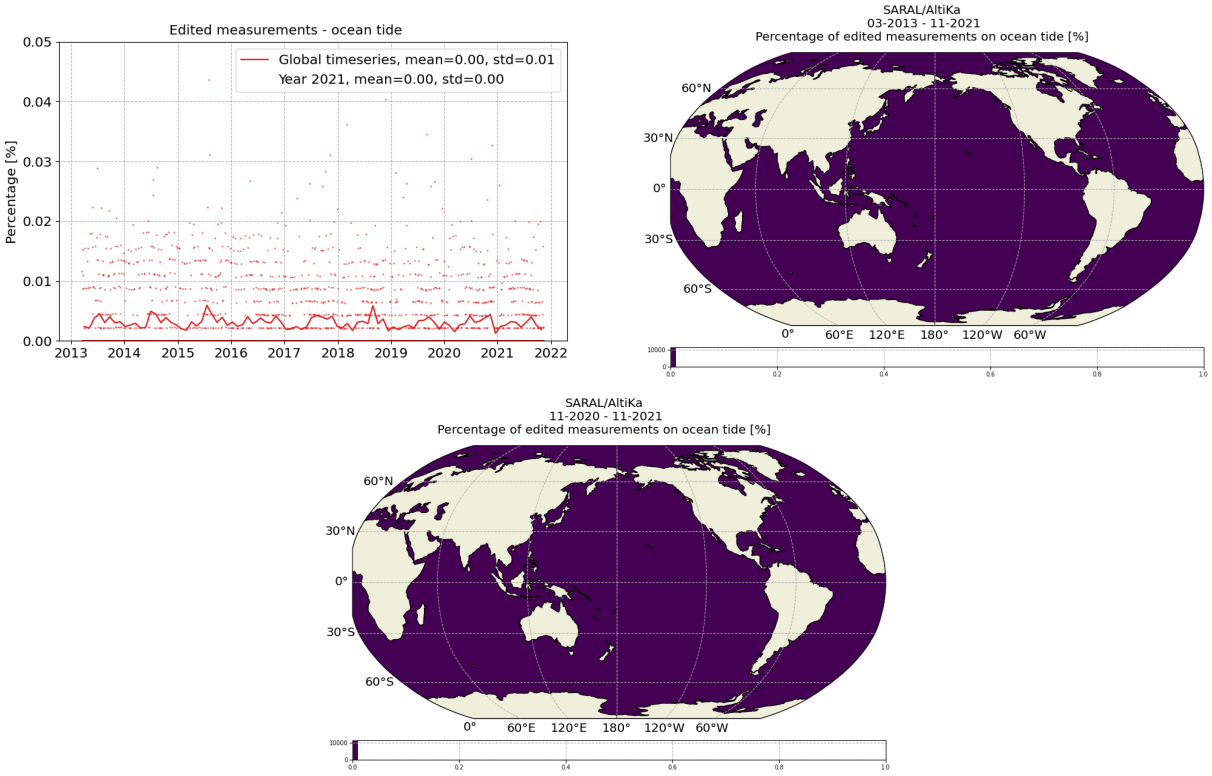

Figure 21: *Percentage of edited measurements by ocean tide criterion. [top] monitoring for GDR data, [right] map since the beginning of the mission (cycles 1 to 155) and [bottom] map over the past year (2021). Dots are daily averages while solid lines correspond to cycle averages.*

3.2.15. Sea surface height

The percentage of edited measurements due to sea surface height (orbit minus range, no corrections applied) criterion is represented in figure 22. On average, **0.64%** of measurements are edited on this criterion. The measurements edited by sea surface height criterion are mostly found near coasts in equatorial and mid-latitude regions, as well as for regions with low significant wave heights (see map 22). As for the track-like patterns, they are the result of the attitude deviation over range computation.

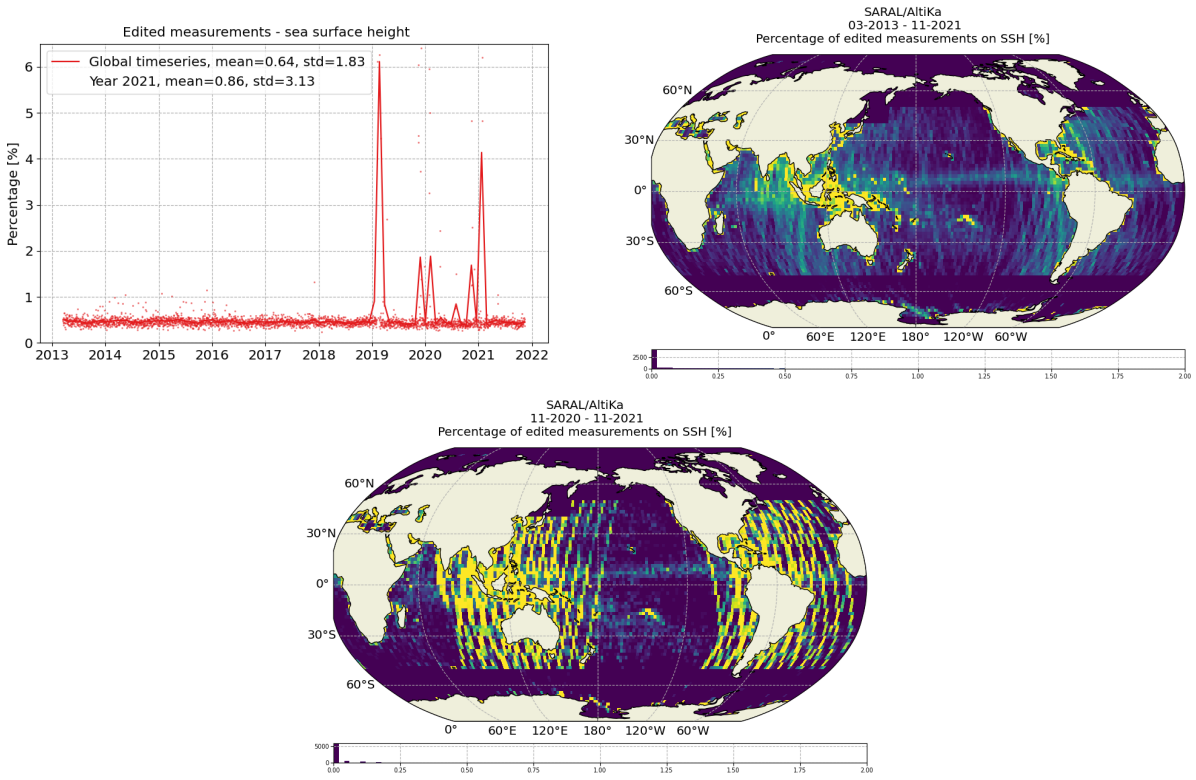

Figure 22: *Percentage of edited measurements by sea surface height criterion. [left] monitoring for GDR data, [right] map since the beginning of the mission (cycles 1 to 155) and [bottom] map over the past year (2021). Dots are daily averages while solid lines correspond to cycle averages.*

3.2.16. Sea level anomaly

The percentage of edited measurements due to the sea level anomaly out of thresholds is represented in figure 23. This percentage is estimated after removing ice flagged data. On average, **1.30%** of data are edited by this criterion. There is a slight increase of this percentage since March 2015 approximately when the ground track was loosely maintained, resulting in higher MSS errors. Also, we can observe an annual signal since March 2016 (left plot of figure 23) linked to the lower percentage of edited measurements by the ice flag (see figure 6) and proving its limitations. As for the peaks observed since February 2019, they are related to the attitude deviation's impact on most involved parameter in SLA computation.

On the other hand, the map is estimated after applying all the previous editing steps, and shows very few measurements edited, mainly located at the coast and around Antartica. This result highlights the efficiency of the previously detailed editing steps in removing erroneous SLA measurements.

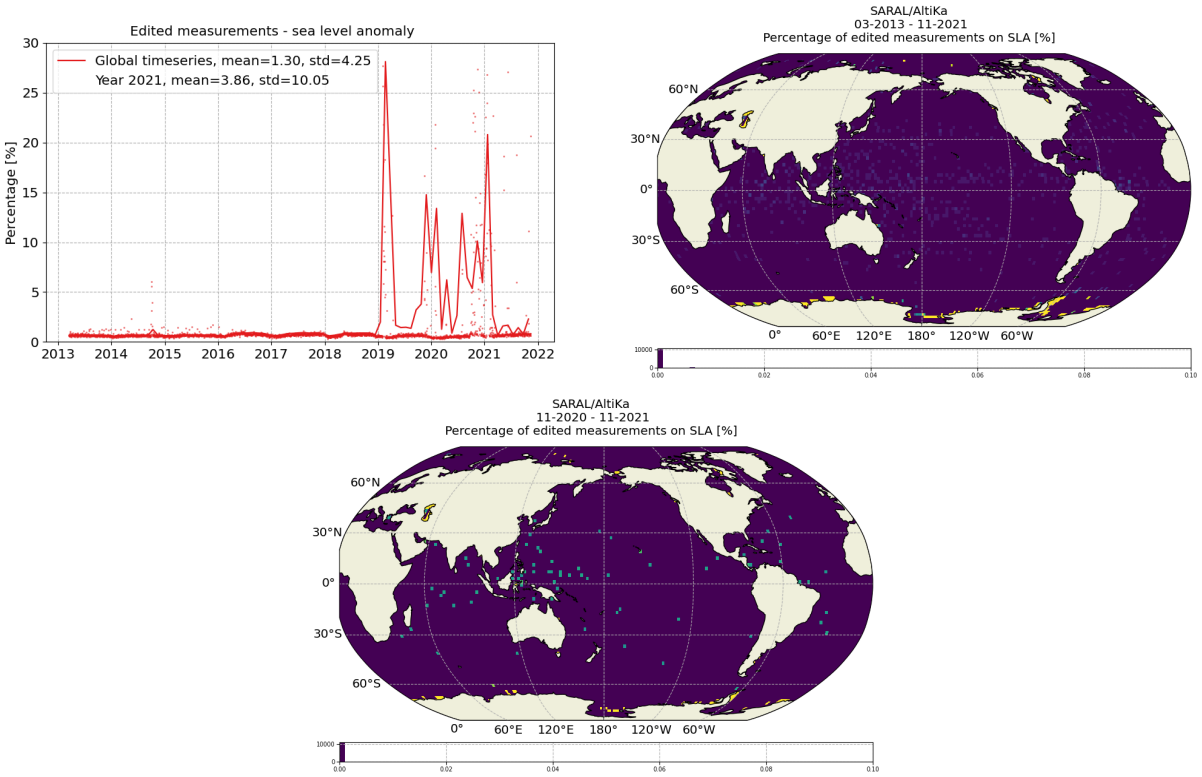

Figure 23: *Percentage of edited measurements by sea level anomaly criterion. [left] monitoring for GDR data, [right] map since the beginning of the mission (cycles 1 to 155) and [bottom] map over the past year (2021). Dots are daily averages while solid lines correspond to cycle averages.*

3.2.17. SLA consistency checks

The last step of the editing procedure is to check for along-track SLA consistency. Two different checks are performed:

- fitting a spline function to SLA values (after all previously mentionned editing criteria have been applied),
- checking that pass mean and standard deviation do not exceed certain thresholds.

Figure 24 shows the monitoring of the percentage of edited points by these two criteria. Very few points are edited by these two editing steps, **0.04%** for splines, and **0.01%** for pass statistics. In the latter case, the whole pass is edited, leaving a large gap in the data. This happened a few times, generally when crossing very large eddies in the Southern Ocean, or in the case of high editing rates in the previous steps leaving only short portions of tracks at this stage (that do not fit the thresholds based on whole tracks statistics).

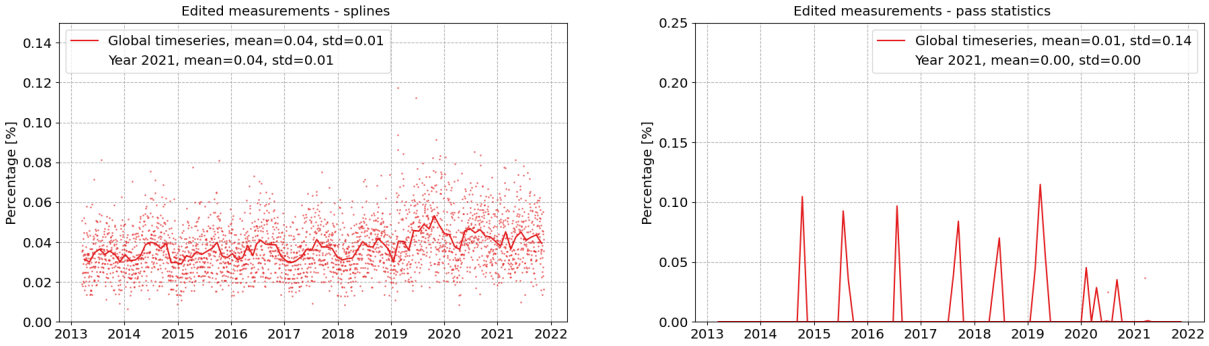

Figure 24: *Monitoring of the percentage of edited measurements by [top] spline criterion and [botom] pass statistics. Dots are daily averages while solid lines correspond to cycle averages.*

4. Monitoring of altimeter and radiometer parameters

4.1. Methodology

Statistics for the main parameters of SARAL/AltiKa have been routinely monitored since the beginning of the mission. Systematic monitoring aims at detecting changes in parameter statistics, that would indicate a problem on the mission. Comparisons with model outputs or other missions (mainly Jason-2 and Jason-3) are also performed as part of the systematic Cal/Val activities.

For SARAL/AltiKa, pass by pass, daily and cyclic statistics are computed after applying the editing process so that the statistics are not skewed by erroneous data. In this section, we mainly present results from daily and cyclic average estimates. The measurements distribution is not homogeneous within latitudes, and can skew the statistics to values of the data in high latitudes. This can be important when comparing to other missions, like Jason-2 and Jason-3 that do not reach the same latitudes as SARAL/AltiKa.

To overcome this issue when needed, we estimate box averages (generally on a 2 degree cartesian grid) before estimating global averages. For quite a few parameters, more precise comparisons are performed by estimating short time differences at crossovers.

Note that for the same reasons as mentionned in the previous section (several SHM periods for Jason-2 in 2017), monitorings of the different parameters will include Jason-2 and Jason-3 to cover up for Jason-2's gaps and have a continuous comparisons over SARAL/AltiKa's lifetime. Also, in order to have a consistent geographical comparison, all the maps of this section are based on GDR data over the lifetime of Jason-3, and averages are estimated over the whole oceanic domain.

4.2. 40 Hz Measurements

Number and standard deviation of 40 Hz elementary range measurements used to derive 1 Hz data are two parameters computed during the altimeter ground processing. For SARAL/AltiKa Jason-2 and Jason-3 a MQE (mean quadratic error) criterion is used to select valid 40/20 Hz measurements before performing a regression to derive the 1 Hz range from high rate (40 Hz or 20 Hz) data.

The MQE criterion checks that the high rate waveforms can be approximated by a Brown echo model (Brown, 1977 [1], Thibaut et al. 2002 [4]). Then elementary ranges too far from the regression line are discarded, through an iterative regression process, until convergence is reached. Thus, monitoring the number of 40/20 Hz range measurements and the standard deviation computed among them is likely to reveal changes at instrumental level.

4.2.1. Number of 40 Hz measurements

The mean number of elementary 40 Hz range measurements for SARAL/AltiKa is close to **38.5**

(see figure 25, where Jason-2 and Jason-3 values were doubled). Before the correction of the PF/RF alignment (alignment between the platform and the radiofrequency axis) on 25th of April 2013 this value was slightly higher (around **38.6**). Jason-2 and Jason-3 have an average number of elementary 20 Hz range measurements of **19.6**, which represents a higher number than SARAL/AltiKa. Jason-2 and Jason-3 also show a smaller day to day variability than SARAL/AltiKa.

On average **1.5%** of the 40 Hz elementary range measurements are removed during the 40 Hz to 1 Hz compression by the MQE criteria. Note that before Patch1 version (not the case here since GDR were reprocessed in GDR-F), the MQE threshold was not applied during the 40 Hz to 1 Hz compression (IGDR data till cycle 4, pass 394), leading to a higher mean of the number elementary 40 Hz range measurements (**39.0**).
Anyway, the discarded data might be due to perturbations in the footprint (rain events, sigma blooms). For these three missions, the number of elementary range measurements is correlated with the significant wave height (and, for SARAL/AltiKa, with sea ice extent). Figure 26 shows less elementary range measurements around rain areas, and also Indonesia, the Mediterranean Sea and costal areas, which are all regions of low significant wave heights (see also map of SWH 38) and therefore regions where sigma bloom may occur. High latitudes also show a lower number of range elementary measurements, due to the presence of sea-ice (that is not well-detected by the ice flag during the editing process). Also, as shown in figure 25, the number of 40 Hz elementary range measurement used to derive 1 Hz data is slightly larger since Ferburary 2019 (reccurent mispointing events since SSA). It is probably linked to the higher percentage of rejected measurement (figure 11), since a larger number of low values rejected during the editing process, skews the statistic closer to 40.

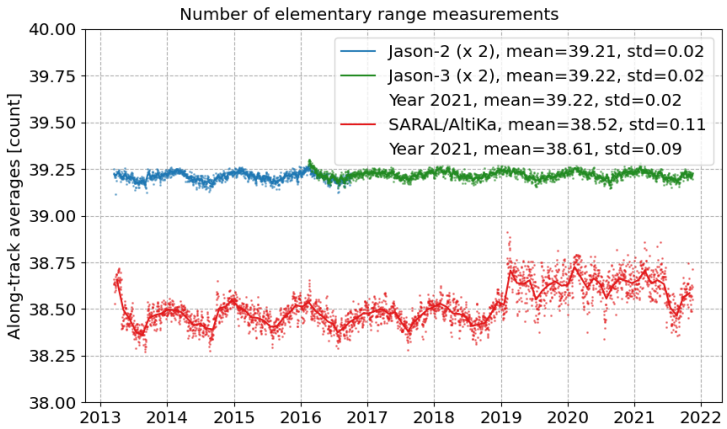

Figure 25: *Daily monitoring of mean of number of elementary measurements for SARAL/AltiKa (ref) , Jason-2 (blue) and Jason-3 (green). Dots represent daily averages, the lines correponds to cycle averages. Jason-2 and Jason-3 data are multiplied by two to account for the 40Hz/20Hz difference between the two missions.*

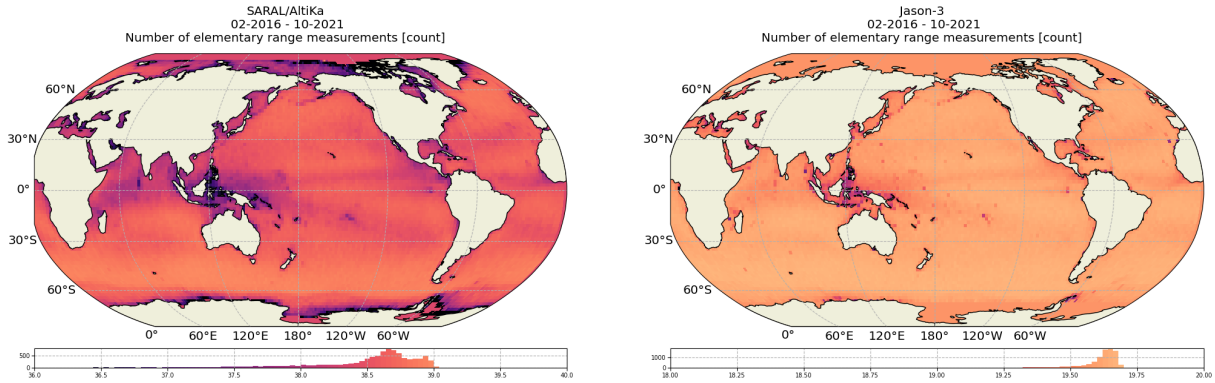

Figure 26: *Average map of number of SARAL/AltiKa elementary 40 Hz range measurements (left) and Jason-3 elementary 20 Hz range measurements (right).*

4.2.2. Standard deviation of 40 Hz measurements

Considering along-track data, SARAL/AltiKa's standard deviation of 40 Hz measurements is **5.8 cm**, compared to **8.0 cm** for Jason-2 and Jason-3 (right side of figure 27). When considering latitude weighted box statistics (left side of figure 27), these values decrease to respectively **5.6 cm** and **7.7 cm**.

A lower value for SARAL/AltiKa compared to Jason-2 and Jason-3 is expected due to different band-widths on the two missions: 480 MHz for SARAL/AltiKa instead of 320 MHz for Jason-2 and Jason-2 (see [45]). As for the number of elementary range measurements, the standard deviation of the elementary range measurements is correlated to significant wave height (see maps on figures 28 and 38), and is slightly impacted by the recent mispointing events (figure 27).

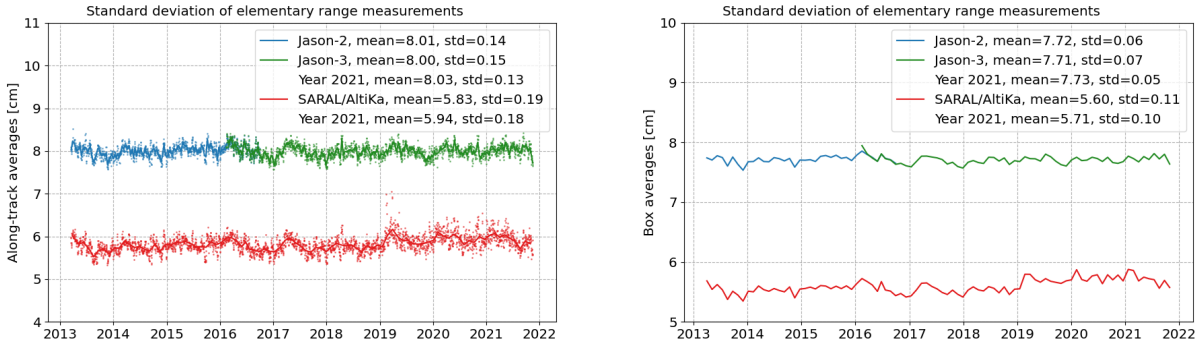

Figure 27: *Monitoring of rms of elementary 40/20 Hz range measurements for SARAL/AltiKa , Jason-2 and Jason-3, either computing latitude weighted box statistics (top) or along track averages (botom). Dots are daily averages while solid lines correspond to cycle averages.*

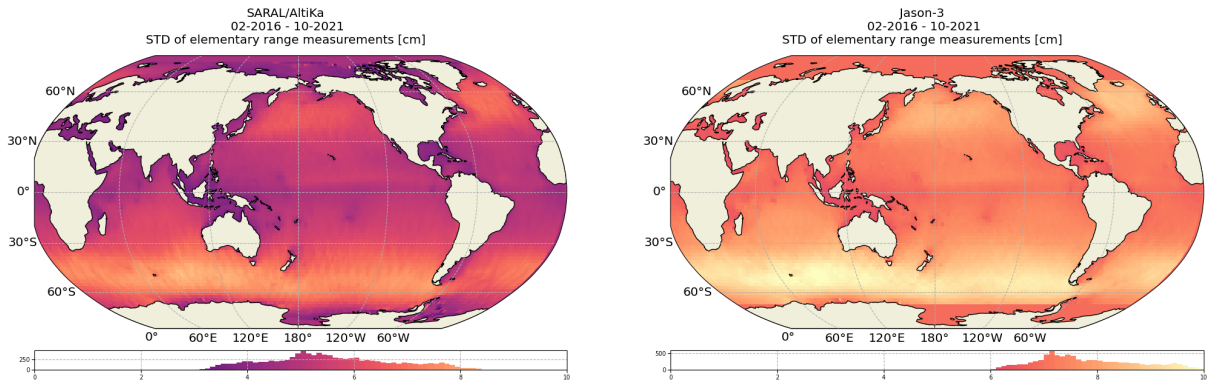

Figure 28: *Average map of rms of SARAL/AltiKa elementary 40 Hz range measurements (left) and Jason-3 elementary 20 Hz range measurement (right).*

4.3. Off-Nadir Angle from waveforms

The off-nadir angle is derived from the slope of the trailing edge of the waveform during the altimeter processing. It can either be the result of real platform mispointing or of backscattering properties of the surface. Figure 29 displays the evolution of the mean and standard deviation of this quantity over time for SARAL/AltiKa, Jason-2 and Jason-3. Jason-2 and Jason-3 show more variations of the off-nadir angle from waveforms due to its larger antenna aperture. Note that these metrics are estimated on valid measurements only. Jason-2 and Jason-3 have an antenna beamwidth of **1.29**°, whereas SARAL/AltiKa has only **0.6**°. In addition Jason-2 and Jason-3's orbit is higher, resulting in a larger footprint radius (9.6 km) than SARAL/AltiKa (4 km). Therefore the probability of perturbations within the footprint - which modify the backscattering properties of the surface - is higher for Jason-2 and Jason-3 than for SARAL/AltiKa.

In the beginning of the SARAL/AltiKa mission the off-nadir angle from waveforms was slightly positive (around $\mathbf{0.003}deg^2$). Following an X-cross calibration maneuver ($\mathbf{+0.3}°/\mathbf{-0.3}°$ in pitch followed by $\mathbf{+0.3}°/\mathbf{-0.3}°$ in roll) done on April, 22$^{\text{nd}}$ 2013 (see N. Stenou [45]) a correction of **-0.045**° in pitch direction was applied from April 25$^{\text{th}}$ onwards. A second X-cross calibration on April 30$^{\text{th}}$, 2013 showed that the correction was successful. Off-nadir angle from waveforms stayed close to zero and very stable spatially and temporally up to February 2019 (SSA).

During summer 2014 a rise in reaction wheel friction due to movement of lubricant resulted in an increase of the variability of the off-nadir angle. This event ended with the loss of a wheel and an important increase of the daily mean of the off-nadir angle leading to a safe-hold mode between October 6$^{\text{th}}$ and 9$^{\text{th}}$, 2014. After the safe-hold mode, the spacecraft has been reconfigured to use only three wheels, resulting in a lower pointing accuracy at zero crossings of RW speed. A patch to the command law allowed to avoid these situations.

In February 2019, SARAL/AltiKa satellite encountered a Star Sensor Anomaly, affecting the nadir pointing accuracy. Since that day, the spacecraft attitude is maintained using waveform derived pointing information (square off nadir angle) to regularly correct the star trackers drift. Hence, most of SARAL/AltiKa's mispointing events remain within the altimeter pointing specifcations. Anyway, the main mispointing events are mentioned in cyclic Cal/Val reports. As for further details

about Jason-3's mispointing events feel free to check out the dedicated yearly report ([67]).

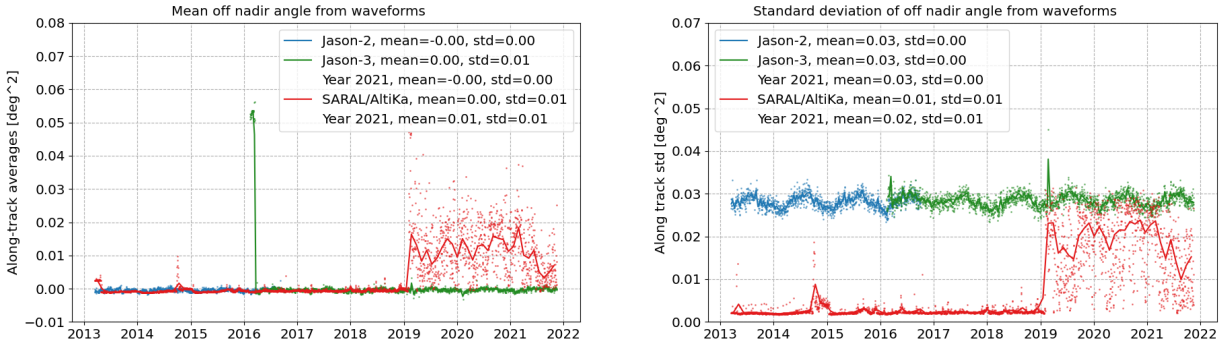

Figure 29: *Monitoring of mean (left) and standard deviation (right) of , Jason-2 and Jason-3 off-nadir angle from waveforms. Dots represent daily averages, the lines correponds to cycle averages.*

The map of SARAL/AltiKa off-nadir angle from waveforms (left of figure 30) is not homogeneous with track patterns mainly due to star sensors issues. The map of Jason-3 (right of figure 30) shows higher values of mispointing at high latitudes close to sea ice, around Indonesia, Equator and close to coasts, which is likely a result of both platform mispointing and surface heterogeneities. These patterns are hardly observable on SARAL/AltiKa's map since the global values of mispointing have significantly increased during the past years. These features were observable before the SSA when pointing was nominal (see SARAL/AltiKa's 2018 annual report here [57]).

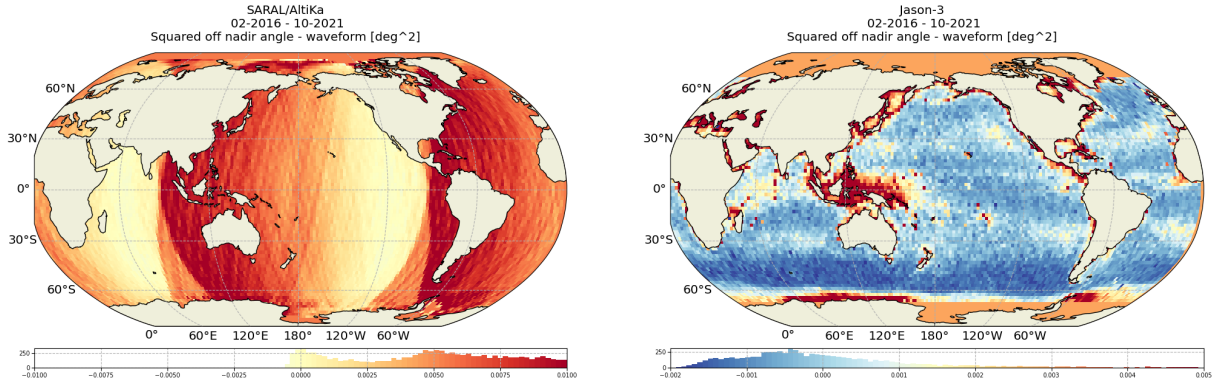

Figure 30: *Average map of off-nadir angle from waveforms for SARAL/AltiKa (left) and Jason-3 (right).*

Following the loss of the RW, ISRO has started sending platform pointing information derived from onboard star trackers. These data are now available in GDR-F products and are very usefull to perform comparisons between platform and waveform mispointing. Figure 31 compares waveform and plaftorm mispointing estimates. Over time, there is a good agreement between waveform and platform estimation. However, since the SSA, platform pointing derived from onboard star trackers is no longer relevant. The map of plaform mispointing is mush more homogeneous than the one derived from waveforms (30), as it is not impacted by neither pseudo mispointing due to heterogeneous surface properties in the radar footprint, nor SSA.

In order to get a better picture of SARAL/AltiKa mispointing events, we detect mispointed track sections. Track sections are defined as 15 consecutive measurements with mispointing values greater than **0.015** deg^2. Results of this detection algorithm are presented in figure 32. Before SSA, there

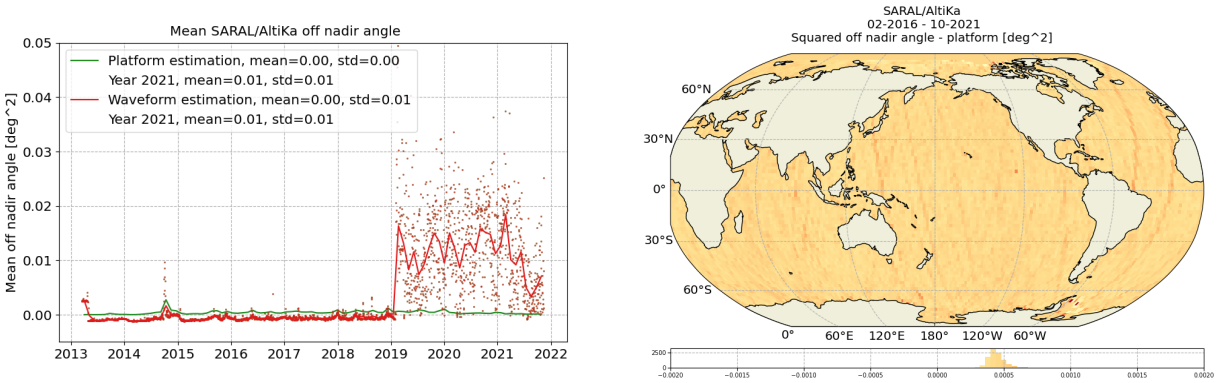

Figure 31: *Monitoring of off-nadir angle from waveform and platform for SARAL/AltiKa (left) and map of platform off-nadir angle (right). Dots are daily averages while solid lines correspond to cycle averages.*

was an excellent agreement between the number of mispointed sections detected from waveforms and platfom data, indicating that, when consecutive measurements are affected by mispointing, it is likely a real platform pointing issue. Before October 2014, small peaks are associated with maneuvers. From October 2015 to February 2015, mispointed sections are associated with zero crossings of the RW speed. The command law was changed to avoid zero crossings and mispointing events occur randomly since then. From February 2019, only waveform derived mispointing shows higher values as expected.

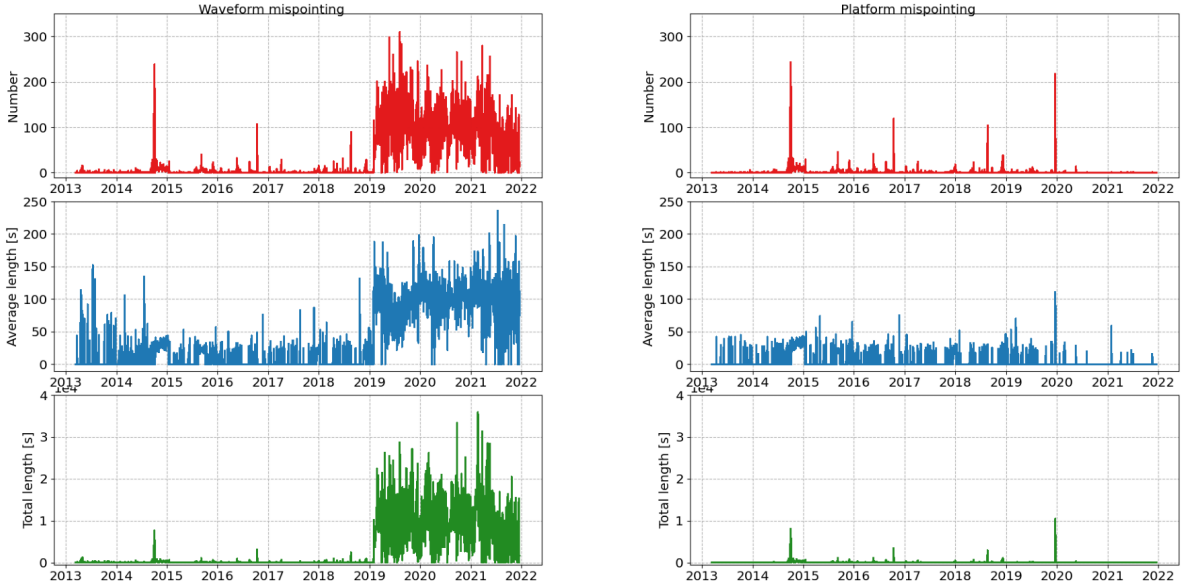

Figure 32: *Monitoring of mispointed track sections from waveform (left) and platform (right) data.*

4.4. Backscatter coefficient

SARAL/AltiKa is the first altimeter mission using the Ka-band frequency and was expected to show a different behavior than altimeters using Ku-band frequency. Several preparatory studies were done before launch, predicting that the Ka-band backscattering coefficient would be about 3.5 dB smaller than the Ku-band backscattering coefficient (see [45]). Note that the backscattering coefficient used here is corrected for atmospheric attenuation.

In flight assessment shows that the difference with respect to Ku-band backscattering coefficient is smaller than expected: **2.5 dB** in average (see bottom of figure 33).

Please note that GDR-F version introduces a small bias of 0.08dB, mainly explained by the evolution in CAL2 computation as the low pass filter is now normalized using the maximum value instead of the average.

The daily evolution of SARAL/AltiKa backscattering coefficient shows the same signals as the one of Jason-2 and of Jason-3 (top left of figure 33), the dispersion diagram of backscattering coefficients at 3h crossover points with Jason-3 (36) shows also a good correlation , and maps show consistent patterns (34).

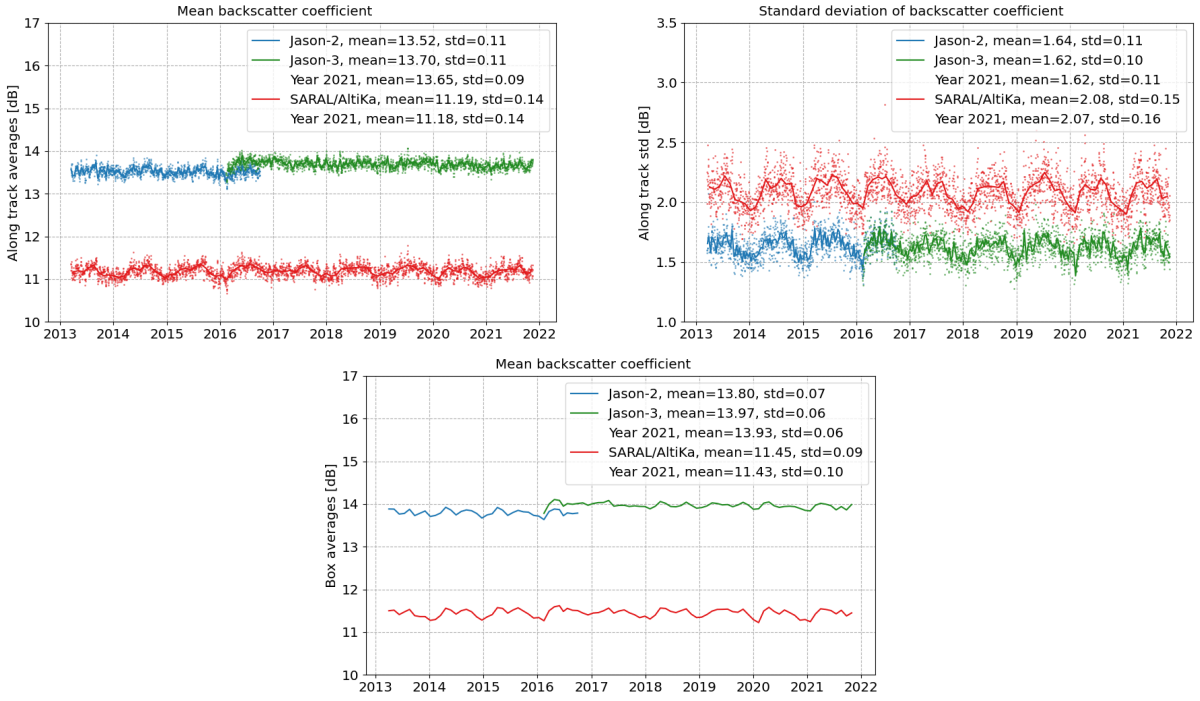

Figure 33: *Daily monitoring of mean (top) and standard deviation (center) of SARAL/AltiKa, Jason-2 and Jason-3 backscattering coefficient and cyclic monitoring of box averaged latiude weighted mean (bottom). Dots are daily averages while solid lines correspond to cycle averages.*

However the backscattering standard deviation is higher for SARAL/AltiKa than for Jason-2 and Jason-3 (top right of figure 33). While maps of backscattering coefficient show the same structures (see figure 34), the amplitudes of the observed structures are slightly larger for SARAL/AltiKa than for Jason-3. Indeed the difference between Ka- and Ku-band backscattering coefficient is not a simple bias, as shown on the map (left of figure 35), which shows a latitude dependency and/or

signals related to waves and rain events. Note that the differences between the two missions are highly related to the sea surface temperature (right of figure 35) so that hot surface temperature of low latitude implies a stronger difference between the two bands ([15]).

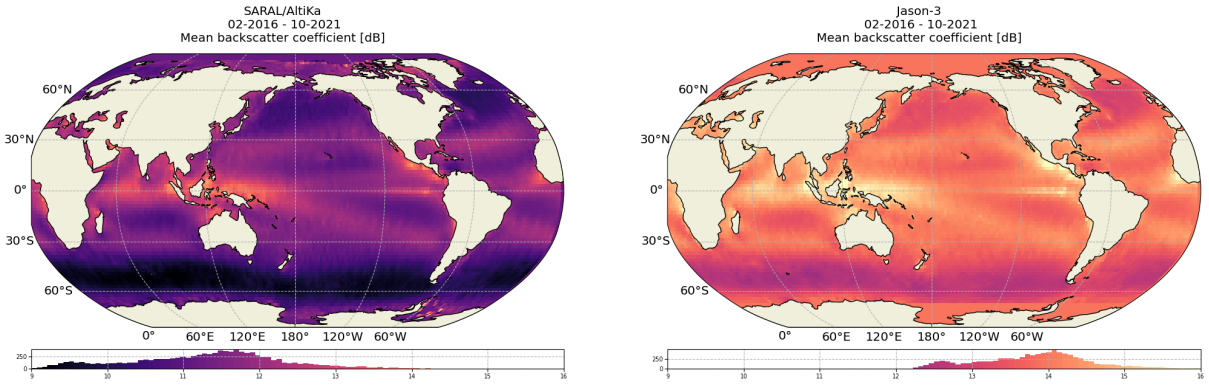

Figure 34: *Average map of backscattering coefficient for SARAL/AltiKa (left) and Jason-3 (right).*

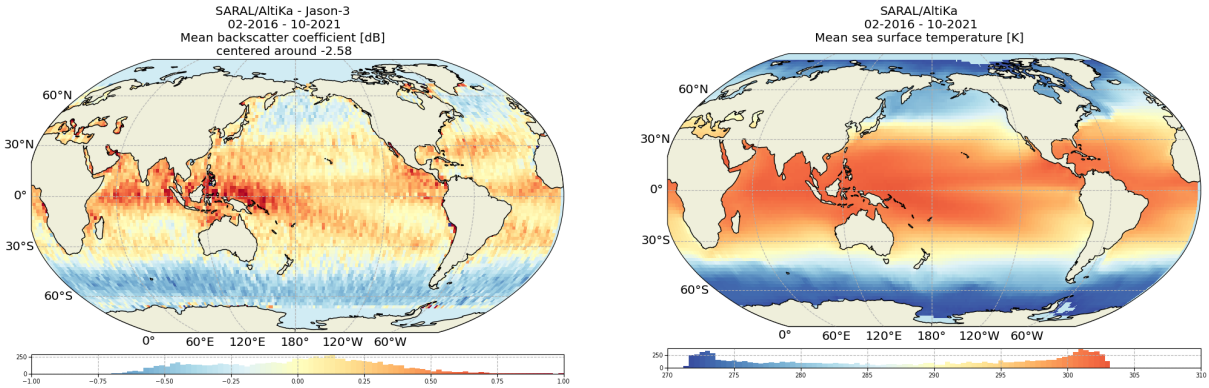

Figure 35: *Difference map of SARAL/AltiKa and Jason-3 backscattering coefficient (left) and map of sea surface temperature (right) .*

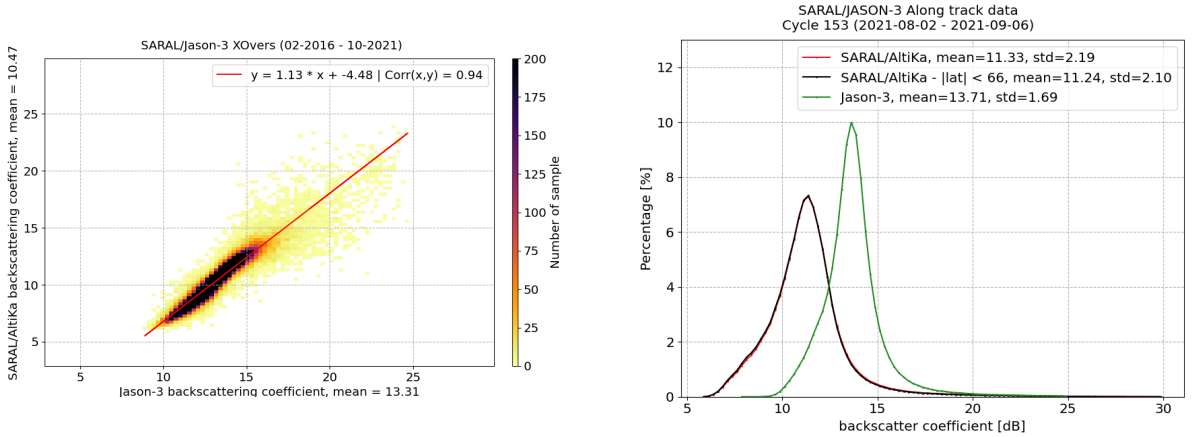

Figure 36: *Dispersion diagram of backscattering coefficient between SARAL/AltiKa and Jason-3 at 3h crossover points (left) and histogram of along-track data computed over SARAL/AltiKa 153 (right).*

Figure 36 displays the dispersion diagram between SARAL/AltiKa and Jason-3 backscatter, esti-

mated at 3h crossovers, as well as the histogram of backscatter. While a good correlation between the two missions is observed, the relation is not strictly linear. The population distribution is different for the Ka- and Ku-band frequencies: the SARAL/AltiKa histogram is tilted with a larger number of measurements at low backscatter values.

4.5. Significant wave height

The significant wave height (SWH) is one of the parameters derived from the waveforms. Monitoring of mean and standard deviation of SWH show a very good agreement between SARAL/AltiKa Jason-2 and Jason-3 (see top of figure 37).

When accounting for the different data distribution with latitude (see bottom of figure 37), the difference between SARAL/AltiKa and the Jason's missions is in average only of **5 cm**. When taking into account all latitudes, SWH is largely reduced for SARAL/AltiKa as small SWH occur in very high northern latitudes when the sea ice recedes (see also left map of figure 38).

The maps of SWH show the same structures: low SWH around Indonesia, in the Mediterranean Sea and the Gulf of Mexico and high SWH around **50°S** (as well as in North Atlantic). The difference map between the two satellites (bottom of figure 38) is centered around a difference of **2 cm**, with slightly higher values for SARAL/AltiKa.

Although this might appear to contradict top left of figure 37, it is only the result of different ways to estimate the mean. Stronger differences occur in high latitudes (in regions, where SWH is higher than **2-3 m**). When considering the dispersion diagram between SARAL/AltiKa and Jason-3 SWH at 3 hours crossovers (left of figure 39), a strong correlation coefficient ($r > 0.98$) is obtained, with an almost perfectly linear relationship between the two missions.

Please note that the new Look Up Table (taking into account the real antenna apperture in GDR-F version) introduces small biais of 5 cm in SWH estimates compared to GDR-T version.

When considering crossover points between SARAL/AltiKa and Jason-3 (figure 39, left) mean SWH values are **3.08 m** for SARAL/AltiKa and **3.09 m** for Jason-3. This is much higher than the mean values of daily along-track SWH (around **2.54 m**), and results from the geographical distribution of 3h crossover points: most crossover points are located in high SWH areas (latitudes around 50°), which biases the mean towards high SWH. Nevertheless, this diagnosis shows that for the same positions (SARAL/AltiKa/Jason-3 crossovers) with a time difference lower than 3h, SARAL/AltiKa SWH and Jason-3's are pretty equivalent. This is also the case when computing latitude weighted box statistics (in order to compensate for uneven data distribution), as shown on bottom of figure 37, where Jason-2's and Jason-3's SWH is quite the same SARAL/AltiKa's. When considering along-track statistics (top of figure 37), Jasons' SWH appears higher than SARAL/AltiKa SWH, this is again an effect of geographical data distribution.

The shapes of the histograms are very similar (see right side of figure 39) for Jason-3 and SARAL/AltiKa, except for small SWH. The minimum SWH value of SARAL/AltiKa SWH is around **12 cm** (related to the look-up table), it is **0** for Jason-3. Nevertheless, small SWH of current Jason-2 and Jason-3 data are not precise (errors of about **15 cm**), as the look-up table correction for small SWH is not accurate, whereas the SARAL/AltiKa look-up tables were updated in GDR-F. Furthermore, the histogram for SARAL/AltiKa shows a small hump for SWH around **50 cm**. Note that in the wave forecasting systems of Meteo-France, altimeter significant wave height from SARAL/AltiKa are

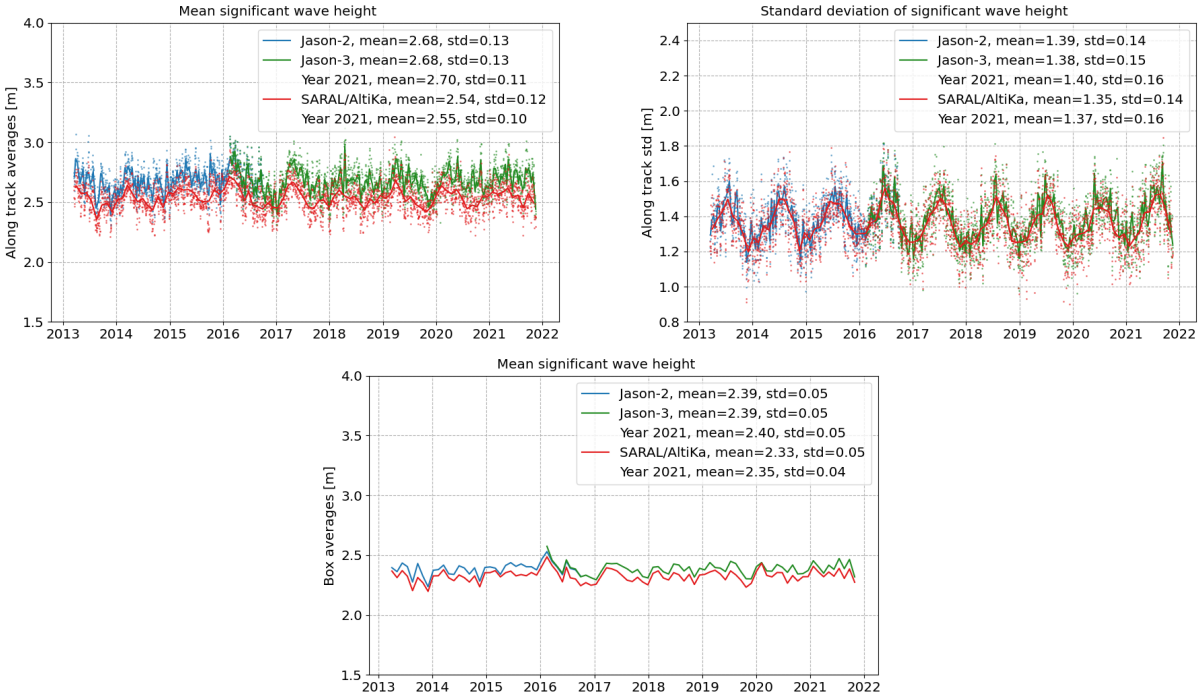

Figure 37: *Daily monitoring of mean (top) and standard deviation (center) of significant wave height for SARAL/AltiKa, Jason-2 and Jason-3 and cycle per cycle monitoring of box averaged latitude weighted mean (botom). Dots are daily averages while solid lines correspond to cycle averages.*

only assimilated for values higher than **50 cm**. According to L. Aouf, the SARAL/AltiKa SWH data have a positive impact on the wave analysis and forecast of the Meteo-France wave analysis model ([9]).

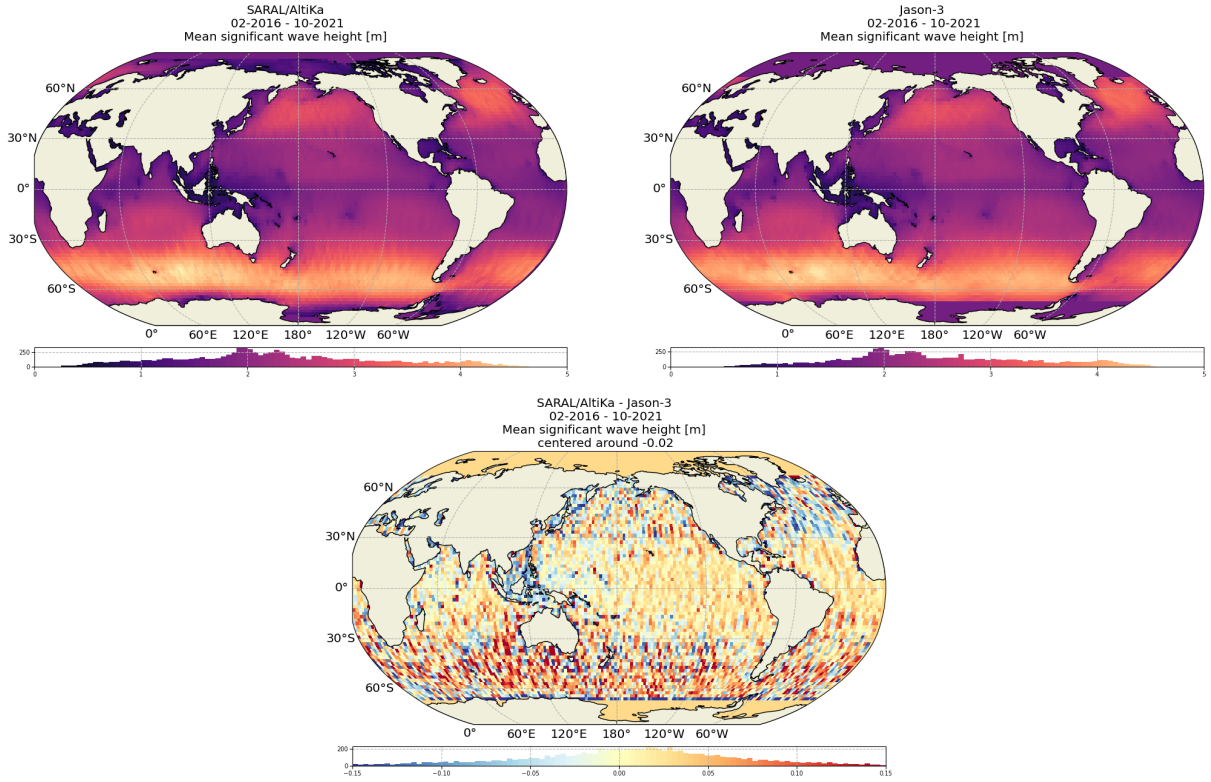

Figure 38: *Average map of significant wave height for SARAL/AltiKa (left) and Jason-3 (right) . Difference map of SARAL/AltiKa and Jason-3 significant wave height.*

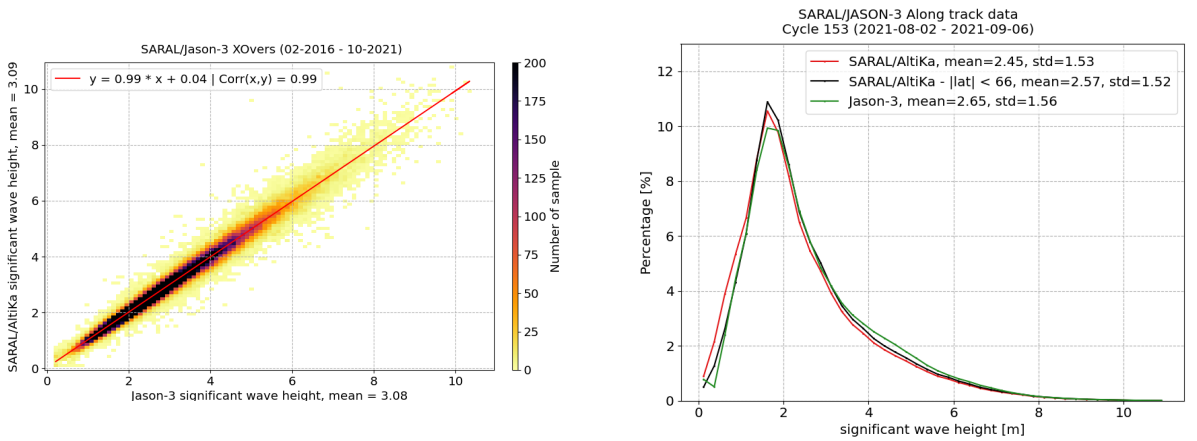

Figure 39: *Dispersion diagram of significant wave height between SARAL/AltiKa and Jason-3 at 3h crossover points on the left and histogram of along-track data computed over SARAL/AltiKa cycle 153 the right.*

4.6. Ionosphere correction

As SARAL/AltiKa uses a single frequence, no dual frequency ionosphere correction is available, GIM model is used instead. This is not an issue as the SARAL/AltiKa altimeter uses a frequency of 35.75 GHz (Ka-band), and ionospheric effects are therefore very small (divided by roughly seven compared to Ku-band frequency). In this section, Jason-2 and Jason-3 ionospheric correction values were scaled to be compared to SARAL/AltiKa ones. The scaling factor is based on the radar frequency ratio: $\frac{(f_{ku})^2}{(f_{ka})^2} = \frac{(13.575)^2}{(35.75)^2} \approx 0.14$ between instruments. Monitoring the evolution of the ionospheric correction on SARAL/AltiKa, Jason-2 and Jason-3 shows very similar evolution (40), with a slightly higher variability for Jason-2 and Jason-3, likely related to small scale features the GIM model is unable to reproduce. Effects of varying local times on Jason-2 and Jason-3 are also visible.

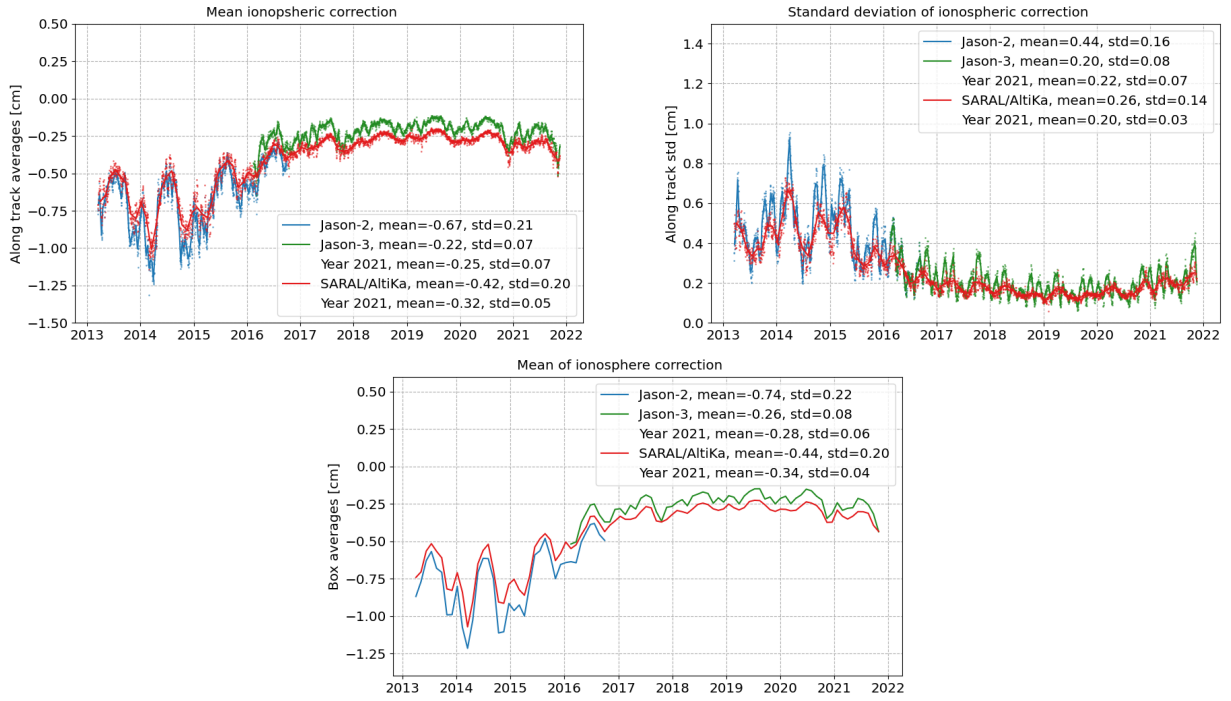

Figure 40: *Daily monitoring of mean and standard deviation ionosphere correction for SARAL/AltiKa (GIM), Jason-2 and Jason-3 (filtered dual-frequency ionosphere correction with scale factor 0.14418 for mean computation). Dots are daily averages while solid lines correspond to cycle averages.*

Small differences between the missions are still observed, which may also be due to the fact that SARAL/AltiKa is a sun-synchronous satellite with 6:00 local time for ascending node and 18:00 local time for descending node. As ionosphere correction varies with local time, it is very small for ascending (morning) passes and has absolute values up to 2 cm in the equatorial region for descending (evening) passes. Jason-2 and Jason-3 on the other hand are not sun-synchronous and revisits only every 12 cycles the same local hours. Different altitudes between Jasons and SARAL/AltiKa might also impact the observed ionospheric content.

Highest ionosphere correction (absolute values) can be found in the same regions (equatorial region) for SARAL/AltiKa and Jason-3 (see maps of figure 41, where Jason-3 data are not scaled), but the

amplitude is of course very different (due to the different frequencies).

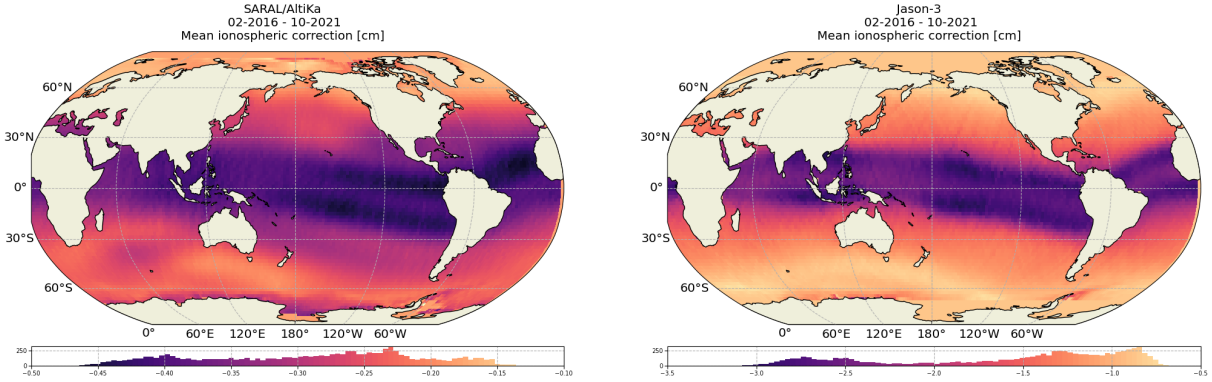

Figure 41: *Average map of ionosphere correction for SARAL/AltiKa (GIM, left) and Jason-3 (filtered dual-frequency ionosphere correction, right). Note that color scales are different for SARAL/AltiKa and Jason-3.*

The dispersion diagram of ionosphere corrections (figure 42, Jason-3 is rescaled to Ka-band frequency) at 3h crossovers shows a correlation level of **0.76** between the two missions. Histograms are slightly different, with a bi-modal distribution for Jason-3 that is less visible on SARAL/AltiKa.

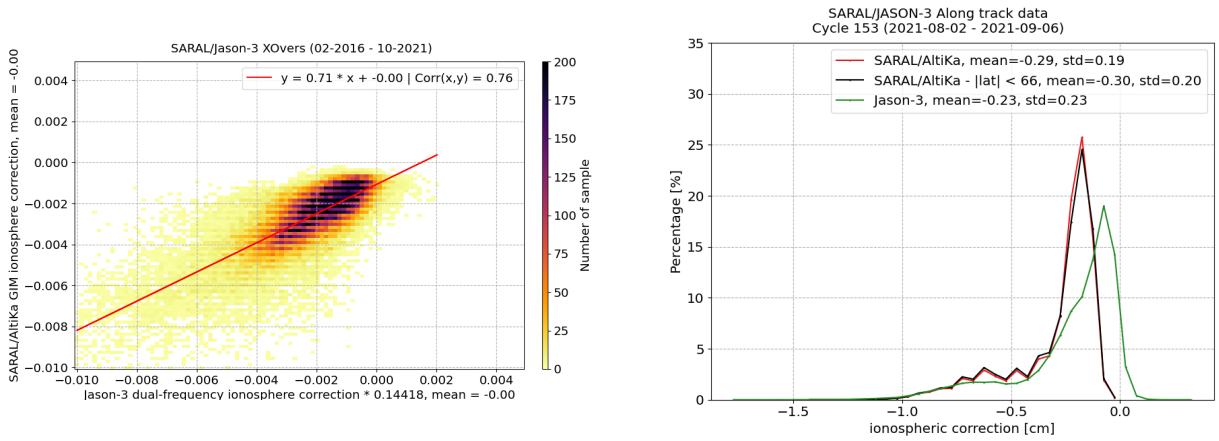

Figure 42: *Dispersion diagram of ionosphere correction between SARAL/AltiKa (GIM) and Jason-3 (filtered dual-frequency with scale factor of **0.14418** for Jason-3) at 3h crossover points on the left and histogram of along-track data computed over SARAL/AltiKa cycle 153 on the right.*

4.7. Radiometer wet troposphere correction

4.7.1. Overview

In order to have access to radiometer wet troposphere correction, liquid water content, water vapor content and atmospheric attenuation, SARAL/AltiKa uses a dual-frequency radiometer (23.8 GHz +/- 200 MHz & 37 GHz +/- 500 MHz), whereas Jason-2 and Jason-3 have a similar three-frequency radiometer (18.7, 23.8 and 34.0 GHz). In the lack of a 18.7 GHz channel as in CNES/JPL Jason's radiometer series, the performances of the WTC estimation have found to be improved with the use of two additional input parameters [6]:

- the sea surface temperature (SST) completes the information of the backscattering coefficient for a better estimation of the surface emissivity
- the atmospheric temperature lapse rate improves the performances of the retrieval, reducing systematic biases over upwelling regions

Figure 43 shows the daily mean and standard deviation of radiometer wet troposphere correction for SARAL/AltiKa, Jason-2 and Jason-3. With Patch4, the standard deviation is similar for SARAL/AltiKa and for Jasons. Concerning the mean of radiometer wet troposphere correction, Jason-2 and Jason-3 has dryer values than SARAL/AltiKa. This is on the one hand related to different radiometer wet troposphere correction retrieval algorithms, but on the other hand, this can also be related to different local times of the satellites (sun-synchronous 6h/18h for SARAL/AltiKa).

Please note that the GDR-F version introduces a new algorithm to compute the gains and residual temperatures that has been developed to correct the saturation of the radiometer 37GHz channel for the cycles which are saturated (cycle 3 to 7). The use or not of this specific treatment depends on a flag added in the radiometer characterization file.

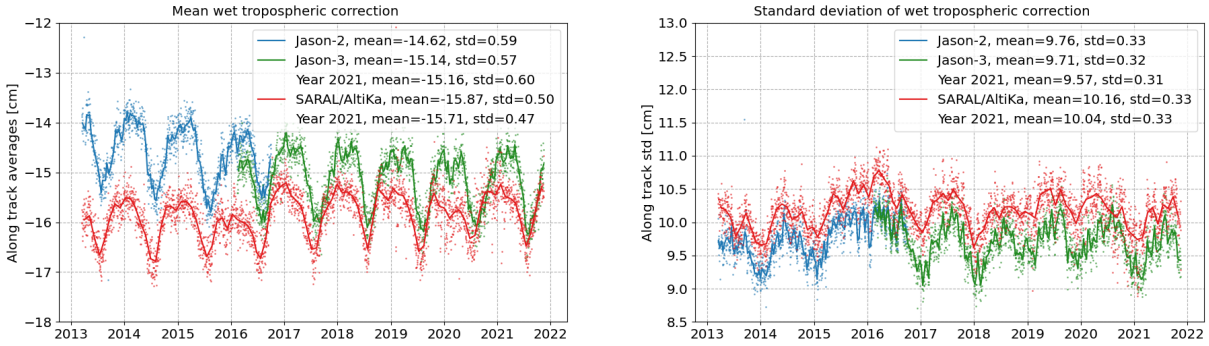

Figure 43: *Monitoring of mean and standard deviation of radiometer wet troposphere correction for SARAL/AltiKa (red) Jason-2 (blue) and Jason-3 (green). Dots are daily averages while solid lines correspond to cycle averages.*

4.7.2. Comparison with the ECMWF model

The ECWMF wet troposphere correction is used as a reference to investigate small differences between SARAL/AltiKa Jason-2 and Jason-3 radiometer corrections. Daily differences are calculated and plotted in figure 44.

In average the difference between radiometer and ECMWF wet troposphere correction for SARAL/AltiKa is around **-1.8 mm** thanks to Patch 4 retrieval algorithm. Thanks to GDR-F dataset, for Jason-3 it is around **0.3 mm**. As for Jason-2 it's performance regarding the wet troposphere correction has been severely impacted by the several SHM modes experienced since Mars 2016. The two ECMWF model updates that occurred during June and November 2013, which might have an impact on the model wet troposphere correction, did not show any impact on the data.

The standard deviation of radiometer minus model wet troposphere correction is slighly higher for SARAL/AltiKa (around **1.4 cm**) compared to Jasons (around **1.2 cm**), shown on left of figure 44 and also on the histogram on figure 46. With the new GDR-F standard, wet troposphere correction shows a better performance with a decrease of 0.2 cm of the standard deviation of radiometer minus model wet troposphere correction compared to GDR-T (Patch 3 retrieval algorithm).

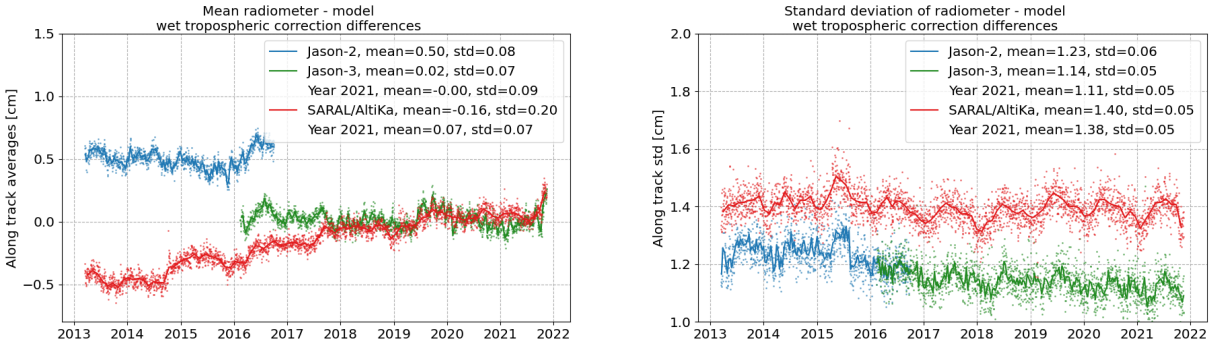

Figure 44: *Monitoring of mean and standard deviation of radiometer minus model wet troposphere correction differences for SARAL/AltiKa Jason-2 and Jason-3. Dots are daily averages while solid lines correspond to cycle averages.*

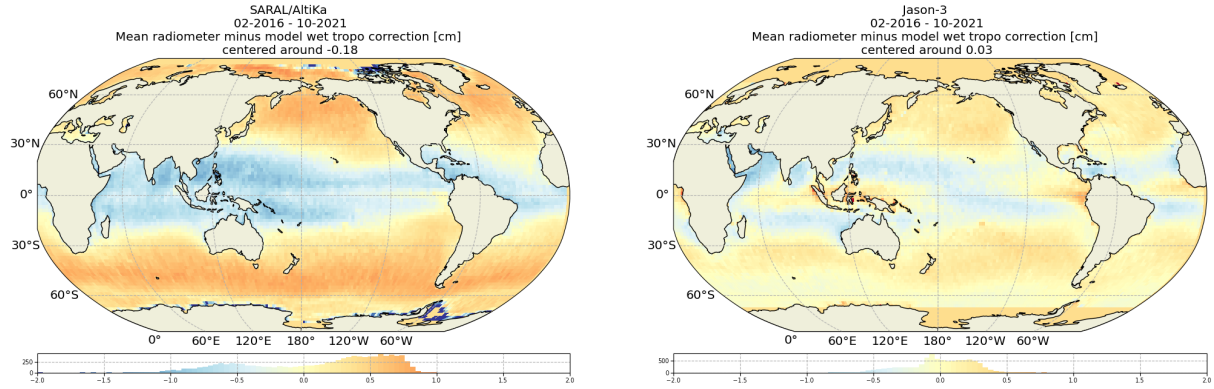

Figure 45: *Average map of radiometer minus ECMWF model wet troposphere correction for SARAL/AltiKa (left) and Jason-3 (right).*

The maps of radiometer minus ECMWF model wet troposphere correction (figure 45) are centered around the mean value (**0.2 mm** for Jason-3, **-1.8 mm** for SARAL/AltiKa). The mean of the SARAL/AltiKa map is impacted by some boxes near the frontier between sea-ice and free water (which tends to underestimate the mean). These boxes with strong negative values are an indication that not all sea ice cases are well-detected. Geographical structures of the radiometer minus model wet troposphere corrections are similar for the two satellites in high latitudes (around $\pm$ 50°), but quite different for low latitudes. This is also observed on the histogram of wet troposphere differences (figure 46) which is slightly wider for SARAL/AltiKa than for Jason-3.

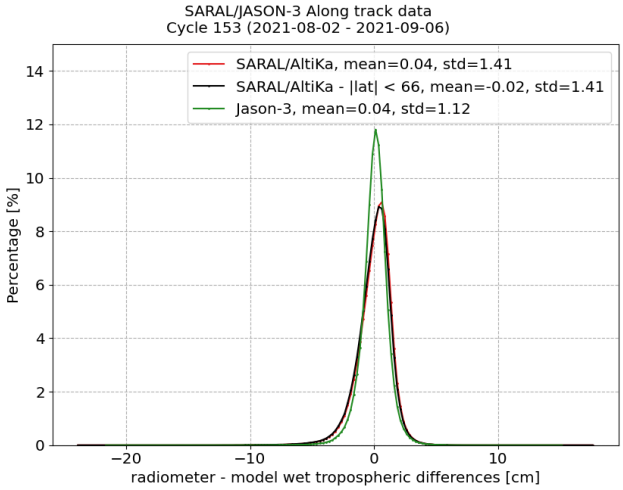

Figure 46: *Histogram (of along-track data) of radiometer minus ECMWF model wet troposphere correction between SARAL/AltiKa and Jason-3 computed for SARAL/AltiKa cycle 153.*

4.8. Altimeter wind speed

The Patch1 version of the products used the wind look-up table from Jason-1 which, with the Ka-band backscattering coefficient produced erroneous wind speeds. In the Patch2 version, the altimeter wind speed algorithm developed by [26] for Ka-band altimetry is used. GDR-F version introduces new wind look up tables based on the method proposed by N. Tran [33] using both significant wave height and backscatter coefficient. Figure 47 shows the daily monitoring of the mean and standard deviation of altimeter wind speed for SARAL/AltiKa, Jason-2 and Jason-3.

The SARAL/AltiKa wind speed is equivalent to Jasons' with very similar daily standard deviation.

The maps of altimeter wind speed for SARAL/AltiKa and Jason-3 are consistent (see 48). Figure 49 shows a good correlation of wind speed data between the two missions ($r = 0.95$). The relationship between both missions' wind speed is truly linear. Thanks to GDR-F standards, SARAL/AltiKa's wind speed no longer saturates for values greater than 16 m/s which tended to underestimate the wind speed compared to Jason-3 (see [58]).

The distribution of SARAL/AltiKa wind speed values shows two modes, this feature is less present on Jason-3 data.

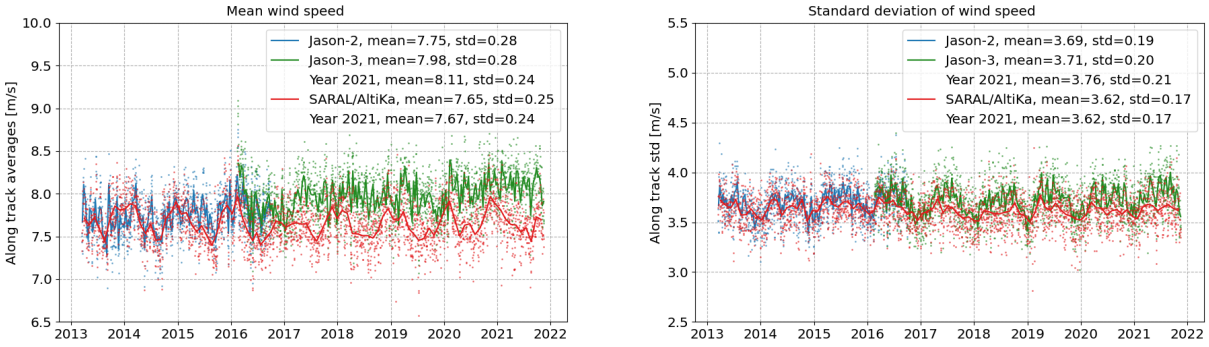

Figure 47: *Monitoring of mean and standard deviation of altimeter wind speed for SARAL/AltiKa and Jason-3. Dots are daily averages while solid lines correspond to cycle averages.*

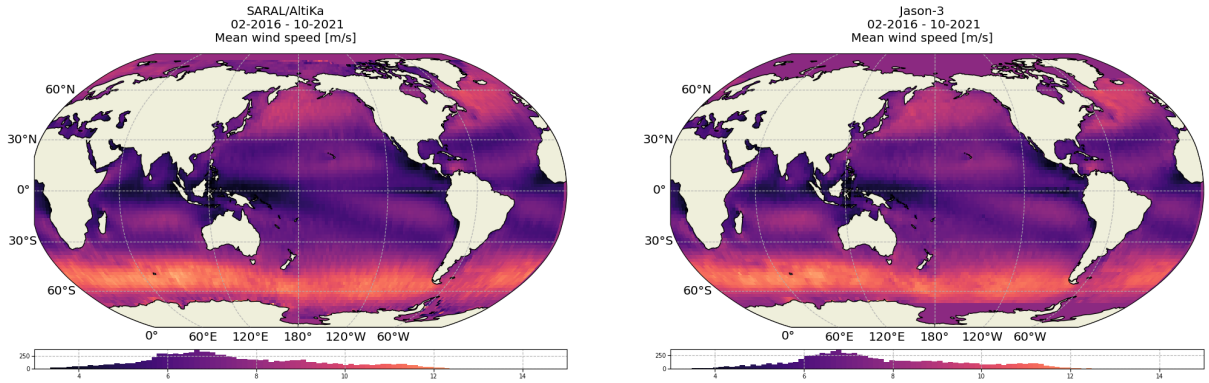

Figure 48: *Average map of altimeter wind speed for SARAL/AltiKa (left) and Jason-3 (right).*

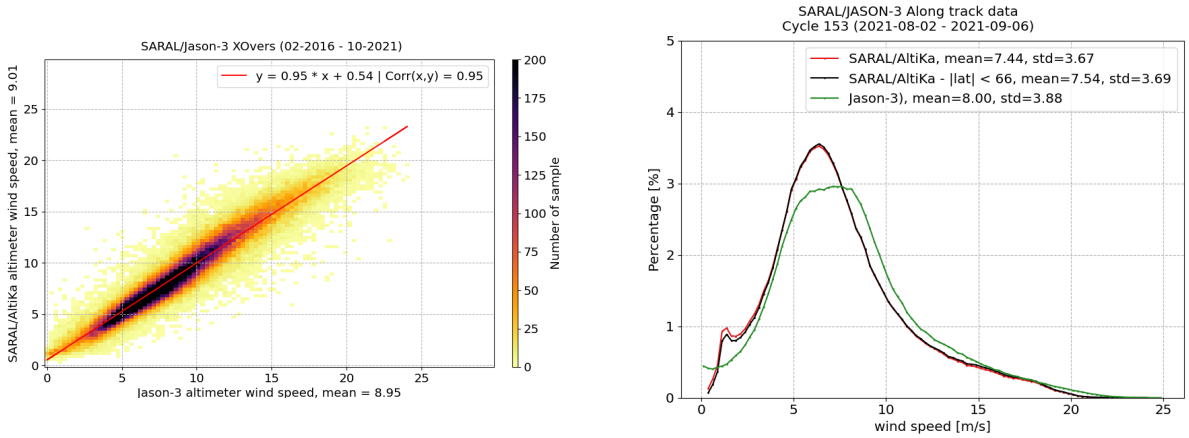

Figure 49: *Dispersion diagram of altimeter wind speed between SARAL/AltiKa and Jason-3 at 3h crossover points (left) and histogram of along-track data computed for SARAL/AltiKa cycle 153 (right).*

4.9. Sea state bias

In Patch1 version, the sea state bias was as a first approximation set to **-3.5%** of SWH. For Patch2 a hybrid SSB solution developed by R. Scharroo [25] was used (but only with SWH as an input). The Patch2 SSB solution is in absolute values around **1.8 cm** stronger (which increases the Patch2 SLA) than the Patch1 solution.

The GDR-F version implements the new SSB tables, based on the method proposed by [33] computed using 2015 test dadaset. The GDR-F solution is in absolute values around **4.4 cm** stronger than the Patch2 solution (which increases the GDR-F SLA). The daily monitoring of the along-track sea state bias for SARAL/AltiKa Jason-2 and Jason-3 shows a similar temporal evolution, but SARAL/AltiKa's SSB has lower absolute values than Jason-2 and Jason-3 (around 3.86 cm lower than Jason-3, see left side of figure 50). This is also the case when considering latitude weighted box statistics (bottom of figure 50). On the other hand the daily standard deviation is smaller for SARAL/AltiKa compared to Jasons (see right side of figure 50).

The bias between SARAL/AltiKa's and Jasons' SSB is not homogeneous but varies geographically, as shown on bottom of figure 51.

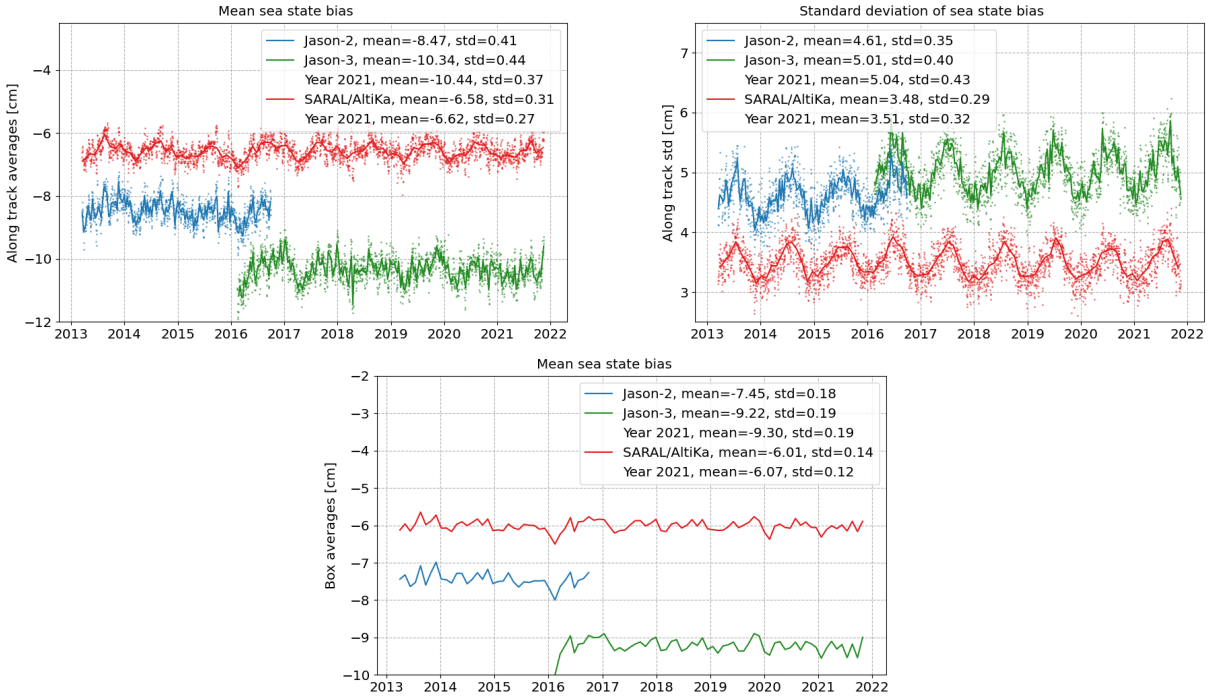

Figure 50: *Monitoring of mean (top) and standard deviation (center) of (along-track) sea state bias of SARAL/AltiKa Jason-2 and Jason-3. Cycle per cycle monitoring of latitude weighted box averaged mean (botom). Dots are daily averages while solid lines correspond to cycle averages.*

SARAL/AltiKa's SSB shows the same patterns as Jason-3 but with lower amplitudes. (top of figure 51). The different nature of the SSB models used for SARAL/AltiKa and Jason-3 (dedicated model) is visible on the right side of figure 52, showing very different shapes of histograms. A new version of the SSB will be produced for Jason-3 with a similar method (with the upcoming GDR-F version for Jason-3 products).

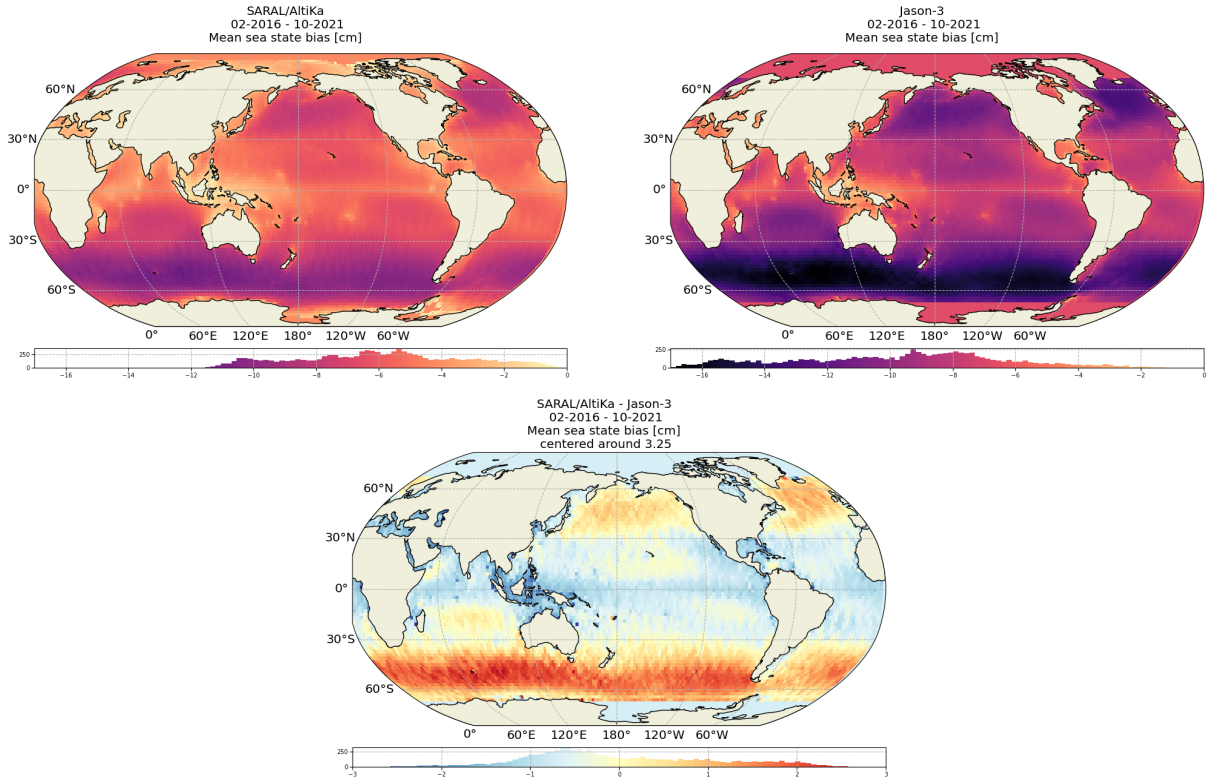

Figure 51: *Average map of sea state bias for SARAL/AltiKa (left) and Jason-3 (right). Map of differences of gridded SARAL/AltiKa and Jason-2 sea state bias.*

This difference in sea state bias between the two missions has also an impact on the geographically correlated biases between the two missions, as shown in chapter 5.3., concerning maps of sea surface height differences at multi-mission crossover points.

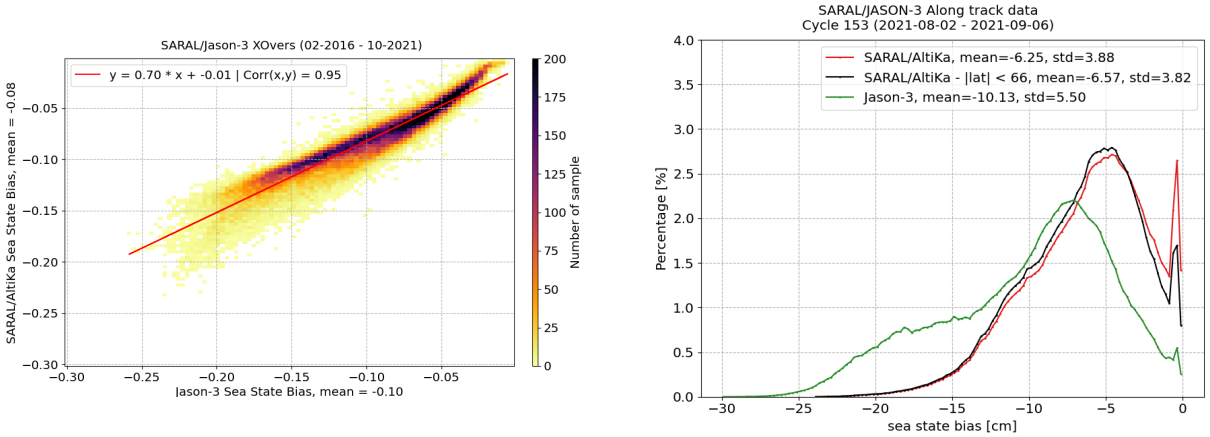

Figure 52: *Dispersion diagram of sea state bias between SARAL/AltiKa and Jason-3 at 3h crossover points (left). Histogram (of along-track data) computed for SARAL/AltiKa cycle 153 (right).*

5. SSH crossover analysis

5.1. Overview

SSH crossover differences are the main tool to analyze the whole altimetry system performance. Crossovers measure the SSH consistency between ascending and descending passes. At each crossover, the observed difference of SSH measurements between ascending and descending arcs results from the sum of errors in the system and ocean variability. In order to reduce the impact of ocean variability, only crossovers with a maximum time difference of 10 days are selected. This gives a measure of the mission performance on mesoscale time/space scales. Mean and standard deviation of SSH crossover differences are computed from the valid data set to estimate maps and cycle per cycle monitoring over the altimeter period. In order to monitor the performances over stable surfaces and homogenious distributions of crossovers, additional selections are applied :

- Remove shallow waters (bathymetry above -1000 m), areas of high ocean variability (variability above 20 cm rms) and high latitudes ($|lat| < 50\,\text{deg}$).
- Weighting the crossovers distribution by latitudes. This process is used to avoir skewing the metrics by downweighting crossovers at high latitudes following the method described in [55] and it also reduces the amplitude of the annual signal.

Under these conditions, SSH performances are always estimated with equivalent conditions.

Please note that, only valid data is used to compute SSH difference at crossovers. As demonstrated in the editing section (3.2.), the late mispointing events are properly discarded during the validation process. Hence the number of SARAL/AltiKa's valid SSH at crossovers is slightly reduced since SSA. As shown in figure 53, the number of valid crossovers decreased of about 17% to 19% depending on the selection applied. The geographycal density of valid crossovers in figure 54 indicates that most of mispointing events slightly impact the distribution of crossovers over ocean.

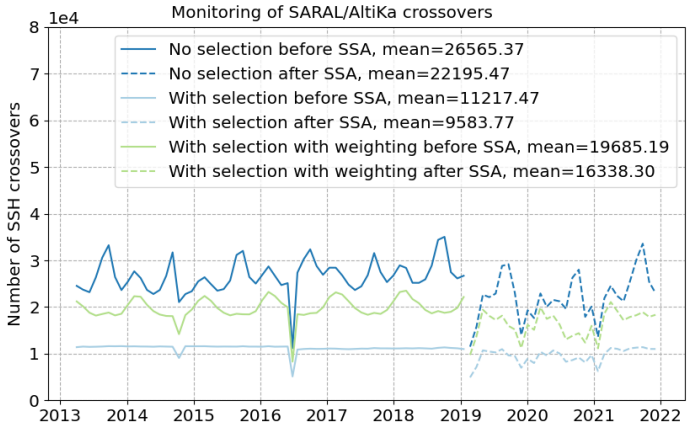

Figure 53: *Monitoring of SARAL/AltiKa's number of valid crossovers per cycle.*

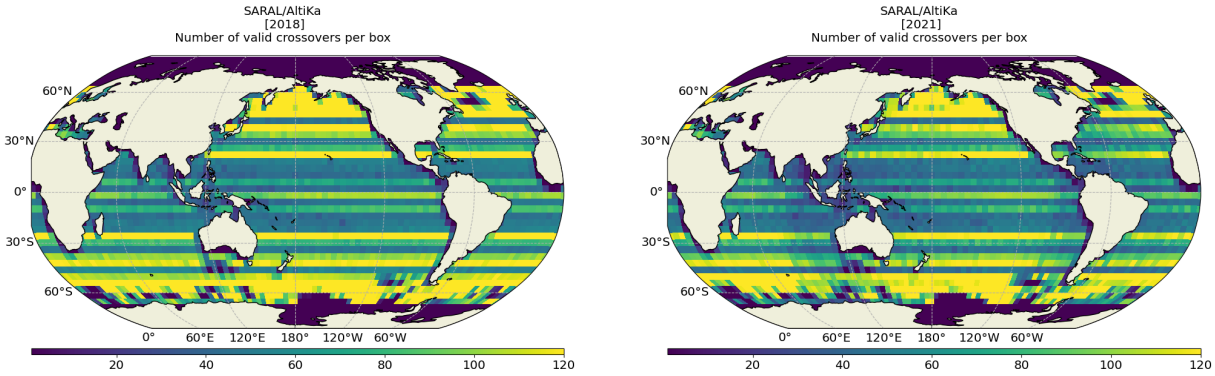

Figure 54: *Number of valid crossovers per box for SARAL/AltiKa over (left) 2018, and (right) 2021.*

The formula used to estimate a fully corrected SSH for SARAL/AltiKa and Jason-3 is defined below:

$$SSH = Orbit - Altimeter\ Range - \sum_{i=1}^{n} Correction_i \quad (1)$$

where the sum of corrections expands as:

$$\begin{aligned} \sum_{i=1}^{n} Correction_i &= Dry\ troposphere\ correction \\ &+ Dynamical\ atmospheric\ correction \\ &+ Radiometer\ wet\ troposphere\ correction \\ &+ Ionospheric\ correction \\ &+ Sea\ state\ bias\ correction \\ &+ Ocean\ tide\ correction\ (including\ loading\ tide) \\ &+ Earth\ tide\ height \\ &+ Pole\ tide\ height \\ &+ Internal\ tide \end{aligned}$$

The corrections effectively used to generate the metrics presented in this report are summarized in table 6 for SARAL/AltiKa and Jason-3. The standards correspond to the current version of the GDR products: GDR-F for SARAL/AltiKa and Jason-3.

Parameter	SARAL/AltiKa	Jason-3
Orbit	CNES POE-F	
Dynamic atmospheric correction	Computed from ECMWF atmospheric pressures after removing S1 and S2 atmospheric tides (for inverse barometer) + Mog2D High Resolution ocean model	
Radiometer wet troposphere correction	MWR using P4 neural network	Radiometer
Ionospheric correction	GIM model	dual-frequency altimeter ionosphere correction
Sea State Bias	SSB compute whith SSB tables based on significant wave heigt and wind [33]	
Global ocean tide	FES 14B ocean tide	
Earth tide	From Cartwright and Taylor tidal potential	
Pole tide	DESAI with new IERS linear mean pole [36]	
Mean Sea Surface	CNES_CLS_2015	
.../...		

Parameter	SARAL/AltiKa	Jason-3
Internal tide	Zaron with M2, K1, S2, O1 waves (version HRET v7.0, see [40])	Zaron with M2, K1, S2, O1 waves (version HRET v8.0)

Table 6: *S*tandards used for SSH estimation on SARAL/AltiKa and Jason-3

When not otherwise stated, the standards from table 6 are used.

5.2. Mean of SSH mono-missioon crossover differences

The map of SSH mean ascending/descending differences at crossovers should ideally be close to zero: only time differences shorter than 10 days are selected in order to be as close as possible to the steady ocean hypothesis while maintaining a global sampling by crossovers. Of course this is untrue due to quickly evolving mesoscale ocean features, yet, large geographically correlated patterns on such maps indicate systematic differences between ascending and descending passes, which are generally errors. This can indicate either problems in the orbit computation or in geophysical corrections. Figure 55 shows the map of mean SSH differences at crossovers for SARAL/AltiKa and Jason-3, computed over the same period in a similar way (based on SARAL/AltiKa cycles).

Both missions show geographically correlated patterns of low amplitudes. The mean difference is slightly negative on SARAL/AltiKa and Jason-3, with a larger mean difference observed on SARAL/AltiKa. Locally differences remain below 1 *cm* on both SARAL/AltiKa and Jason-3.

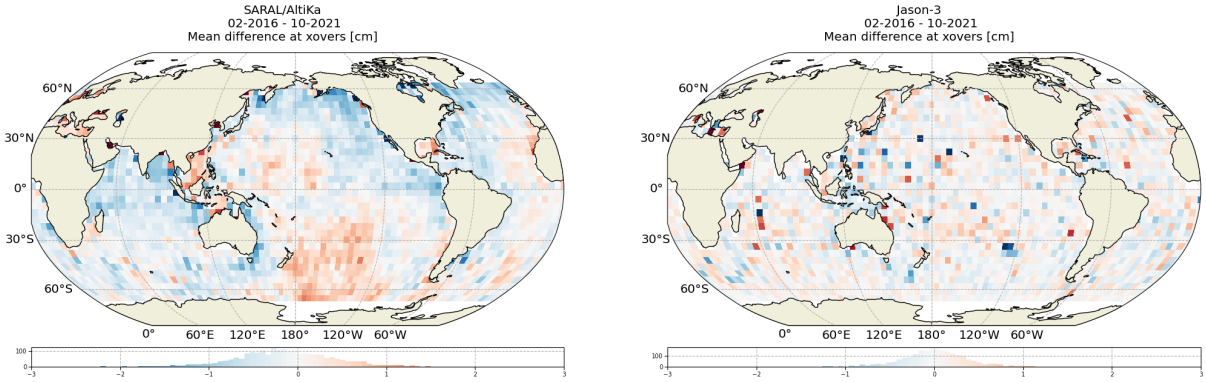

Figure 55: *Map of mean of SSH crossovers differences for [left] SARAL/AltiKa and [right] Jason-3.*

In addition to mapping the differences accumulated over several cycles, the global mean of SSH differences at crossovers is estimated for each cycle. This quantity is monitored over time to detect any issue on the mission.

Over SARAL/AltiKa lifetime, the evolution of the cycle-average mean SSH difference at crossovers is plotted on figure 56 for SARAL/AltiKa, Jason-2 and Jason-3. The left and right panels correspond to two different selections of crossovers used to estimate the mean (no selection at all and selection on bathymetry, latitude and oceanic variability), while plain and dotted lines correspond to two ways of averaging the SSH differences at crossovers (a simple ensemble mean and a latitude weighted mean based on the crossovers' theoretical density). The weighted averaging method was described in the SARAL/AltiKa yearly report 2014 [55]. The mean difference is slightly negative $\approx -1\ mm$ for SARAL/AltiKa, Jason-2 and Jason-3. The mean value is very stable over time for the three missions, with a slightly larger cycle to cycle variability on Jason-2 and Jason-3 than on SARAL/AltiKa, but note that the samples used for Jason-2 and Jason-3 are smaller than those for SARAL/AltiKa due to different cycle lengths. One can also note a periodic signal around one year on SARAL/AltiKa, which is related to the β angle (see [21] for an in-depth analysis of such signals). Please note that the various mispointing events observed so far have no visible impact over the metrics shown here.

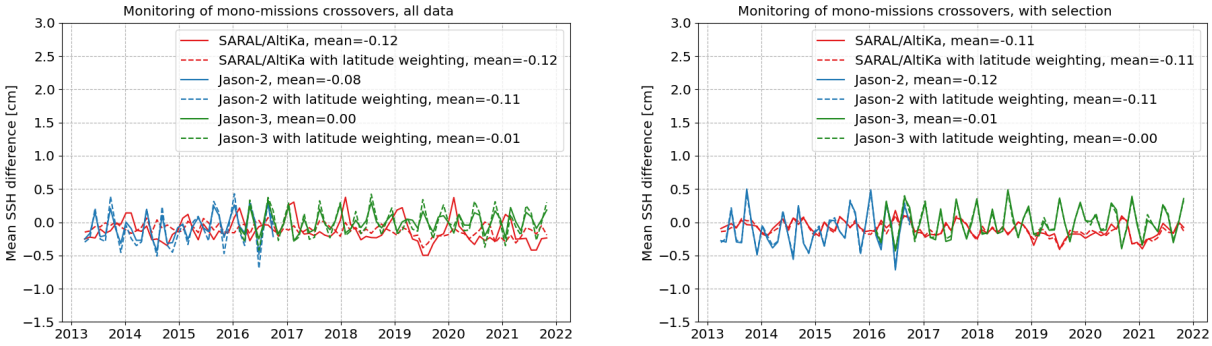

Figure 56: *Cycle per cycle monitoring of ascending/descending SSH differences at mono-mission crossovers for SARAL/AltiKa Jason-2 and Jason-3 for Saral cycles 1 to 155.*

5.3. Mean of SSH multi-mission crossover differences

On top of monomission crossovers that permits to detect systematic biases on one mission, crossovers differences are also estimated between different missions. In this case they are used to check for geographically correlated biases or drifts that could happen between two missions. Here SARAL/AltiKa is compared to Jason-2 and Jason-3 through their SSH differences at crossovers.

The temporal evolution of the mean of SARAL/AltiKa minus Jason-2 and SARAL/AltiKa minus Jason-3 SSH differences at crossovers is shown on figure 57. A selection for latitudes lower than 50°, deep ocean and low oceanic variability areas is used here, along with a mean estimation based on latitude weighted averages. The bold lines were computed using the radiometer wet tropospheric correction while the dotted lines are based on the model correction. In all cases the temporal evolution of SSH differences at crossovers is very steady for both SARAL/AltiKa / Jason-2 and SARAL/AltiKa / Jason-3 crossovers:

- the mean bias between SARAL/AltiKa and Jason-2 is around 71 *mm*,
- the mean bias between SARAL/AltiKa and Jason-3 is around 68 *mm*,
- there is no significant drift between SARAL/AltiKa and Jason-2 nor SARAL/AltiKa and Jason-3.

Thanks to Patch4 wet troposphere retrieval algorithm, there is no drift between the radiometer and model wet troposphere corrections (see [58]).

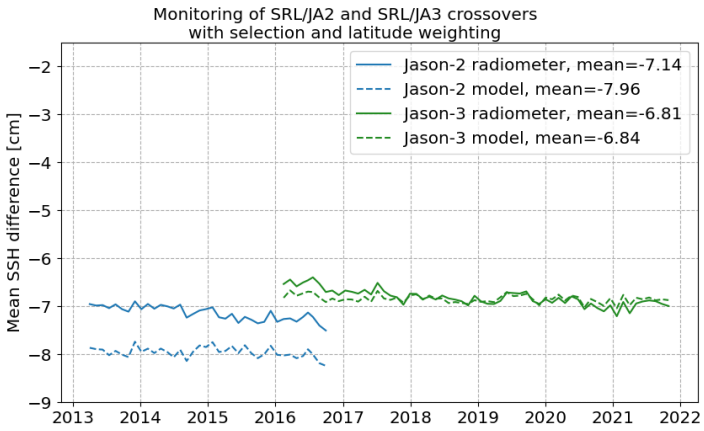

Figure 57: *Monitoring of mean of SARAL/AltiKa minus Jason-2 and SARAL/AltiKa minus Jason-3 differences at crossovers using radiometer wet troposphere correction (bold line) or ECMWF model wet troposphere correction (dotted line) for GDR data, latitude weighed mean.*

Rather than looking at the temporal evolution, mapping the SSH differences between SARAL/AltiKa and Jason-3 provides information about geographically correlated biases between the two missions. Such maps are shown on figure 58, they are both computed over the whole available period of Jason-3 to have a suitable comparison and both maps are centered before plotting. Large scale biases are visible between the two missions with amplitudes up to ±2 cm. Using the radiometer on both missions (left of figure 58) shows positive patches centered around the equator. As observed for mono-mission crossover differences, part of the observed pattern might come from orbit related issues and/or from geophysical corrections. Using the model wet tropospheric correction on both

missions (right of figure 58) creates North/South patch with smaller amplitudes.

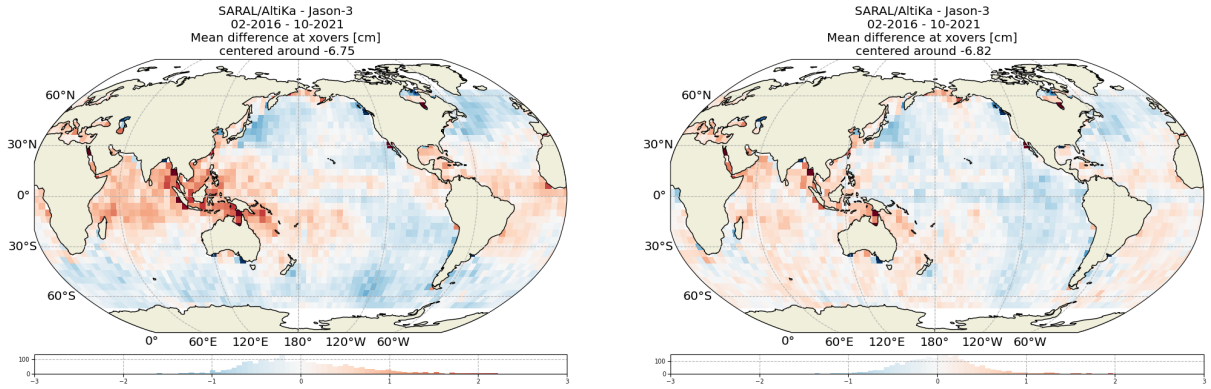

Figure 58: *Map of mean of SSH crossovers differences between SARAL/AltiKa and Jason-3 using the radiometer wet tropospheric correction (left) or the ECMWF model wet troposphere correction (right) for both missions. The maps are centered around the mean.*

5.4. Standard deviation of SSH crossover differences

The standard deviation of SSH differences at crossovers is a key performance metric for satellite altimetry missions. In this section the standard deviation of SSH differences at crossovers is investigated for SARAL/AltiKa and compared to Jason-2 and Jason-3.

The cycle per cycle standard deviation of SSH differences at crossovers is plotted on the left of figure 59 for different selections and averaging methods:

- solid black: no selection is applied, and the ensemble standard deviation is estimated without any weighting. In this case the standard deviation amounts to 6.41 *cm* and its temporal evolution is impacted by an annual signal due to varying sea ice extent.
- dotted black: no selection is applied on the crossovers, but the standard deviation is estimated after weighting the crossovers following the method described in [55]. This process slighlty reduces the standard deviation (5.93 *cm*) due to downweighting of crossovers at high latitudes and it also reduces the amplitude of the annual signal.
- solid red: shallow waters (bathymetry < -1000 *m*), high latitudes and high variability areas have been removed. This is as close as possible to the steady ocean hypothesis and the standard deviation of SSH differences drops to 5.00 *cm*, no more annual cycle is observed.
- dotted red: uses the same selection as above, combined to a latitude weighting of the crossovers before estimating the standard deviation. Using this method leads to a small increase of the standard deviation of SSH differences at crossovers (at 5.21 cm)

The right part of figure 59 displays the geographical distribution of the standard deviation of SSH differences at crossovers. This map shows the expected patterns with high standard deviation observed in high ocean variability areas and in the Arctic Ocean (where some geophysical corrections such as tides, are less accurate).

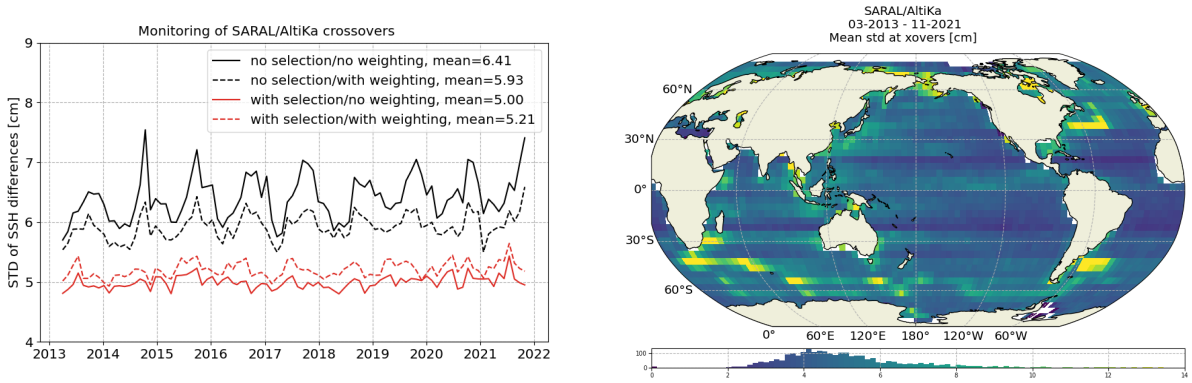

Figure 59: *Cycle by cycle standard deviation of SSH crossover differences for SARAL/AltiKa using different selections and averaging methods (left) and map of standard deviation at crossover points. In both cases the radiometer wet tropospheric correction is used.*

As part of the routine Cal/Val activities, the performance of SARAL/AltiKa is compared to Jason-2 and Jason-3 through the use of the standard deviation of SSH differences at crossovers. Figure 60 display comparisons between SARAL/AltiKa Jason-2 and Jason-3 performance at crossovers for different selections. In each case the performance using the radiometer and the model are displayed.

To account for the uneven distribution of crossover points, we estimate weighted statistics (figure 60) where the weights applied are based on the crossovers density. This allows to better compare two missions that do not share the same ground track. Similar results are obtained with these weighted statistics: SARAL/AltiKa's performance is excellent and slightly below Jasons'.

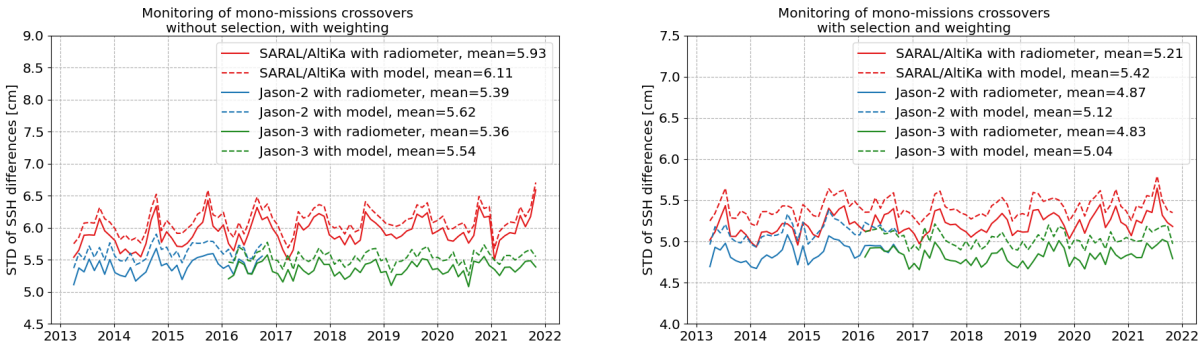

Figure 60: *Monitoring of the standard deviaiton of SSH differences at crossovers for SARAL/AltiKa Jason-2 and Jason-3 without any selection (left) and after removing high latitudes, shallow waters and high variability areas (right). A weighting based on crossovers density is applied.*

5.5. Performances of the different product types

Saral/AltiKa data are also available as OGDR and IGDR products, which are more rapidly available than GDR products. The main differences between these products are listed in table 7.

Auxiliary Data	Impacted Parameter	OGDR	IGDR	GDR
Orbit	Satellite altitude, Doppler correction, ...	DORIS Navigator	Preliminary (Doris MOE)	Precise (Doris + Laser POE)
Meteo Fields	Dry/wet tropospheric corrections, U/V wind vector, Surface pressure, Inverted barometer correction,...	Predicted	Restituted	
	Waves	Not Available	MFWAM	
Pole Location	Pole tide height	Predicted		Restituted
Mog2D	HF ocean dealiasing correction	Predicted	Preliminary	Precise
GIM	Ionosphere correction	Predicted	Restituted	
Platform Pointing	Platform pitch, rall, yaw and mispointing angles	Not available		HK Telemetry
SST	sst, wet tropospheric correction	Seasonal ma or static		Restituted

Table 7: *D*ifferences between the auxiliary data for the O/I/Gdr products (from [52])

Figure 61 displays the monitoring of the cycle per cycle mean and standard deviation of SSH differences at crossovers for the OGDR, IGDR and GDR products. Regarding the mean, all three products show a good stability, of course the temporal variablity is greater for OGDR and IGDR than for GDR data. As for the bias observed for OGDR crossover differences, it is due to the attitude deviation experienced by SARAL/AltiKa's platform since SSA, that leads to a much less accurate orbit estimation. This feature is not observed for IGDR and GDR for which orbit determination methods are less sensitive to such deviations. GDR-F standard starts cycle 137 for IGDR and cycle 138 pass 37-38 for OGDR products.

Also as expected, GDR products provide the best performance with a standard deviation of the differences at crossovers of 5.00 cm. But IGDR data also exhibits a very good performance especially since the switch to IGDR-F, with an average standard deviation of 5.37 cm, very close to the GDR value despite degraded standards at the beginning of the period and a less accurate orbit solution (MOE vs. POE). OGDR data show a higher standard deviation of $\approx$ 6.69 cm.

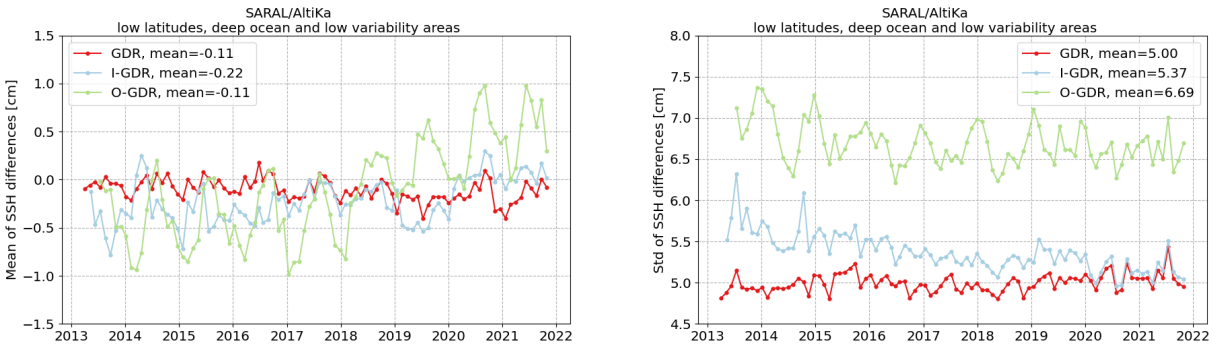

Figure 61: *Cycle per cycle monitoring of mean and standard deviation of SSH crossover differences for SARAL/AltiKa using radiometer wet troposphere correction and geographical selection ($|latitude| < 50°$, bathymetry < -1000 m and ocean variability < 20 cm rms).*

5.6. Estimation of pseudo time-tag bias

The pseudo time tag bias is found by computing at crossovers the regression between SSH differences and orbital altitude rate ($\dot{H}$), also called satellite radial speed :

$$\Delta SSH = \alpha \dot{H}$$

This method allows to estimate the time tag bias but also absorbs other errors correlated with $\dot{H}$ as for instance orbit errors. Therefore it is called "pseudo" time tag bias.

Figure 62 shows the monitoring of the pseudo datation bias for SARAL/AltiKa Jason-2 and Jason-3 on a cyclic basis. On average SARAL/AltiKa has a slightly higher pseudo time-tag bias than Jason-2 and Jason-3, around 0.08 ms, but appears to be more stable over time (0.1 standard deviation for Jasons which is twice higher as SARAL/AltiKa's).

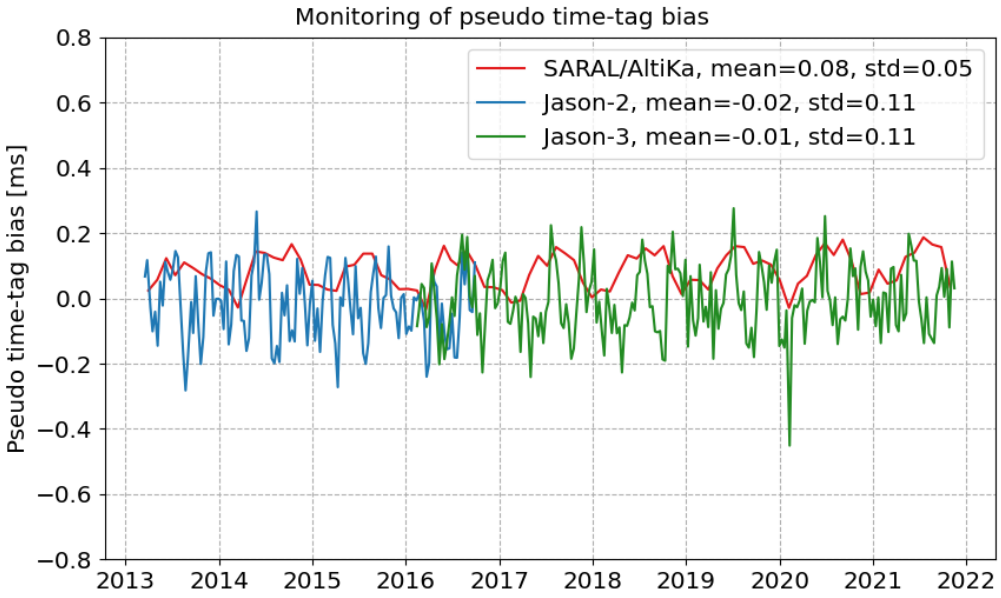

Figure 62: *Cycle per cycle monitoring of the pseudo time tag bias for SARAL/AltiKa and Jason-2*

6. Sea Level Anomalies along-track analysis

6.1. Overview

The Sea Level Anomalies (SLA) are computed along track from the SSH minus the mean sea surface where the SSH is estimated as defined in the previous section (5.1.):

$$SLA = SSH - MSS$$

Please keep in mind that only valid data is used here so that all mispointing events are properly discarded during the validation process and thus have no significant impact on the following metrics.

Figure 63 shows two maps of SLA from SARAL/AltiKa and Jason-3 over one cycle of SARAL/AltiKa (here cycle 153). The two maps show very similar patterns.

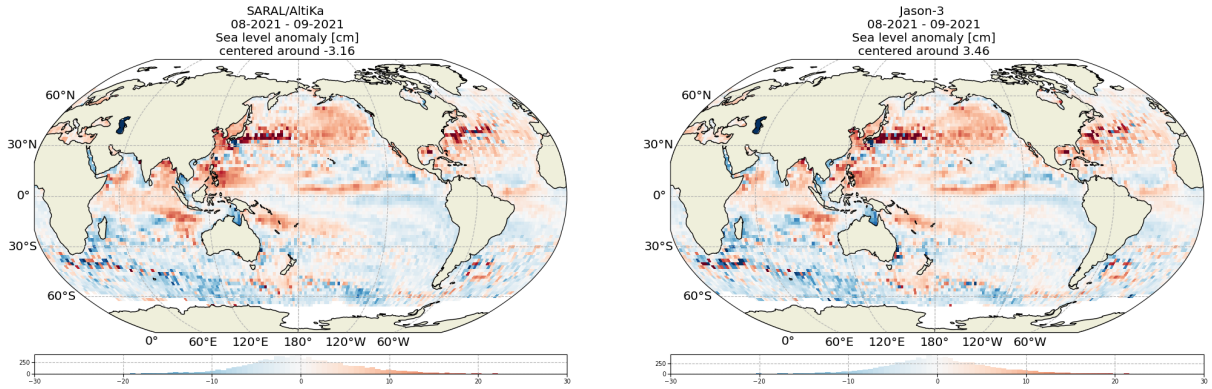

Figure 63: *SLA map for SARAL/AltiKa 153 cycle using the radiometer wet tropospheric correction (left) from SARAL/AltiKa data, and (right) from Jason-3 data over the same period.*

Computing differences between SARAL/AltiKa and Jason-3 allows a better appreciation of potential discrepancies between the two missions than individual maps. Figure 64 displays the average SLA differences between SARAL/AltiKa and Jason-3, for the radiometer and the modeled wet tropospheric correction. Both maps show geographically correlated differences with amplitudes up to ≈ 2 cm. The patterns are very similar to the ones observed at SARAL / Jason-3 crossovers with a positive patch arround the equator. When using the model wet tropospheric correction on both missions, the amplitude of the differences is slightly reduced and with North/South patches.

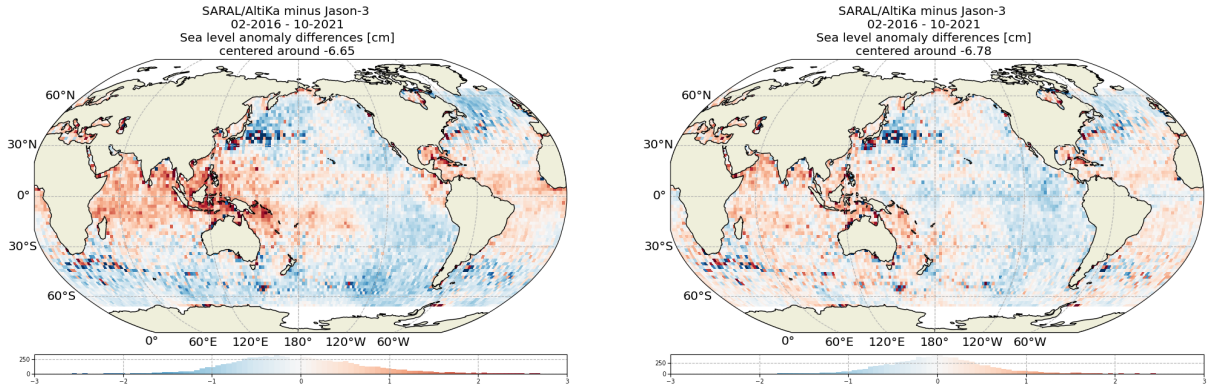

Figure 64: *Map of mean SLA differences between SARAL/AltiKa and Jason-3 using (left) the radiometer and (right) model wet tropospheric correction.*

6.2. Along-track SLA performances compared to Jason-2 and Jason-3

Looking at along-track SLA provides additionnal metrics to estimate the altimetry system performances. The evolution of the mean SLA allows the detection of shifts, drifts or geographically correlated biases, while looking at the SLA variance may also highlight changes in the long-term stability of the altimeter's system performance. Figure 65 displays the temporal evolution of the daily mean and standard deviation of SARAL/AltiKa Jason-2 and Jason-3 SLA, while figure 66 shows SLA differences between SARAL/AltiKa and both Jason-2 and Jason-3.

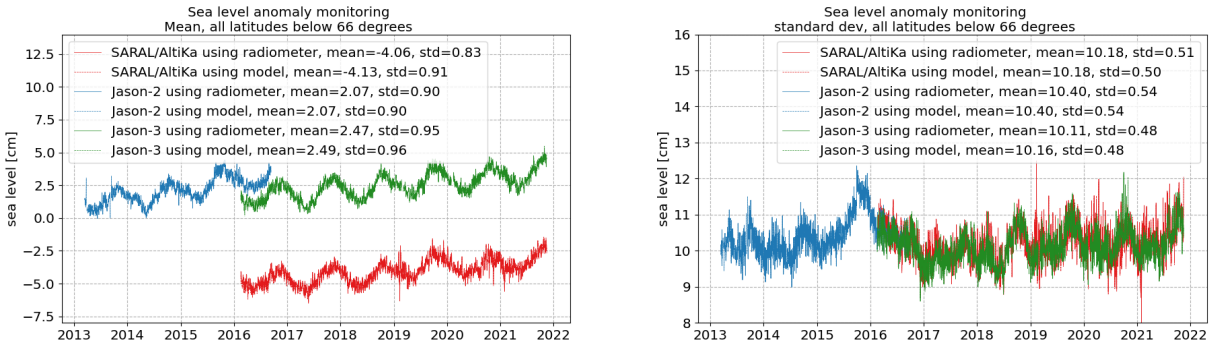

Figure 65: *Monitoring of daily mean (left) and daily standard deviation (right) of SLA of GDR data using the radiometer (plain lines) and the model (dotted lines) wet tropospheric corrections. Global statistics are estimated for all latitudes between* $-66°$ *and* $66°$.

SARAL/AltiKa Jason-2 and Jason-3 daily mean and standard deviation of SLA show similar signals and evolution.
There is an offset between SARAL/AltiKa and Jason-3 of around **-6.5** *cm* (see figure 66), which is quite consistent with the multi-mission crossovers analysis. The standard deviation of daily averages of SLA differences is $\approx$ **5** *mm*. No statistically significant drift is observed between SARAL/AltiKa and Jason-2 nor with Jason-3 (see figure 57). Switching from the radiometer to the model wet tropospheric correction has little impact on daily averages of SLA differences between SARAL/AltiKa and Jason-2 or Jason-3, as daily SLA variations are much larger than the difference between wet tropospheric corrections.

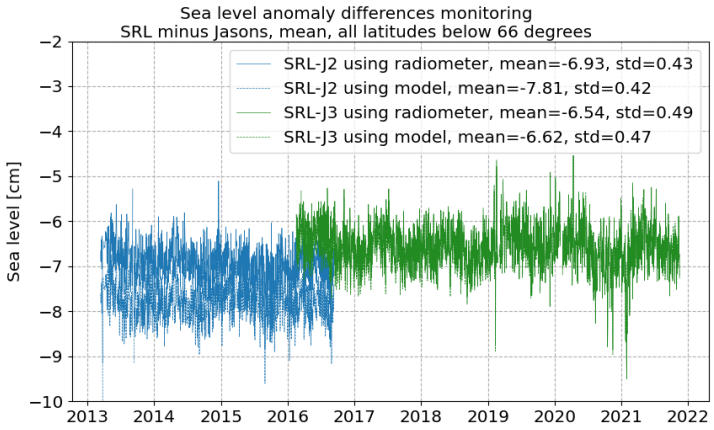

Figure 66: *Monitoring of the daily mean SLA difference between SARAL/AltiKa and Jason-2 / SARAL/AltiKa and Jason-3, using the radiometer and model wet tropospheric corrections.*

6.3. Along-track performances of the different product types (OGDR/IGDR/GDR)

SARAL/AltiKa products are available for three data types (with different latencies and precision): OGDR, IGDR and GDR. These products show somes differences in the product content which are summarized in table 7). Figure 67 displays the evolution of the mean and standard deviation of global SLA, as it is in the different products currently available. There are several shifts on the mean OGDR and IGDR values:

- in Feb 2014, when OGDR and IGDR, changed from Patch 1 to Patch 2,
- in July 2014, due to mean sea surface and editing changes.
- in Jan 2020, when OGDR and IGDR, changed from GDR-T to GDR-F,

Regarding standard deviation, GDR products show the lower standard deviation with 10.66 *cm*, while IGDR and OGDR data show a higher SLA variability, which is expected from less accurate geophysical corrections and orbit solutions. As for the peaks observed at the begining of February 2019, they are explained by the large amplitude of attitude deviation right after SSA. It impacts direclty the orbit estimation, harshly for OGDR data and to a lesser extent for IGDR and GDR data.

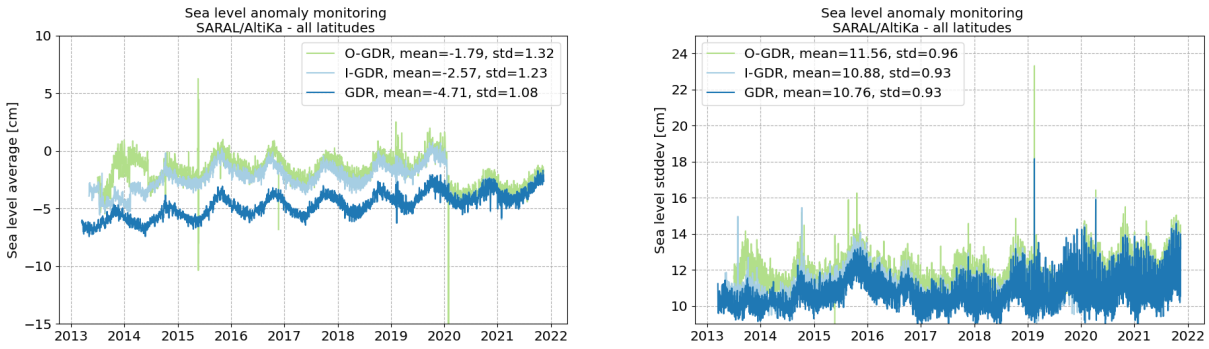

Figure 67: *Daily monitoring of the mean (left) and standard deviation [right] of global average SARAL/AltiKa SLA, using the radiometer wet tropospheric correction, for OGDR, IGDR and GDR products.*

6.4. SARAL/AltiKa as part of the GMSL record

SARAL/AltiKa data can easily be merged to the global Global Mean Sea Level (GMSL) record.

Left of figure 68 displays how SARAL/AltiKa blends in with the reference GMSL record while right is a focus on the SARAL/AltiKa period. Even though SARAL/AltiKa is not used to build the reference GMSL indicator (see [18] for further details) , with nearly seven years of data, and Jason-2/ Jason-3 covering the same period, we can give some credit to SARAL/AltiKa's global sea level trends estimates. Over the same periods SARAL/AltiKa shows very similar global mean sea level rise rates compared to Jason-2 and Jason-3 respectively.

A slight drift is observed since 2019 and is under investigation. It may come from the new method of calculating the inter-mission biais. It is no longer computed for each mission (SARAL/AltiKa/Jason-2 and SARAL/AltiKa/Jason-3) but only one biais is computed between SARAL/AltiKa and reference GMSL. Please note a study [68] report that Jason-3's radiometer has a drift of ≈ 0.5 mm/year. When using model Wet tropospheric corection, see botom of figure 68, the drift start later and is less significative.

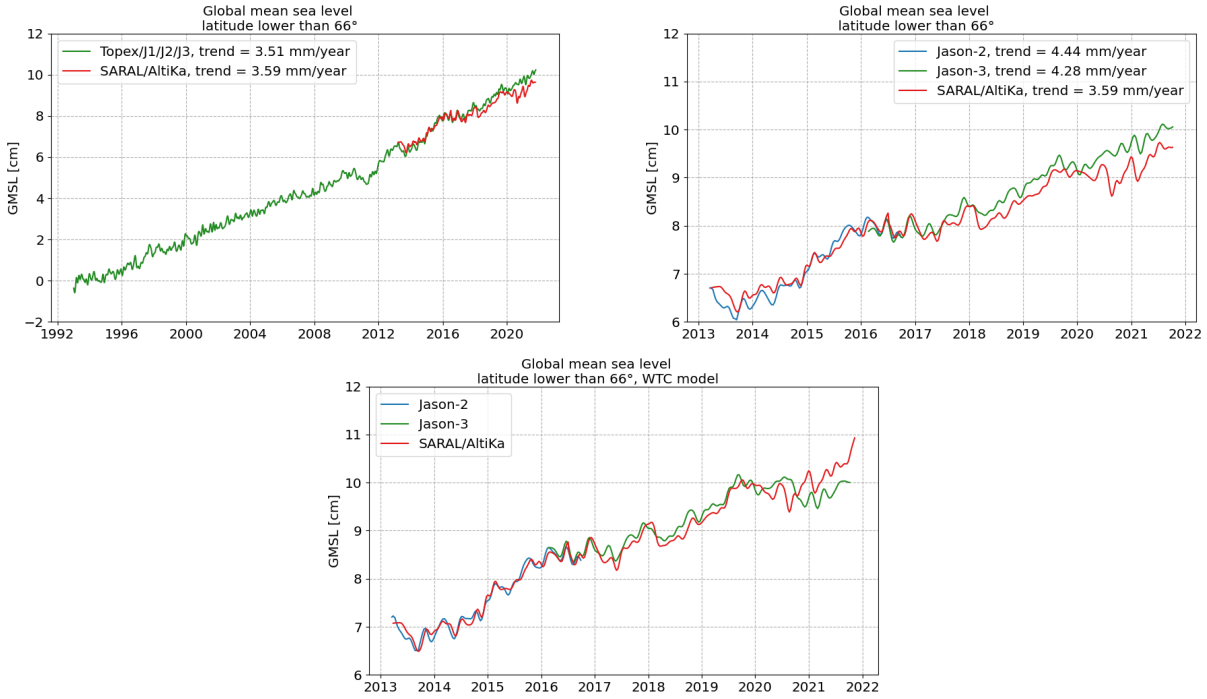

Figure 68: *[left] SARAL/AltiKa global mean record compared to the reference global mean sea level from TOPEX/Poseidon, Jason-1 and Jason-2 and Jason-3, and [right] a zoom on the SARAL/AltiKa period. [botom] GMSL with model wet tropospheric correction.*

As for tide gauge comparison, figure 69 shows SLA differences between the altimeters and the GLOSS/CLIVAR tide gauge network for Jason-3 (left) and SARAL/AltiKa (right). For more details about the calculation methods and the data used to have such comparisons, please feel free to check it out in the annual report of MSL activities [19]. As shown in the right panel of figure 69, the difference between SARAL/AltiKa's and tide gauge's SLA estimation is lower than $5mm$. As with the GMSL, a slight drift is visible since 2020, but it is still within the incertitude range.

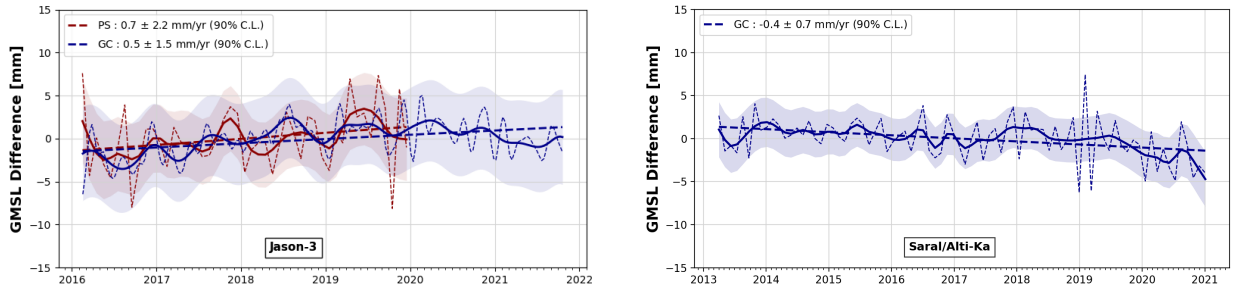

Figure 69: *SLA differences between the altimeters and the GLOSS/CLIVAR tide gauge network for Jason-3 (left) and SARAL/AltiKa (right).*

7. Particular Investigation : Mission error budget

The present section documents the activities undertaken in the framework of the CALVAL activities to assess SARAL/AltiKa's GDR-F ocean error budget. Computing the error budget of a mission is a very complex work that was initiated on older altimetric missions and for GDR-D dataset. The first envisat error budget was addressing each post of error, integrated in time and space [61]. Then Jason-2's error budget mainly adressed the 10 days correlated errors and long term trends [62]. Studies showed that the errors made on of each correction could be decomposed spectrally for different wavelengths, highlighting the different behaviors of each component of the sea suirface signals ([46] & [47]). In 2018, with Sentinel3-A (*Sentinel3-A STM error budget from MPC project*) and SARAL/AltiKa GDR-D's ocean error budget, the higher frequencies are addressed more closely, including different sea surface features and instrumental and processing effects. This error budget update for the latest "GDR-F" standards covers the same features as the ones presented in the 2018 Annual Report for the "GDR-D" standard.

7.1. Temporal and spatial error scales

In altimetry, several types of errors can be assesed. They are mainly defined by temporal and spatial scales :

- Sub mesoscales and mesoscales errors
  - White noise: this error is a high frequency uncorrelated error (in space and time) and is often due to instrumental noise (altimeter).
  - Short timescale errors ($<$ 10 days): these errors include both temporally correlated and uncorrelated errors for time scales lower than 10 days. They are important to define for mesoscale/sub-mesoscale oceanography applications.
- Climate scales errors
  - Medium temporal errors (2 months – 1year): these errors include all temporally correlated errors at medium scales such as periodic signals (annual, semi-annual...). The description of these errors is useful for climate application.
  - Long-term errors ($>$ 1 year): these errors include inter-annual signals and drifts. It is the most important for climate applications as for instance the global mean sea level evolution.

In this study we will focus mainly on the first type of errors. Our objective here is to give a feedback on instrumental and processing performances and not to determine potential limitations at large temporal scales.

7.2. Error estimation techniques

Assessing the errors on altimeter's parameters and the resulting geophysical corrections is not straight forward. Errors can be indeed of a very different and complex nature since they can be correlated to both spatial and temporal scales. Several methods can be used to compute their estimations. The following study, will focus mainly on global high frequency errors.

7.2.1. Spectral analysis

The spectral analysis allows to identify the repartition of energy in the sampled signal as a function of the spatial scales involved (wavelength in km). These wavelenghts can be converted into temporal frequencies with the relation: Wavelength = Ground Satellite Speed / Frequency. The method consists in averaging N Fast Fourier Transform computed over a sample of M along-track points. The bandwidth analysed with this method concerns wavelength between the inverse of the spectrogram window's size and the Shannon frequency ($2\Delta x$ where Δx stands for the sampling frequency that is to say the distance between two consecutive measurements.)

The spectral analysis gives access to an estimation of high frequency errors considering that the energy α for very short wavelength (between 500m and 1 km), cannot be related to oceanographic signals but rather to instrumental and processing errors. The high frequency error σ is extracted from the PSD white noise floor as follows :

$$\sigma = \sqrt{\frac{\alpha}{2\Delta x}} \tag{2}$$

where α corresponds to the ordinate of the fitted value of the noise floor and $2\Delta x$ to the Shanon frequency.
Note that Δx is a sampling-dependant parameter : Δx = Ground Satellite Speed / Sampling Frequency. However, Thibaut et al showed that high frequency errors σ do not depend on the sampeling frequency since they demonstrated that 40Hz and 20 Hz spectral analysis of SARAL/AltiKa's data give the same results in terms of high frequency noise (20 Hz data obtained by under-sampling the 40Hz dataset, see [48] for more details). Hence, we can compare the high frequency errors of SARAL/AltiKa to Jason-3 and Sentinel3-A regardless of their sampeling frequencies (40 Hz, 20Hz, 20Hz respectively).
Note also that the resulting error describes high frequency errors mixing different kind of sea state (high/low sea state areas). To be consistent with the requirements which specify a noise level for SWH equal to 2m, we will use the next method based on the standard deviation computed while averaging the 40Hz parameters into 1Hz measurements.

7.2.2. Standard deviation analysis

For needs of most users, the altimeter dataset is compressed from 40 Hz to 1Hz. The standard deviation derived from averaging forty consecutives high resolution (40Hz) measurements into 1Hz measurements can give an estimation of the noise at 40 Hz. The underlying hypothesis that over 7 km along-track portions (which stands here for the distance between 2 consecutive 1Hz measurements for SARAL/AltiKa), there is no or few geophysical signals is in general reliable. The benefit of this methods is to have an estimation of the noise as a function of SWH which is in line with the mission's specifications.

7.2.3. From 40 Hz to 1 Hz

The two methods described so far give an estimate of the noise for 40 Hz measurements whereas the requirements' specifications are given for 1Hz averaged values. According to Zanife et al. [28], the 40Hz noise estimation can be approximately related to the 1Hz noise level using the decorrelation assumption of the high rate data over 1s, thus the division by $\sqrt{40}$ results in the 1Hz noise level. This assumption will be used in the following over 40Hz and 20Hz data- hence $\sqrt{20}$ - as Jason-3 and Sentinel3-A are two 20Hz missions SARAL/AltiKa will be compared to.

7.3. Dataset and requirements

7.3.1. Dataset

If not specified otherwise, this study was led on the so-called GDR-F product version, detailed in SARAL/AltiKa's handbook [52]. GDR-D product version is used for comparison. Validation report of GDR-F product [59] detailed differences between the two versions. Sentinel3-A's datatset used for comparison purposes only, is Sentinel3-A's PDGS product. As for Jason-3's, the comparisons were led on the GDR-F standards of GDR products. For Jason-3, only 1Hz dataset is used because the validity flag is not currently available for the 20Hz dataset. Table 8 lists the various corrections applied to retrieve the SLA. As SARAL/AltiKa uses a single frequency, no dual frequency ionosphere correction is available and thus GIM model is used instead.

Parameter	SARAL/AltiKa GDR-F	SARAL/AltiKa GDR-D	Sentinel3-A	Jason-3
Orbit	POE-F standard	POE-E standard	POE-F standard	POE-F standard
Range	MLE4	MLE4	MLE4	MLE4
Wet troposphere correction	Radiometer (NN patch4)	Radiometer (NN patch2)	Radiometer	Radiometer
Dry troposphere correction	ECMWF model	ECMWF model	ECMWF model	ECMWF model
Ionosphere correction	GIM model	GIM model	GIM model	GIM model
Dynamycal atmospheric correction	High resolution MOG2D model	High resolution MOG2D model	High resolution MOG2D model	High resolution MOG2D model
Sea state bias	SSB compute with SSB tables (method proposed by Tran, 2018 [34] and [33])	Empirical model	SSB compute with SSB tables	SSB compute with SSB tables
Ocean tide correction	FES14B	GOT4.10	FES14B	FES14B
		.../...		

Parameter	SARAL/AltiKa GDR-F	SARAL/AltiKa GDR-D	Sentinel3-A	Jason-3
Pole tide correction	DESAI with new IERS linear mean pole	Wahr 85 model	DESAI with new IERS linear mean pole	DESAI with new IERS linear mean pole
Solid earth tide correction	Cartwright Tayler 71 model	Cartwright Tayler 71 model	Cartwright Tayler 71 model	Cartwright Tayler 71 model
Internal tide correction	Zaron with M2, K1, S2, O1 waves	None	Zaron with M2, K1, S2, O1 waves	Zaron with M2, K1, S2, O1 waves
Mean Sea Surface	CNES-CLS 2015 model	CNES-CLS 2015 model	CNES-CLS 2015 model	CNES-CLS 2015 model

Table 8: *Main parameter used in sea surface height (SSH) computations.*

7.3.2. Requirements

Table 9 provides a summary of the preliminary error budget derived from [51].

Error type	Req	Goals
Altimeter Noise	1.5 cm	1 cm
Sea state bias	2 cm	2 cm
Wet troposphere	1.2 cm	1 cm
Dry troposphere	0.7 cm	0.7 cm
Ionosphere	0.3 cm	0.3 cm
Altimeter range after corrections (RSS)	2.9 cm	2.6 cm
Orbit radial component (RMS)	3 cm	2 cm
Total sea surface height (RSS)	4.2 cm	3.2 cm
.../...		

Error type	Req	Goals
Significantg wave height	6.3 cm	3.9 cm
Sigma naught Absolute Value after in-flight calibration	0.7 db	0.5 db
Wind speed	1.7 m/s	1 m/s

Table 9: *Preliminary error budget for 1Hz measurements at 2m average SWH.*

Generally speaking SARAL/AltiKa has been specified based on Jason-2's state of the art, including improvements in payload technology, data processing and algorithms. The sea-surface height shall be provided with a globally averaged (RMS) error of 4.2 cm or better (1 sigma), assuming 1 second averages. The instrumental and environmental corrections are provided with the appropriate precision to meet this requirement. In addition to these requirements, a set of measurement-system goals was established based on the anticipated impact of off-line ground processing improvements. These improvements are expected to reduce sea-surface height errors down to 3.2 cm (RMS).

7.4. Global high frequency errors

This section details the estimation of high frequency errors for the main parameters of table 9 when possible.
The spectral analysis is done over a 20 days period, two times 10 consecutive days with a 6 months gap (from 18/02/2017 to 28/02/2017 and from 17/08/2017 to 27/08/2017), for the segments to be sampled over different kind of sea states and seasonnal features. On the other hand, the noise estimation derived from the standard deviation method is applied over a longer period to have consolidated statistics for all the values of SWH, here cycle 106 of SARAL/AltiKa. High latitudes and costal areas have been removed to keep only open ocean data and an appropriate editing has been applied to remove outliers.

7.4.1. Altimeter range

The sea level content provided by most of the conventional altimeters in low resolution mode (LRM) does not allow the observation of ocean scales smaller than 80-100 km (Dibarboure et al.,2014 [12]). This limitation is mainly due to surface heterogeneities in the altimeter footprint (e.g. rain, sigma blooms) and the white noise level due to instrumental and processing features. The spectral analysis of the sea level anomaly defined as in equation 3 allows to precisely assess the range high frequency signals since orbit and mean sea surface (MSS) are low frequency quantities.

$$SLA_{raw} = Orbit - Altimeter\ Range - Mean\ Sea\ Surface \tag{3}$$

Fitting the PSD floor plotted figure 70 gives access to the white noise estimate σ using 2. The three spectra exhibits the same signals at large scales ($> 100km - 80km$) wherease at smaller scales (below $50km$), they show different behaviors. While LRM altimeters data present a white noise floor, SARM data exhibit a red noise signal explained by the sensitivity of the SAR mode to the swell direction and period (Raynal et al [49]).
Anyway, table 10 summerizes the noise estimate for the three datasets. The 1Hz white noise is computed from the 40Hz /20Hz white noise as explained in section 7.2.3..

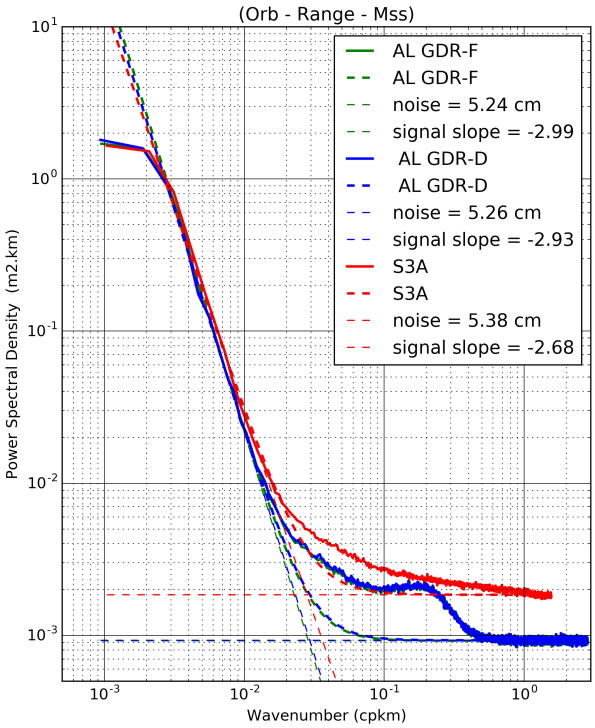

Figure 70: *SLA spectra for SARAL/AltiKa GDR-F, SARAL/AltiKa GDR-D, and Sentinel3-A.*

Mission	40Hz error	1 Hz error
SARAL/AltiKa GDR-F	5.24 cm	0.83 cm
SARAL/AltiKa GDR-D	5.26 cm	0.83 cm
Sentinel3-A (20 Hz)	5.38 cm	1.20 cm

Table 10: *Range high frequency error estimate for 40Hz and 1Hz dataset using spectral analysis.*

The spectral analysis method is very appropriate to assess and compare high frequency energies, but it does not consider a specific sea state as mentioned in the requirements' specification table 9. Indeed, the segments selected before the Fast Fourier Transform computation are representative of a global sea state as shown figure 71. The average sea state sampeled here is quite in line with the 2m-SWH described in the requirements, thus the noise estimate is in line with the requirements.

The map of SARAL/AltiKa's range standard deviation is showed figure 72). The geophysical distribution of the values is clearly related to the SWH distribution (Figure 72 right) so that the range standard deviation values could be naturally extracted for different kinds of sea states.

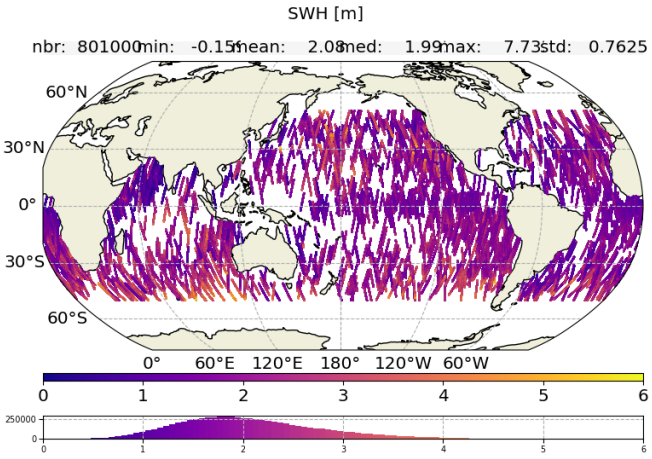

Figure 71: *Global sea state for the selected segments for all the following PSD analysis.*

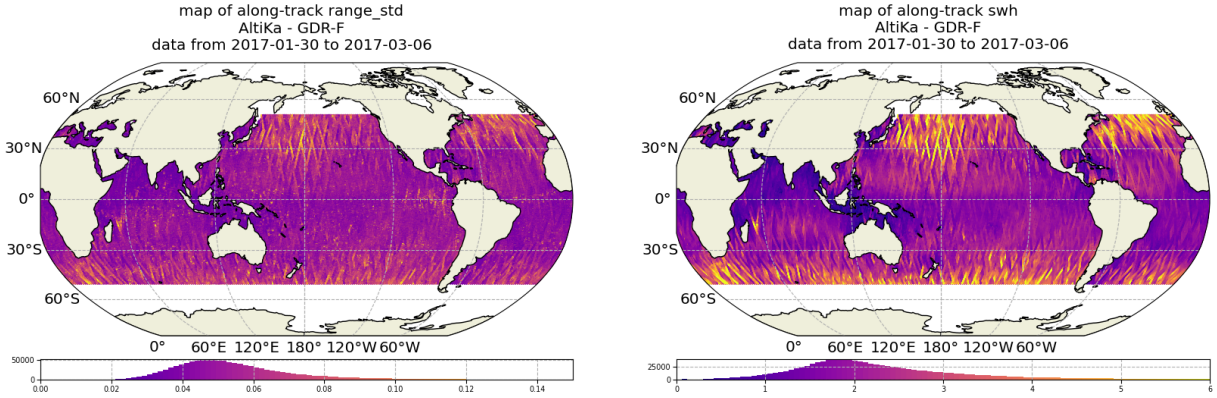

Figure 72: *Std. Range and SWH global distribution (Cycle 106).*

The standard deviation estimated within a series of 40 high resolution measurements considered as independent is supposed to give an estimate of the 40Hz range white noise. Indeed, for this range of wavelength , 7 Km for 40 consecutive high resolution measurements, we make the assumption that the signal observed does not contain any oceanic structures, hence the range variations between the 40Hz measurements are at this point only related to the noise.
But, this assumption is quite questionable since the white noise plateau of SARAL/AltiKa's range spectrum does not reach 7 Km where indeed the signal observed includes an important part of the hump. For a 2m SWH, the 40Hz and 1 Hz metrics have been reported in Table 11, they are fully in line with the requirements (9).
Even though the average sea state sampeled for the PSD (figure 71) is close to 2m-SWH, it includes errors due to sea states up to 4m-SWH, whereas the latter method takes into account only 2m-SWH errors. Hence, the figures are indeed slightly below the ones derived from the spectral method but still of the same order of magnitude.
As expected, there is no significant difference betwen GDR-D and GDR-F for range high frequency error estimate. The only differences between both versions are instrumental corrections which have no impact on spectral analysis.

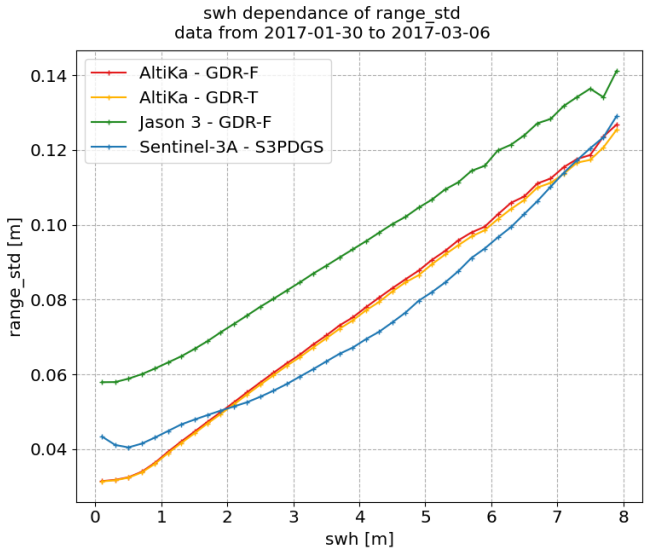

Figure 73: *Evolution of the 40Hz range standard deviation (20Hz for Sentinel3-A and Jason-3) wrt SWH (Cycle 106).*

Mission	40Hz error	1 Hz error
SARAL/AltiKa GDR-F	5 cm	0.8 cm
SARAL/AltiKa GDR-D	5 cm	0.8 cm
Sentinel3-A (20 Hz)	5 cm	1.1 cm
Jason-3 (20 Hz)	7.1 cm	1.6 cm

Table 11: *Range heigh frequency error estimate for 40Hz and 1Hz dataset using Std analysis for SWH = 2 m.*

7.4.2. Sea Surface Height

In the following, SLA_{raw} and SLA_{corr} and SLA will refer to :

$$SLA_{corr} = SLA_{raw} - \sum_{i=1} Correction_i \tag{4}$$

where SLA_{raw} stands for the SLA as defined in equation 3 and the sum of corrections expands as:

$$\begin{aligned} \sum_{i=1} Correction_i &= Dry\ troposphere\ correction \\ &+ Dynamical\ atmospheric\ correction \\ &+ Radiometer\ wet\ troposphere\ correction \\ &+ Ionospheric\ correction \\ &+ Sea\ state\ bias\ correction \end{aligned}$$

$$SLA = SLA_{corr} - \sum_{i=1} TidalEffect_i \tag{5}$$

where the sum of tidal effects expands as:

$$\begin{aligned} \sum_{i=1} TidalEffects_i &= Ocean\ tide \\ &+ Pole\ tide \\ &+ Earth\ tide \\ &+ Internal\ tide \end{aligned}$$

Internal tide was not available for GDR-D dataset.
PSD of SLA_{raw}, SLA_{corr} and $SLA_{raw} - SSB$ are plotted for SARAL/AltiKa and Sentinel3-A on figure 74. On the right plot of figure 74, we can easily see how the blue curve is quite comparable to the red curve showing the poor impact of the corrections other than SSB on the high frequency components of the SSH. That is to say that all the atmospheric effects accounted for here seem to have no high frequency content, at least not at the scales assessed so far. The left plot of figure 74 shows the same features on Sentinel3-A's spectra. Anyway, the total SSH high frequency errors are reported in table 12, and the value for SARAL/AltiKa is well within requirements.

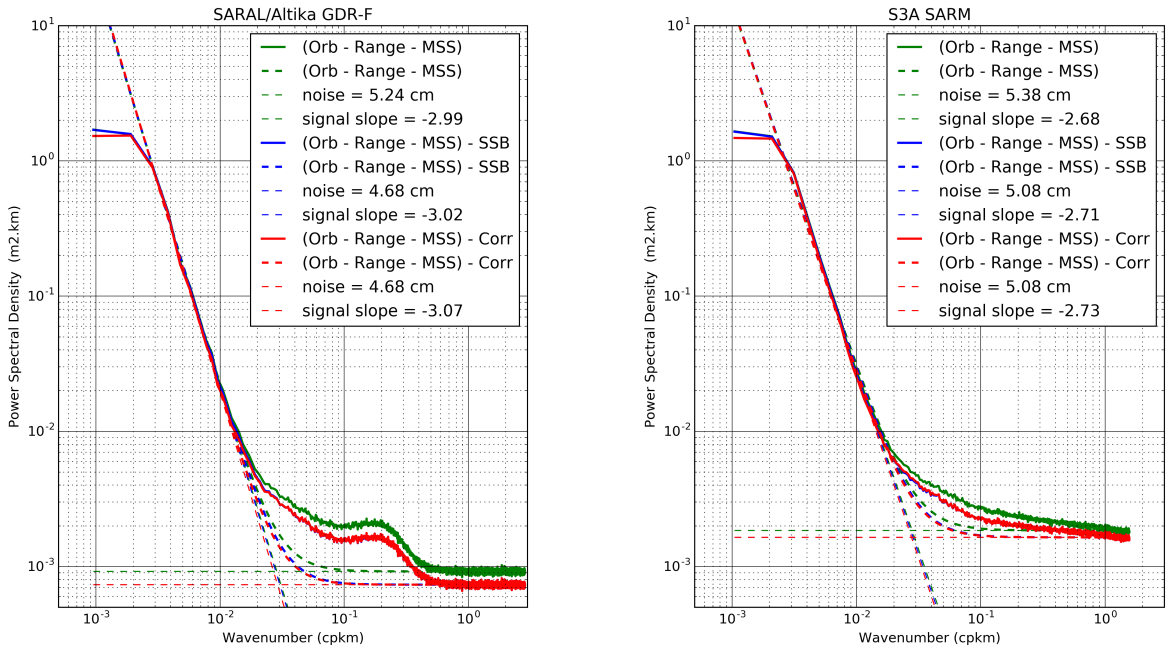

Figure 74: *Corrected range and SSH spectra .*

Mission	40Hz error	1 Hz error
SARAL/AltiKa GDR-F	4.68cm	0.74 cm
Sentinel3-A (20 Hz)	5.08 cm	1.14 cm

Table 12: *SSH high frequency error estimate for 40Hz and 1Hz dataset.*

7.4.3. Significant Wave Height

SWH spectra have been computed for both version of SARAL/AltiKa and Sentinel3-A. Fitting the plateau of the PSD spectra plotted in figure 75 gives access to the noise on SWH measurements following equation 2.

The results reported in table 13 show that SARAL/AltiKa's noise on SWH is of $32cm$. SARAL/AltiKa's SWH PSD exhibits a double bump (compared to Jason-3 that shows only one hump and Sentinel3-A no hump at all) that is yet to be investigated.
The 1Hz error of $5.1cm$ is above the aimed value specified in Table 9 but clearly below the required value of $6.3cm$. The metrics given before are for the same global sea state represented in figure 71.

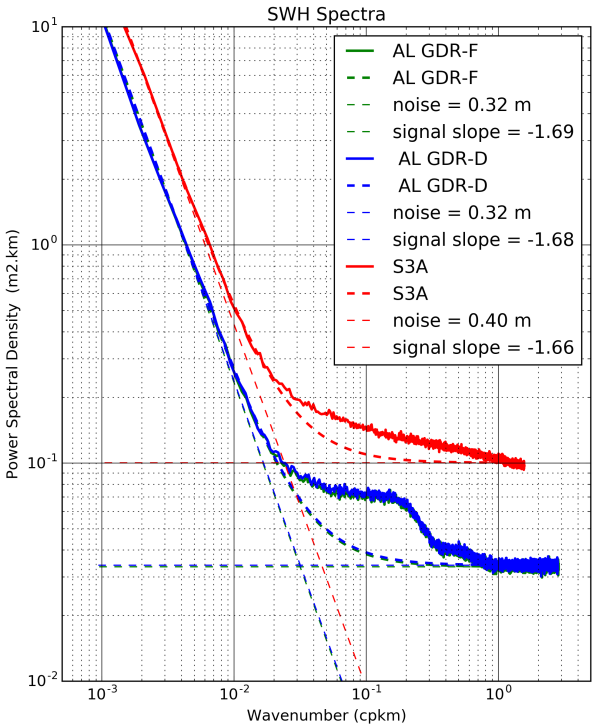

Figure 75: *SWH spectra for SARAL/AltiKa and Sentinel3-A*

There is no significant difference between GDR-F and GDR-D dataset.

Mission	40Hz error	1 Hz error
SARAL/AltiKa GDR-F	32 cm	5.1 cm
SARAL/AltiKa GDR-D	32 cm	5.1 cm
Sentinel3-A (20 Hz)	40 cm	8.9 cm

Table 13: *SWH high frequency error estimate for 40Hz and 1Hz dataset.*

The map of SARAL/AltiKa's SWH standard deviation on the left of figure 76 shows a clear correlation between the geophysical distribution of the standard deviation of SWH and the SWH distribution itself (figure 76 right). Hence figure 77 where the standard deviation of 40 Hz SWH measurements is extracted for different kinds of sea states. Table 14 reports the results obtained for a 2 m sea state.

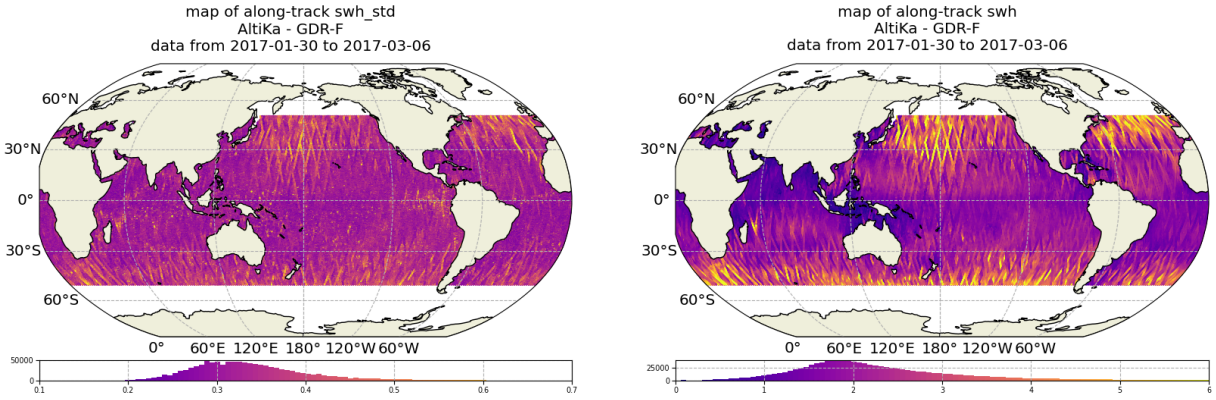

Figure 76: *Std. SWH and SWH global distribution (Cycle 106).*

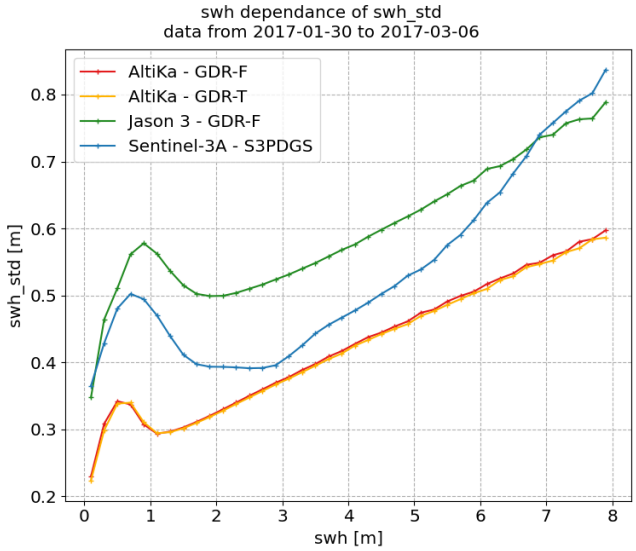

Figure 77: *Evolution of the 40Hz (20Hz for Sentinel-3A and Jason 3) swh standard deviation as function of the SWH (Cycle 106).*

The SWH noise values obtained with this method are perfectly in line with those derived from spectral analysis.
The results summarized in table 14 are very satisfying concerning SARAL/AltiKa since they are still within requirements (below 6.3cm).

Mission	40Hz error	1 Hz error
SARAL/AltiKa GDR-F	32 cm	5.1 cm
SARAL/AltiKa GDR-D	32 cm	5.1 cm
Sentinel3-A (20 Hz)	39 cm	8.7 cm
Jason-3 (20 Hz)	50 cm	11.2 cm

Table 14: *SWH heigh frequency error estimate for 40Hz and 1Hz dataset for SWH = 2 m.*

7.4.4. Sigma Naught

Sigma naught spectra have been computed for both version of SARAL/AltiKa and Sentinel3-A.The results summarized in table 17 show how SARAL/AltiKa's noise level is quite lower than Sentinel3-A, and fifty times lower than the required value of 0.5 dB.

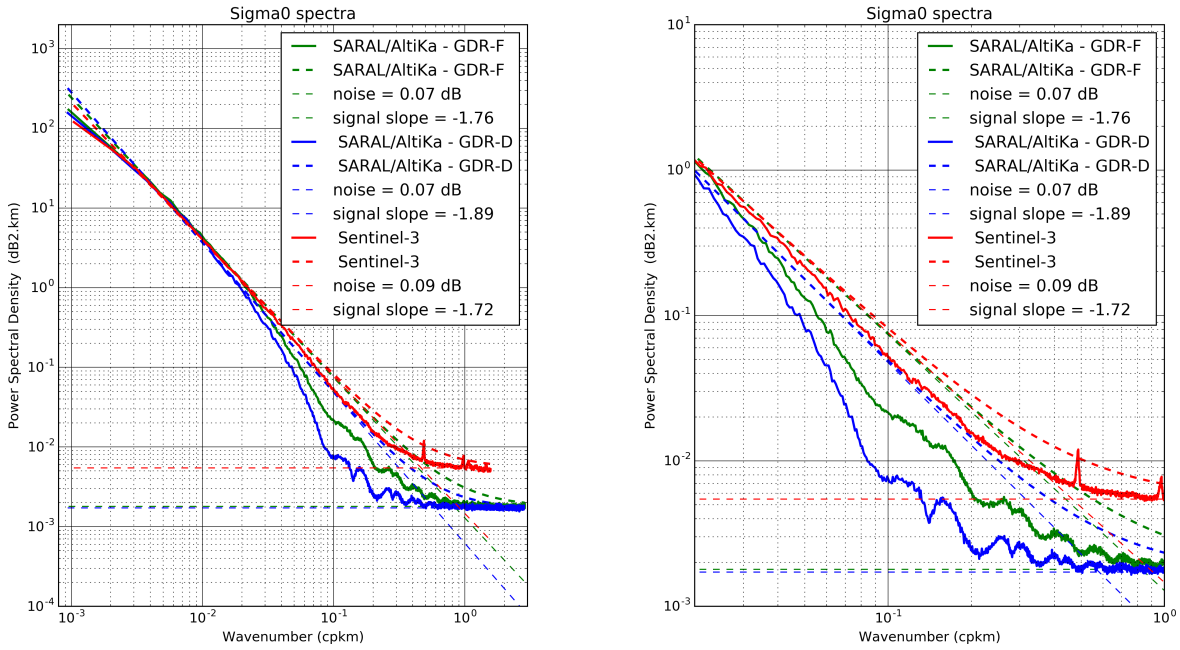

Figure 78: *40 Hz Sigma naught spectra for both version of SARAL/AltiKa and Sentinel3-A [left]. Zoom over 50km-1km scale [right]*

GDR-F and GDR-D reach the same noise level but with significant signal differences between 50km

and 1km. There are two main differences between both versions of the backscatter coefficient, the updated atmospheric atenuation and the CAL2 computation. The low pass filter of CAL2 is now normalized using the maximum value instead of the average, which could explains the differences in spectral analysis.

Mission	40Hz error	1 Hz error
SARAL/AltiKa GDR-F	0.07 dB	0.01 dB
SARAL/AltiKa GDR-D	0.07 dB	0.01 dB
Sentinel3-A (20 Hz)	0.09 dB	0.02 dB

Table 15: *Sigma naught high frequency error estimation for 40Hz and 1Hz dataset.*

The map of SARAL/AltiKa's Sigma naught standard deviation on the left of figure 79 shows no real correlation between the geophysical distribution of the standard deviation of Sigma naught and SWH distribution (figure 76 right) but rather to the variation of Sigma naught itself (right of figure 79).

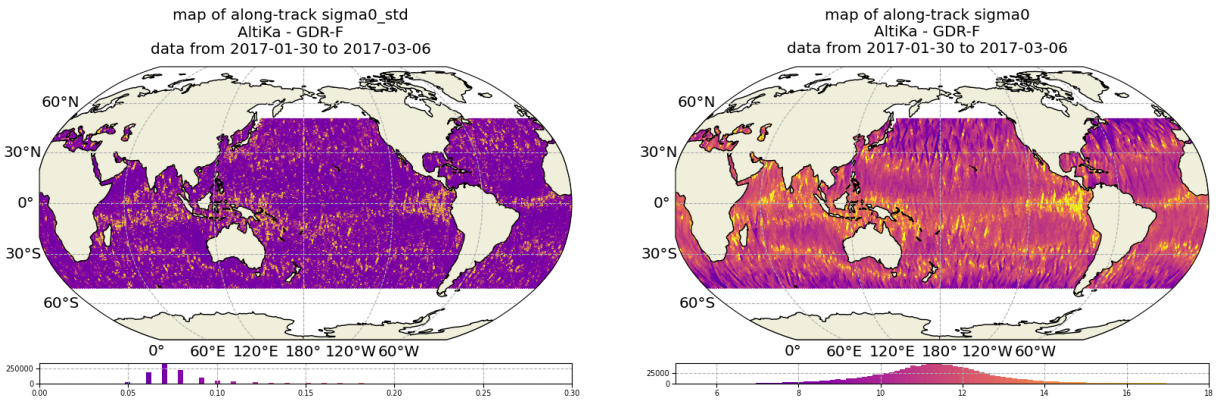

Figure 79: *Std. Sigma naught (letf) and Sigma naught(right) global distribution (Cycle 106).*

Figure 80 shows the standard deviation of 40 Hz SWH measurements extracted with respect to wave height (right) but also with respect to sigma naught (left).
As reported in table 16 the results obtained for an average 2m wave height and also for an average 11.25dB sigma naught are substantially the same and largely within requirements.

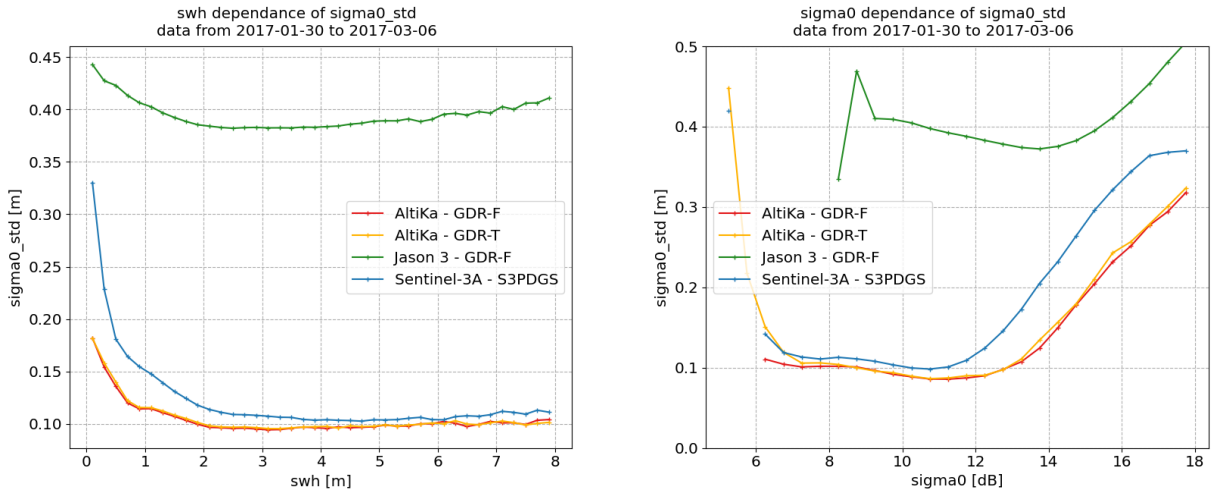

Figure 80: *Std. Sigma naught wrt SWH (left) and Sigma naught(right) distribution (Cycle 106).*

Mission	40Hz error (SWH)	1 Hz error (SWH)	40Hz error (SIG0)	1 Hz error (SIG0)
SARAL/AltiKa GDR-F	0.10 dB	0.016 dB	0.09 dB	0.014 dB
SARAL/AltiKa GDR-T	0.10 dB	0.016 dB	0.09 dB	0.014 dB
Sentinel3-A (20 Hz)	0.12 dB	0.025 dB	0.10 dB	0.022 dB
Jason-3 (20 Hz)	0.39 dB	0.087 dB	0.39 dB	0.087 dB

Table 16: *Sigma naught high frequency error estimation for 40Hz and 1Hz dataset.*

7.4.5. Wind Speed

In the GDR-F dataset, wind speed is provided within the 40-Hz products using a 2D empirical model developped by N.Tran [33] based on SWH and Sig0. That was not the case in the GDR-D dataset. For 2018's GDR-D error budget, 40-Hz wind speed had been recomputed from the 40-Hz sigma0 by applying the same equation as the one used in the 1Hz GDR-D production (1D version from Lillibridge et al [26]).

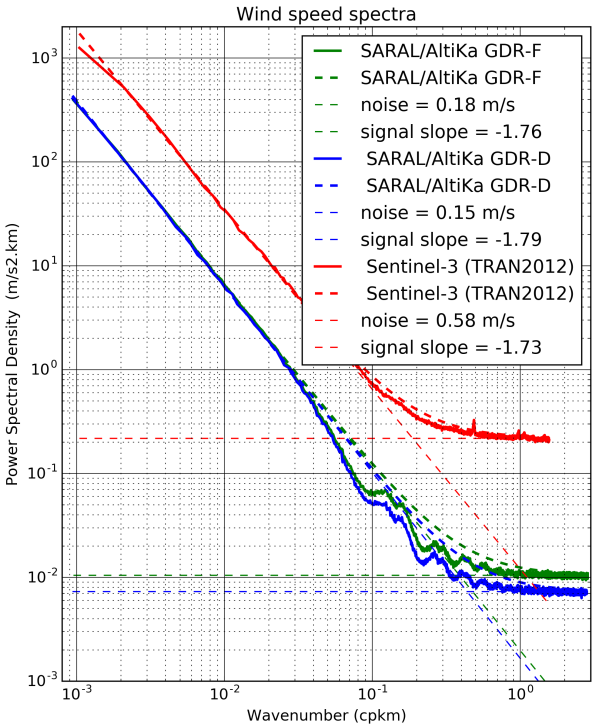

Figure 81: *40 Hz wind speed spectra for SARAL/AltiKa GDR-F compared to GDR-D and Sentinel3-A.*

As seen for all the previously assessed parameters, SARAL/AltiKa has the lowest noise level compared to Sentinel3-A. The noise of GDR-F wind speed is slightly higher than the one of GDR-D, but still well below the requirements ($1m/s$). The high frequency error estimates summarized in table 17.

Mission	40Hz error	1 Hz error
SARAL/AltiKa GDR-F	18 cm/s	2.85 cm/s
SARAL/AltiKa GDR-D	15 cm/s	2.37 cm/s
Sentinel3-A (20 Hz)	81 cm/s	18.11 cm/s

Table 17: *Sigma error estimation for 40Hz and 1Hz dataset.*

7.4.6. Sea State Bias

The non-Gaussian nature of the ocean surface induces a range bias in the instantaneously retrieved sea surface height (SSH). This effect is known as the electromagnetic bias and should be removed for accurate altimetry measurement of the sea level. This correction is now provided in the 40 Hz GDR-F products. It was not the case in the GDR-D dataset. In the 2018's ocean error budget, to assess high frequency signals, the sea state bias has been re-computed using GDR-D SWH and Wind speed (method proposed by N. Tran, 2018 [34] and [33]). This approach is the one used to generate the GDR-F reprocessed SSB.

Figure 82 shows the PSD of the SSB and its impact when applied to the range (as defined in equation 3).

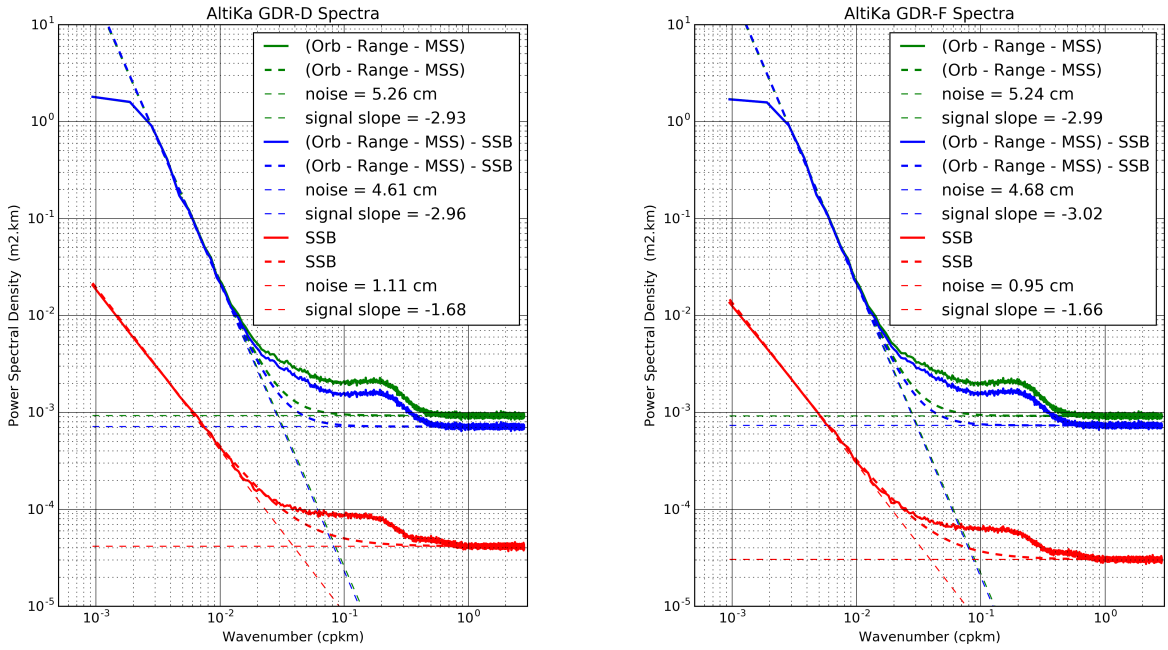

Figure 82: *SLA raw, SLA raw - SSB and SSB spectra for SARAL/AltiKa GDR-D [left] and -F [right].*

Two points can be highlighted: (1) above 200 km, SSB is a minor correction to the range and (2) below 100 km, SSB is a major player given the scales of wind and wave phenomena. The PSD of the reference SLA (Orbit - Range - MSS) displays a white noise floor of $5.24cm$. It reduces down to $4.68cm$ when the SSB correction is applied. The white noise floor observed on the PSD of the SSB correction alone is of $0.95cm$.

Mission	40Hz error		1 Hz error	
	GDR-D	GDR-F	GDR-D	GDR-F
SLA_{raw}	5.26 cm	5.24 cm	0.83 cm	0.83 cm
$SLA_{raw} - SSB$	4.61 cm	4.68 cm	0.73 cm	0.74 cm
SSB	1.11 cm	0.95 cm	0.18 cm	0.15 cm

Table 18: *SLA raw, SLA raw - SSB and SSB heigh frequency error estimate for 40Hz and 1Hz dataset.*

Tran et al ([34]) discussed the effects of sea-state related errors on high-rate altimeter sea level data. Intended to be a large-scale correction by design, the empirical form of the SSB correction introduces small-scale content because of the noisy nature of its inputs. As a consequence, some of the correlated tracker-related errors are also removed through the SSB correction when applied at high-rate, leading to a lower SLA high-frequency variability. Since the high-frequency content of the SSB correction is not large enough to remove completely the correlated errors coming from both random errors in waveform data and systematic errors in the waveform model, a high-frequency adjustment (HFA) depending on instrument, retracking algorithm and SSB version, can be additionally applied to achieve further noise mitigation objectives. Note that the HFA correction is implemented in the L2E products (Level 2 Expertise) that can be made available on request [22]. As it is not yet in the GDR products, we do not consider this correction here. Anyway, the estimates of the SSB white noise are given in Table 18, and they are way below specifications.

7.5. Global ocean error budget

Usually, the total sea surface height error is computed as follows:

$$Total\ Sea\ Surface\ Height\ Error(RSS) = \sqrt{\sum \sigma_i^2} \tag{6}$$

Where σ_i is the individual error for each i-parameter. This method is based on the assumption that all parameters involved in the computation are independant wich is obviously not true given the nature of some fields (e.g SSB correlated to the range as shown figure 82). Note that only high frequency errors have been assessed in this study. Dry troposphere and ionosphere corrections are respectively derived from ECMWF and GIM models and do not add extra noise at the scales assessed and thus have no high frequency content.
The results cannot be directly compared to those of GDR-D since SSB was computed using a "GDR-F" like method.
To have comparable metrics to those of the requirement table 9, we procede as follows :

- For high frequency quantities - that is to say *Altimeter noise, Significant wave height, Sigma naught, Wind speed* - the higher estimate of the noise is taken.
- For SSB, the value derived from the spectral analysis is used for high frequency errors. As for global errors, it is yet to be determined.

- For Dry troposphere and ionosphere corrections, there are no high frequency contents (at least not at the scale we're interested in), and global errors have not been tackled in this study.
- For Wet troposphere, the high frequency content have not been assessed yet. The global error is estimated using the difference between the radiometer and the ECMWF model wet troposphere. In fact, the standard deviation of the differences gives access to the sum of both errors, which is of $1.40cm$ for SARAL/AltiKa (see dedicated section 4.7.2.) . We assume that the model and radiometer wet troposphere contribute equaly in the total error, thus a division by $\sqrt{2}$ (see figure 44) is necessary to obtain the value reported in table 19. GDR-D's standard deviation of the differences was of $1.57cm$ (see 2018 error budget [57]), significantly higher than GDR-F value.
- For the orbit error (radial component), the global error was estimated using SLR RMS residuals method (detailed for Jason-1 and Jason-2 in [35]). Figure 83 shows the evolution of the error during 2018. The means value used here is the one direved from the red/green curve using only high elevation SLR stations.
- As for the global error on SSH, the value is derived from long term crossovers monitoring, where the standard deviation of the difference can be considered as a fair estimate of the global errors on SSH. Assuming that both arcs contribute equally in the global error, a division by $\sqrt{2}$ is applied to the mean value of the standard deviation ($5.0cm$). The value used here is the one refered to as *with selection , no weighting* in figure 59.

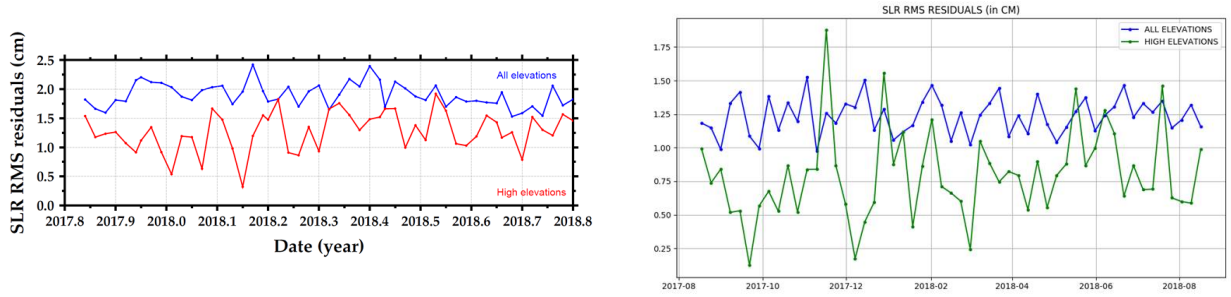

Figure 83: *Monitoring of the orbit error using SLR RMS residual over 2018 for POE-E [left] and POE-F [right]. (courtesy of A.Couhert)*

Error type	Req	Goals	Short scales (< 7km)		Large wavelenght short time scales (> 50 km,< 10 days)	
			GDR-D	GDR-F	GDR-D	GDR-F
Altimeter Noise	1.5 cm	1 cm	0.83 cm	0.83 cm	-	-
Sea state bias	2 cm	2 cm	0.18 cm	0.15 cm	TBI	TBI
Wet troposphere	1.2 cm	1 cm	TBI	TBI	1.1 cm	1.0 cm
Dry troposphere	0.7 cm	0.7 cm	-	-	0.7 cm	0.7 cm
Ionosphere	0.3 cm	0.3 cm	-	-	0.3 cm	0.3 cm
Altimeter range after corrections	2.9 cm (RSS)	2.6 cm (RSS)	0.73 cm	0.74 cm	TBI	TBI
Orbit radial component	3 cm	2 cm	-	-	1.3 cm	0.80 cm
Total sea surface height	4.2 cm	3.2 cm	0.73 cm	0.74 cm	3.7 cm	3.5 cm
Significantg wave height	6.3 cm	3.9 cm	5.1 cm	5.1 cm	-	-
Sigma naught Absolute Value after in-flight calibration	0.7 dB	0.5 dB	0.016 dB	0.016 dB	-	-
Wind speed	1.7 m/s	1 m/s	0.15 m/s	0.18 m/s	-	-

Table 19: *GDR-D and GDR-F estimated error budget*

The conclusion of this investigation is twofold. First, SARAL/AltiKa's instrumental and processing performances in terms of high frequency content was compared to Ku-band 20Hz SAR (Sentinel3-A) altimeter. We mainly focused on the assessment of very high frequency signals to give the order of magnitude of instrumental and processing impacts. On this occasion, we have clearly put in evidence that not only SARAL/AltiKa is in line with requirements, but also that the metrics obtained are pretty comparable to Sentinel3-A in terms of white noise. The performance of GDR-F is similar if not slightly better than the GDR-D products.
The questioning raised in the previous error bugdet are still valid:

- The requirement metrics provided, that are not always relevant as we have seen in section 7.4.6.. Due to the correlation between range and SSB at high frequency, we obtained a total SSH error lower than the range error itself ($0.74cm$ compared to $0.83cm$).
- The estimation methods used to derive the uncertainties at high frequency which are based on different assumptions and do not allow to quantify the same error contents:
  - The spectral analysis method, is the most relevant to estimate the white noise over 40Hz measurements since we can estimate the energy of signals at very low wavelenghts (between 500m and 1 km). But it is harder to select specific sea states. The conversion from 40Hz white noise to 1 Hz white noise based on the assumption of uncorrelated measurements is relevant in this case since the signal converted here contains only white noise.
  - The analysis of the 40Hz standard deviation is a good way to determine the noise level for a given sea state (SWH = 2m and). But it is based on the assumption that the white noise plateau is stable over the forty consecutive measurements (about 7 km in SARAL/AltiKa's case). We have seen that this is not exactly the case since conventional altimetry is impacted by the spectral hump for wavelengths lower than 10 km; and SARM altimetry is impacted by a red signal at these scales. So this estimation integrates an additional error related to these two phenomena. Thus the assumption of uncorrelated 40Hz consecutive measurements is not as relevant as it is for the spectral analysis method.

8. Conclusion

SARAL/AltiKa was launched on February, 25th 2013 and has been providing high quality sea surface height measurements for more than 5 years. This report summarizes a variety of results, including comparisons with Jason-2 and Jason-3 to demonstrate the excellent quality of SARAL/AltiKa data. The main points of this performance assessment are summarized below:

- SARAL/AltiKa provides an excellent coverage of the ocean, with more than 99% of measurements available over ocean.
- The global bias is of 69 mm with respect to Jason-3 and of 65 mm with respect to Jason-2.
- SLA statistics show no long term drifts, SARAL/AltiKa and Jason-2 and Jason-3 observe very similar SLA features when considering temporal evolution of global averages and also geographical patterns.
- Standard deviation of daily SLA averages differences between SARAL/AltiKa and both Jasons is below 5 mm.
- At crossovers SARAL/AltiKa shows a performance similar to Jason-2 with a standard deviation of 5.2 cm.
- Data quality remains excellent, even when considering the various mispointing events due to attitude deviations since SSA (Feb'2019). Only 5.73% of rejected measurements (locally up to 12% e.g. over Indian Ocean) during the editing process (once ice excluded), which is only slightly higher than Jason-2 (3.27%) and Jason-3(3.24%).
- The ocean error budget is largely within requirements with a reduced noise level for the Ka-band compared to Sentinel3-A.

All these metrics confirm the excellent data quality of SARAL's data record. One should bear in mind that 2016 was marked by a milestone for SARAL/AltiKa: the start of the drifting phase on July, 4th. As shown throughout the report, the orbit change does not have any measureable impacts on the instrument's performance. Besides, after more than 4 years on an unmaintained decaying altitude (see [20] for further details about SARAL/AltiKa's sampling during its drifting phase), SARAL/AltiKa provides an extremely dense, albeit random, yearly coverage for geodetic applications (Mean Sea Surface or Bathymetry) and yields an enhanced mesoscale monitoring capability ([20]&[17]).

Mispointing events are still affecting the platform, resulting from random anomalies in reaction wheel friction and since February 2019, caused by the Star Sensor Anomaly. The SSA leads to frequent attitude deviations that are routinely corrected using waveform derived mispointing information.

Thanks to the GDR-F reprocessing, GDR dataset is now homogeneous and shows many improvements. The data and related documentation are available on AVISO (aviso@altimetry.fr). For further information and comparison with GDR-T see [59].

9. Glossary

AMR Advanced Microwave Radiometer

CLS Collecte Localisation Satellites

CNES Centre National d'Etudes Spatiales

CNG Consigne Numerique de Gain (= Automatic Gain Control)

DEM Digital Elevation Model

DIODE Détermination Immédiate d'Orbite par Doris Embarqué

ECMWF European Centre for Medium-range Weather Forecasting

EDP Earliest Detection Part

GDR Geophysical Data Record

GDR-D Geophysical Data Record version D

GDR-F Geophysical Data Record version F

GIM Global Ionosphere Maps

GOT Global Ocean Tide

IGDR Interim Geophysical Data Record

JPL Jet Propulsion Laboratory (Nasa)

MLE Maximum Likelyhood Estimator

MOE Medium Orbit Ephemeris

MQE Mean Quadratic Error

MWR MicroWave Radiometer

MSS Mean Sea Surface

NSIDC National Snow and Ice Data Center

OSTST Ocean Surface Topography Science Team

PEACHI Prototype for Expertise in Altimetry, Coastal, Hydrology and Ice

PF/RF PlatForm / RadioFrequency

PLTM PayLoad TeleMetry

POE Precise Orbit Ephemeris

PSD Power Spectral Density

OGDR Operational Geophysical Data Record

RMS Root Mean Square

RSS Root Sum Square

SALP Service d'Altimétrie et de Localisation Précise

SARAL Satellite with ARgos and ALtika

SSA Star Sensor Anomaly

SSH Sea Surface Height

SLA Sea Level Anomaly

SLR Satellite Laser Ranging

SSB Sea State Bias

SWH Significant Wave Height

TEC Total Electron Content

TBI To Be Investigated

TM TeleMetry

10. References

References

[1] Brown, G.S., 1977, The average impulse response of a rough surface and its application", *IEEE Transactions on Antenna and Propagation*, Vol. AP 25, N1, pp. 67-74

[2] Davis, C.H., A robust threshold retracking algorithm for measuring ice-sheet surface elevation change from satellite radar altimeters, IEEE Transactions on Geoscience and Remote Sensing

[3] Ricker, R., Hendricks, S., Helm, V., Skourup, H., Davidson, M., Sensitivity of CryoSat-2 Arctic sea-ice freeboard and thickness on radar-waveform interpretation, The Cryosphere 2014.

[4] Thibaut, P., O.Z. Zanifé, J.P. Dumont, J. Dorandeu, N. Picot, and P. Vincent, 2002, Data editing: The MQE criterion, *Paper presented at the Jason-1 and TOPEX/Poseidon Science Working Team Meeting, New-Orleans (USA), 21-23 October*

[5] Vincent, P., S. D. Desai, J. Dorandeu, M. Ablain, B. Soussi, P. S. Callahan, and B. J. Haines 2003. Jason-1 Geophysical Performance Evaluation. Mar. Geod. 26(3-4): 167-186.

[6] Obligis, E., Rahmani, A., Eymard, L., Labroue, S., Bronner, E., An improved retrieval algorithm for water vapor retrieval : application to the envisat microwave radiometer, IEEE Transactions on Geoscience and Remote Sensing, 2009, 47 (9), p. 3057-3064. ISSN 0196-2892

[7] Boy, F. and J.-D. Desjonqueres, 2010, Note technique datation de l'instant de reflexion des échos altimètres pour POSEIDON2 et POSEIDON3, *TP3-JPOS3-NT-1616-CNES*

[8] Desjonquères, J. D. , G. Carayon , N. Steunou and J. Lambin, 2010, Poseidon-3 Radar Altimeter: New Modes and In-Flight Performances, *Marine Geodesy*, 33:1, 53–79, available at http://pdfserve.informaworld.com/542982__925503482.pdf

[9] Aouf, L. and J.-M. Lefèvre, 2013, The impact of Saral/Altika wave data on the wave forecasting system of Météo-France : update, Oral presentation at SARAL/AltiKa 1st Verification Workshop, Toulouse, France, available at http://www.aviso.oceanobs.com/fileadmin/documents/ScienceTeams/Saral2013/24_wave_lotfi.pdf

[10] Faugere, Y., A. Delepoulle, F.Briol, I. Pujol, N. Picot, E. Bronner; 2013, Altika in DUACS: Status after 2 months (and perspectives), oral presentation at SARAL/AltiKa 1st Verification Workshop, Toulouse, France, available at http://www.aviso.oceanobs.com/fileadmin/documents/ScienceTeams/Saral2013/34_Altika_in_Duacs_Faugere.pdf

[11] Griffin, D. and M. Cahill, 2013, Use of AltiKa NRT sea level anomaly in the Australian multi-mission analysis, Oral presentation at SARAL/AltiKa 1st Verification Workshop, Toulouse, France, available at http://www.aviso.oceanobs.com/fileadmin/documents/ScienceTeams/Saral2013/33_multi_mission_gridding_GRIFFIN.pdf

[12] - Dibarboure, G., F. Boy, J. D. Desjonqueres, S. Labroue, Y. Lasne, N. Picot, J. C. Poisson, and P. Thibaut, 2014: Investigating short-wavelength correlated errors on low-resolution mode altimetry. *J. Atmos. Oceanic Technol.*, **31**, 1337–1362, doi:10.1175/JTECH-D-13-00081.1

[13] Frery, M.-L. *et al.*, 2014, Correction du canal 37GHz du radiomètre AltiKa, CLS/DOS/NT-14-115

[14] Le Gac, S., F. Boy, A. Guillot, J.D. Desjonqueres, N. Picot, J.C. Poisson, F. Piras, G. Bracher, P. Thibaut, G. Valladeau , 2015, Impact of the antenna diagram approximation in conventional altimetry WF processing, *Application to SARAL/AltiKa data*, Oral presentation at OSTST, Reston, USA, https://meetings.aviso.altimetry.fr/fileadmin/user_upload/tx_ausyclsseminar/files/OSTST2015/IPM-04-_LeGac_Talk_AltiKaAntennaDiagram_OSTST2015.pdf

[15] Vandemark, D., Chapron, B., Feng, H., Mouche, A., 2016, Sea surface reflectivity variation with ocean temperature at Ka-band observed using near-nadir satellite radar data, *Remote Sensing*

[16] - Dufau, C., M. Orsztynowicz,G. Dibarboure, R. Morrow, and P.-Y. Le Traon (2016), Mesoscale resolution capability of altimetry:Present and future, *J. Geophys. Res.Oceans*, **121**, doi:10.1002/2015JC010904.

[17] Mercator Ocean Journal #56, 2017, *Special Issue CMEMS* section : High-level data processing and observation products (TACs), available at: https://www.mercator-ocean.fr/en/science-publications/mercator-ocean-journal/mercator-ocean-journal-56-special-issue-cmems/

[18] Ablain, M., Taburet, N., Zawadzki, L., Jugier, R., Vayre, M., 2017, SALP annual report (2017) of Mean Sea Level Activities SALP-RP-MA-EA-23189-CLS available from https://www.aviso.altimetry.fr/fileadmin/documents/calval/validation_report/SALP-RP-MA-EA-23189-CLS_AnnualReport_2017_MSL.pdf

[19] Guerou A., 2021, SALP annual report (2021) of Mean Sea Level Activities

[20] Dibarboure, G., Lamy, A., Pujol, M-I., Jettou, G., 2018, The drifting phase of SARAL/AltiKa: securing a stable mesoscale sampling with an unmaintained decaying altitude, *Remote Sensing*

[21] Ollivier, A. 2018, Assessment of Orbit Quality through the Sea Surface Height calculation - Yearly report 2018 - SALP activities, SALP-RP-MA-EA-23080-CLS

[22] Dibarboure, G., L2E project leader at CNES (Gerald.Dibarboure@cnes.fr), Piras, F., L2E project manager at CLS (fpiras@groupcls.com)

[23] Tolman, H. L., 2014, User manual and system documentation of WAVEWATCH III version 4.18. *NOAA / NWS / NCEP / MMAB Technical Note 316, 194 pp.* available at http://polar.ncep.noaa.gov/waves/wavewatch/manual.v4.18.pdf

[24] The WAVEWATCH III Development Group., 2016, User manual and system documentation of WAVEWATCH III version 5.16. *NOAA / NWS / NCEP / MMAB Technical Note 329, 326 pp.* available at http://polar.ncep.noaa.gov/waves/wavewatch/manual.v5.16.pdf

[25] Scharroo, R., and J. L. Lillibridge, 2005, Non-parametric sea-state bias models and their relevance to sea level change studies, in *Proceedings of the 2004 Envisat & ERS Symposium*, Eur. Space Agency Spec. Publ., ESA SP-572, edited by H. Lacoste and L. Ouwehand

[26] Lillibridge, J., R. Scharroo, S. Abdalla, and D. Vandemark, 2013, One-and Two-Dimensional Wind Speed Models for Ka-band Altimetry, *Journal of Atmospheric and Oceanic Technology*, doi: http://dx.doi.org/10.1175/JTECH-D-13-00167.1

[27] B. Chelton, Dudley 1995, The sea state bias in altimeter estimates of sea level from collinear analysis of TOPEX data, *Journal of Geophysical Research Atmospheres*, 99, DOI : 10.1029/94JC02113

[28] Zanife, O. Z., P. Vincent, L. Amarouche, J. P. Dumont, P. Thibaut, and S. Labroue, 2003. Comparison of the Ku-band range noise level and the relative sea-state bias of the Jason-1, TOPEX and Poseidon-1 radar altimeters. Mar. Geod. 26(3-4): 201-238.

[29] Labroue, S., MH. Rio, Y. Faugere, A. Ollivier - Tâche 1.1 - Résolution des produits et filtrage SALP-NT-P-EA-21665-CLS.

[30] Gaspar, P. , S. Labroue, F. Ogor, G. Lafitte, L. Marchal, and M. Rafanel. 2002. « Improving nonparametric estimates of the sea state bias in radar altimetry measurements of sea level », J. Atmos. Oceanic Technol., 19, 1690-1707.

[31] Labroue S., P. Gaspar, J. Dorandeu, O.Z. Zanife, F. Mertz, P. Vincent, and D. Choquet, Non-parametric estimates of the sea state bias for Jason-1 radar altimeter, Mar. Geod., 27, 453-481, 2004.

[32] Tran N., S. Labroue, S. Philipps, E. Bronner and N. Picot: "Overview and Update of the Sea State Bias Corrections for the Jason-2, Jason-1 and TOPEX Missions", Marine Geodesy / special issue on OSTM/Jason-2 calibration/validation, 33(S1): 348 - 362, doi:10.1080/01490419.2010.487788, 2010.

[33] Tran N., D. Vandemark, H. Feng, A. Guillot, N. Picot (2014) Updated wind speed and sea state bias models for Ka-band altimetry, 2014 SARAL/AltiKa workshop, Lake Constance, Germany. Available at https://meetings.aviso.altimetry.fr/fileadmin/user_upload/tx_ausyclsseminar/files/Poster_PEACHI_ssb_tran2014.pdf

[34] Tran N., D. Vandemark, E.D. Zaron, P. Thibaut, G. Dibarboure, and N. Picot (2019): "Assessing the effects of sea-state related errors on the precision of high-rate Jason-3 altimeter sea level data", Advances in Space Research / special issue " 25 Years of Progress in Radar Altimetry", doi:10.1016/j.asr.2019.11.034

[35] Couhert, A., L. Cerri, J-F. Legeais, M. Ablain, N-P. Zelensky, B-J. Haines, F-G. Lemoine, W-I. Bertiger, S-D. Desai, M. Otten, Towards the 1mm/y stability of the radial orbit error at regional scales, *J. Advances in Space Research* ,**#55 (2-23)**, 2015 , http://www.sciencedirect.com/science/article/pii/S0273117714004219

[36] J. C. Ries and S. D. Desai, Conventional model update for rotational deformation, in Fall AGU Meeting, New Orleans, LA, 2017,

[37] Carrere L., F. Lyard, M. Cancet, A. Guillot, N. Picot: FES 2014, a new tidal model - Validation results and perspectives for improvements, presentation to ESA Living Planet Conference, Prague 2016.

[38] Lyard, F. H., Allain, D. J., Cancet, M., Carrere, L., and Picot, N.: FES2014 global ocean tides atlas: design and performances, Ocean Sci. Discuss. [preprint], https://doi.org/10.5194/os-2020-96, in review, 2020.

[39] Edward D. Zaron , Robert deCarvalho, 2016. Identification and Reduction of Retracker-Related Noise in Altimeter-Derived Sea Surface Height Measurements. *Journal of Atmospheric and Oceanic Technology*, p201-210, doi:10.1175/JTECH-D-15-0164.1

[40] Carrere, L., Arbic, B.K., Dushaw, B., Egbert, G., Erofeeva, S., Lyard, F., Ray, R.D., Ubelmann, C., Zaron, E., Zhao, Z., Shriver, J.F., Buijsman, M.C., Picot, N., Accuracy assessment of global internal tide models using satellite altimetry, to be submitted

[41] Mean Sea Surface CNES/CLS models over time https://www.aviso.altimetry.fr/en/data/products/auxiliary-products/mss.html

[42] Schaeffer, P., Pujol, M.-I., Faugere, Y., Picot, N., Guillot, A. 2016: New Mean Sea Surface CNES_CLS 2015 focusing on the use of geodetic missions of CryoSat-2 and Jason-1. Living Planet Symposium

[43] Pujol, M.-I., Y. Faugere, G. Dibarboure, P. Schaeffer, A. Guillot and N. Picot, 2015, The recent drift of SARAL: an unexpected MSS experiment, oral presentation at the 2015 OSTST, Reston, VA

[44] Picot, N., A. Guillot, P. Sengenès, J. Noubel, N. Steunou, S. Philipps, P. Prandi, G. Valladeau, M. Ablain, S. Desai, B. Haines and S. Fleury, 2013, Data Quality Assessment Of The SARAL/AltiKa Ka-band Mission, Oral presentation at OSTST, Boulder, USA, available at http://www.aviso.oceanobs.com/fileadmin/documents/OSTST/2013/oral/Picot_SARAL_Data_Quality_Assessment.pdf

[45] Stenou, N., P. Sengenes, J. Noubel, N. Picot, J.D. Desjonquères, J.C. Poisson, P. Thibaut, F. Robert and N. Tavenea, 2013, AltiKa Instrument : In-Flight Stability And Performances, Oral presentation at OSTST, Boulder, USA, available at http://www.aviso.oceanobs.com/fileadmin/documents/OSTST/2013/oral/Steunou_OSTST2013_AltiKa_Instrument.pdf

[46] Ollivier, A., N. Steunnou, G. Dibarboure, Spectral analysis of altimetric signal and errors Towards a spectral error budget of Nadir Altimetric missions, https://meetings.aviso.altimetry.fr/fileadmin/user_upload/tx_ausyclsseminar/files/30Ball0900-2_Pres_OSTST2014_J2_ErrorBugdet_Spectra_Ollivier.pdf

[47] Ollivier, A. , B. Picard, G.Dibarboure, N. Picot, P. Femenias, Spectral analysis of altimetric signal and errors. Evidencing the skills of different Altimetric missions for different time and space scales, Living Planet Symposium 2016

[48] Thibaut, P., F. Piras, J-C. Poisson, A. Guillot, F. Boy, N. Picot, 2015, Characterization of the Altimeter Mission Performances over Ocean, *Comparison and Interpretation*, Oral presentation at OSTST, Reston, USA, https://meetings.aviso.altimetry.fr/fileadmin/user_upload/tx_ausyclsseminar/files/OSTST2015/ERR-03-Thibaut.pdf

[49] Raynal, M., T. Moreau, N. Tran, s. Labroue, F. Boy, P. Féménias, F. Borde, 2018, Assessment of the SARM processing sensitivity to swell, Oral presentation at OSTST, Ponta Delgada, Azores, Portual, https://meetings.aviso.altimetry.fr/fileadmin/user_upload/ERR_01_Raynal.pdf

[50] Jettou, G., Rousseau, M., Ollivier, A., 2019, GDR-F global quality assessment (over 2015), Oral presentation at 2019's Ocean Surface Topography Science Team meeting, Chicago, USA, available at https://meetings.aviso.altimetry.fr/fileadmin/user_upload/2019/CVL2_04_SARAL_GDRF_GLOBAL_ASSESSMENT_V1.pdf

[51] SARAL System Requirements, *SRL-SYS-SP-010-CNES*

[52] SARAL/AltiKa Products handbook, 2013, *SALP-MU-M-OP-15984-CN* edition 2.3, available at: https://www.aviso.altimetry.fr/fileadmin/documents/data/tools/SARAL_Altika_products_handbook.pdf

[53] Philipps, S., P. Prandi and V. Pignot, 2013, Saral/ Altika validation and cross calibration activities (Annual report 2013) SALP-RP-MA-EA-22271-CLS available from http://www.aviso.altimetry.fr/fileadmin/documents/calval/annual_report_Altika_2013.pdf

[54] Philipps, S. and V. Pignot, 2014, Saral/AltiKa reprocessing GDR-T Patch2, SALP-RP-MA-EA-22345-CLS/CLS.DOS/NT/14-031

[55] Prandi, P., V. Pignot and S. Philipps, 2015, Saral/ Altika validation and cross calibration activities (Annual report 2014), SALP-RP-MA-EA-22418-CLS

[56] Prandi, P., V. Pignot, 2015, Saral/ Altika validation and cross calibration activities (Annual report 2015) SALP-RP-MA-EA-22957-CLS available from http://www.aviso.altimetry.fr/fileadmin/documents/calval/annual_report_al_2015_01.pdf

[57] Jettou, G., Rousseau, M., Ollivier, A., 2018, SARAL/AltiKa validation and cross calibration activities, Annual report 2018 SALP-RP-MA-EA-23188-CLS available from https://www.aviso.altimetry.fr/fileadmin/documents/calval/validation_report/AL/SALP-RP-MA-EA-23249-CLS_Annual_Report_SARAL_2018.pdf

[58] Jettou, G., Rousseau, M., 2019, Saral/ Altika validation and cross calibration activities (Annual report 2019), SALP-RP-MA-EA-23419-CLS

[59] Jettou, G., Rousseau, M., 2020, SARAL/AltiKa GDR-F product - Validation report SALP-RP-MA-EA-23462-CLS

[60] Prandi, P., S. Philipps, V. Pignot and N. Picot, 2015, SARAL/AltiKa Global Statistical Assessment and Cross-Calibration with Jason-2 *Marine Geodesy*, 38, DOI: 10.1080/01490419.2014.995840

[61] Ollivier, A., G. Jettou, Error budget of Envisat altimetry mission - V3 reprocessing version, https://earth.esa.int/documents/700255/3528455/Error_Budget_Envisat_Altimetry_Mission.pdf

[62] Philipps, S., M. Ablain, H. Roinard, E. Bronner, N.Picot, Jason–2 global error budget for time scales lower than 10 days, https://www.aviso.altimetry.fr/fileadmin/documents/OSTST/2012/Philipps_jason2_global_error.pdf

[63] Roinard, H., S. Philipps and O. Lauret, 2016, Jason-2 validation and cross calibration activities (Annual report 2015), SALP-RP-MA-EA-22961-CLS available at https://www.aviso.altimetry.fr/fileadmin/documents/calval/validation_report/J2/annual_report_j2_2015.pdf

[64] Roinard, H., P. Matton and S. Philipps, 2015, Jason-2 validation and cross calibration activities (Annual report 2014), SALP-RP-MA-EA-22409-CLS available at http://www.aviso.altimetry.fr/en/data/calval.html

[65] Roinard, H., Cadier, E., 2017, Jason-2 validation and cross calibration activities (Annual report 2017) SALP-RP-MA-EA-23186-CLS available from https://www.aviso.altimetry.fr/fileadmin/documents/calval/validation_report/J2/SALP-RP-MA-EA-23186-CLS_Jason-2_AnnualReport2017_v1-2.pdf

[66] Lauret, O., 2016, Jason-3 validation and cross calibration activities (Annual report 2016) SALP-RP-MA-EA-23060-CLS available from https://www.aviso.altimetry.fr/fileadmin/documents/calval/validation_report/J3/annual_report_j3_2016.pdf

[67] Roinard, H., Michaud, L., 2019, Jason-3 validation and cross calibration activities (Annual report 2019) SALP-RP-MA-EA-23399-CLS available from https://www.aviso.altimetry.fr/fileadmin/documents/calval/validation_report/J3/SALP-RP-MA-EA-23399-CLS_Jason-3_AnnualReport2019_v1-1.pdf

[68] Barnoud, Anne; Pfeffer, Julia; Guérou, Adrien; Frery, Marie-Laure; Siméon, Mathilde; Cazenave, Anny; Chen, Jianli; Llovel, William; Thierry, Virginie; Legeais, Jean-François; Ablain, Michaël. 2021, Contributions of Altimetry and Argo to Non-Closure of the Global Mean Sea Level Budget Since 2016 Geophysical Research Letters, Volume 48, Issue 14, article id. e92824. 2021-07. doi:10.1029/2021GL092824.

11. Annex

11.1. Content of Patch 1

Hereafter the content of Patch 1 is recalled. All GDR data up to cycle 7 included were initially produced with this patch. It was used to produce IGDR data from cycle 4 pass 395 to cycle 10 pass 565.

Altimeter calibration file : The altimeter calibration stability has been analysed. Based on the actual data, we have implemented an averaging of the calibrations over a 7 days window for the low pass filter (identical to Jason-2) and 3 days for the internal path delay and total power (not used on Jason-2). This will slightly reduce the daily noise observed in the altimeter calibration data.

Altimeter characterization file : We have updated the altimeter characterization file using the flight calibration of the gain values (4 calibrations performed). The impact is very small (of the order of 0.01 dB).

Retracking look-up tables : We have updated the ocean retracking look-up tables using the flight calibration data (PTR). The impact is very small on the range and sigma0 values but of the order of 15 cms on SWH for low sea states.

MQE : We have analyzed the altimeter flight data and based on the observed MQE values over ocean a threshold of 2.3E-3 (Jason-2 value is 8E-3) is used for the 1Hz data computation.

Neural network : A first linear relation has been computed between the measured BT and the simulated one. This linear relation is applied on the 23.8 GHz only – the same analysis will be conducted on the 37 GHz and sigma0. This generates a bias on the radiometer wet tropospheric correction which is now much more consistent with the model one.

Atmospheric attenuation : The value outputted by the neural algorithm is now recorded in the level2 products (it was set to 0 at the beginning of the mission). Rad_water_vapor and rad_liquid_water: The values have been corrected to comply with the actual unit in the level2 products (kg/m^2). But the rad_liquid_water remains not reliable as an anomaly has been noticed in the neural network.

SSHA : The radiometer wet tropospheric correction is now used to compute this value (the model value was used at the beginning of the mission).

Controls parameters : The threshold values have been updated with in-flight data. This is a first tuning – additional work is necessary.

11.2. Content of Patch 2

Hereafter the content of Patch 2 is recalled. GDR data were produced using Patch 2 from cycle 8 onwards. Cycles 1 to 7 were reprocessed with the Patch 2 to provide a consistent dataset

Wind look-up table : The table provided by NOAA is used. This table is only based on the measured sigma0, taking into account the atmospheric attenuation (sigma0 at the surface). (Reference: Lillibridge et al. [26])

SSB look-up table : The table provided by R. Scharroo is used (same method as in [25]). We use only the significant wave height to compute the SSB.

Radiometer neural algorithm : Taking into account several months of AltiKa measurements, the neural network coefficients have been updated. Note that this modifies the radiometer related parameters (radiometer wet troposphere correction, atmospheric attenuation, radiometer liquid water content and radiometer water vapor content).

Ice-2 retracking algorithm : The algorithm has been updated taking into account the AltiKa Ka band specificities (ice2 algorithm was based on ENVISAT Ku band experience).

FES2012 tide model : This new tide model is included, improving the SSH accuracy in coastal zones. (Reference : http://www.aviso.oceanobs.com/en/data/products/auxiliary-products/global-tidefes2004-fes99/description-fes2012.html)

Matching pursuit algorithm : The algorithm based on J. Tournadre proposal has been tuned to comply to AltiKa Ka band specificities.

MQE parameter scale factor : The scale factor of the MQE has been modified.

Update of the altimeter characterization file : The altimeter characterization file has been modified in order to account for 63 values of altimeter gain control loop (AGC). This has impacts over sea ice and land hydrology, in some cases the AGC was set to default value in current P1 products.

Doris on ground processing (Triode) : The Doris navigator ground processing has been upgraded to reduce the periodic signal observed on the altitude differences with MOE/POE.

11.3. Content of GDR-F

Are listed hereafter the major evolutions of SARAL/AltiKA's new GDR-F product. GDR data are produced with this version since cycle 135, whereas IGDR data were only produced with this patch from cycle 137 onwards.

Ocean tide height: ocean_tide_sol2, ocean_tide_equil and ocean_tide_non_equil are now computed with FES2014 instead of FES2012. ocean_tide_sol2 is now used for SLA estimation instead of ocean_tide_sol1 that now contain GOT4V10 instead of GOT4V8.

Pole tide: S. Desai pole tide with new IERS linear mean pole is now provided in product instead of Warh 85 pole tide.

Sea state biais: Sea state biais is now compute with SSB tables based on significant wave height and wind, using 2015 GDR-F dataset for the method proposed by Tran, 2018 [34] and [33].

Off nadir angle look up table: Mispointing look up table is now provided in product, and applied to square off nadire angle.

Orbit: Orbit is now computed with POE-F standard.

Wet tropospheric correction: Patch 4 of neuronal network for wet tropospheric correction is now provided in producted. It is now based on 5 parameters (23.8 GHz and 37 GHz brightness temperatures, Ka-band backscatter coefficient, sea surface temperature and atmospherical temperature lapse rate climatology).